Experimental Investigation on the Desiccation and Fracturing of Clay

Tollenaar , Roderick N.

DOI
10.4233/uuid:40f6b033-0e6a-460b-9501-30cf35a99b8d

Publication date
2017

Document Version
Final published version

Citation (APA)
Tollenaar , R. N. (2017). *Experimental Investigation on the Desiccation and Fracturing of Clay*. [Dissertation (TU Delft), Delft University of Technology]. https://doi.org/10.4233/uuid:40f6b033-0e6a-460b-9501-30cf35a99b8d

Important note
To cite this publication, please use the final published version (if applicable).
Please check the document version above.

Experimental Investigation on the Desiccation and Fracturing of Clay

Experimental Investigation on the Desiccation and Fracturing of Clay

Proefschrift

ter verkrijging van de graad van doctor
aan de Technische Universiteit Delft,
op gezag van de Rector Magnificus prof. ir. K.C.A.M. Luyben,
voorzitter van het College voor Promoties,
in het openbaar te verdedigen op donderdag 15 juni 2017 om 12:30 uur

door

Roderick Nicolaas TOLLENAAR

Master of Applied Science in Mining Engineering,
The University of British Columbia, Vancouver, Canada,
geboren te Chillán, Chili.

Dit proefschrift is goedgekeurd door de

promotor: prof. dr. C. Jommi
copromotor: dr. ir. L.A. van Paassen

Samenstelling promotiecommissie:

Rector Magnificus,	voorzitter
Prof. dr. C. Jommi,	Technische Universiteit Delft
Dr. ir. L.A. van Paassen,	Technische Universiteit Delft
Onafhankelijke leden:	
Prof. dr. A. Ledesma,	Universitat Politècnica de Catalunya
Prof. dr. F. Cotecchia,	Politecnico di Bari
Prof. dr. ir. H.H.M. Rijnaarts,	Wageningen University & Research
Prof. dr. M.A. Hicks,	Technische Universiteit Delft
Overige leden:	
Prof. ir. A.F. van Tol,	Technische Universiteit Delft
Reservelid:	
Prof. dr. ir. J.C. Winterwerp,	Technische Universiteit Delft

Keywords: Soil Cracking, Soil Fracturing, Desiccation, Tensile Strength, Pull Rate, Tensile Test, Geo-PIV, Drying Rate, Suction, Evaporation

Printed by: Ipskamp Printing

Cover Picture: Baggerdepot, Wormer- en Jisperveld, Noord Holland, Nederland

e-mail: rodtol@hotmail.com

ISBN 978-94-92516-59-6

An electronic version of this dissertation is available at
http://repository.tudelft.nl/.

to my parents

Contents

1

Introduction

Victory awaits him who has everything in order; luck, people call it. Defeat is certain for him who has neglected to take the necessary precautions in time; this is called bad luck.

Roald Amundsen

1

1.1. Problem Statement

In low-lying delta areas like the Netherlands, dredging of waterways and lakes is essential for allowing navigation and recreation. Furthermore it helps to maintain the water quality and it allows to efficiently drain the land required for agriculture. One way of dealing with dredged sediments is to store them in upland depots. It has also been suggested that these sediments could be viable as substitute for other materials in civil engineering and agricultural applications.

Dredged sediments often contain an important fraction of fines and organic material, all of them with high water contents. Therefore, it requires a significant amount of time for the sediments to ripen through a combination of drainage, consolidation and evaporation.

After enough dewatering has taken place, cracks will start developing affecting not only the drainage and evaporation, but also producing more deformation. If the dredged material is used in construction, the cracks will affect the geotechnical properties of the material like its strength, stiffness and hydraulic conductivity. While cracks are considered to accelerate evaporation in a ripening soil, they might be detrimental in many civil engineering applications. For instance, they can affect the stability and serviceability of earthworks. Additionally, when the sediments are employed for agricultural purposes, cracks will influence drainage, water infiltration, evaporation, and potentially the soil composition through oxidation and decomposition. Consequently, identifying how cracks occur in the soil is essential for understanding the behavior of the material.

As established by Corte & Higashi (1960), Nahlawi & Kodikara (2006) and Peron et al. (2009), soil cracking is the result of the constrained shrinkage of the soil. Tang et al. (2010a) indicated that the development of suction during the drying of the soil is the driving force behind shrinkage and cracking, which is the direct consequence of the water loss during evaporation. At the same time, evaporation also influences suction development (Kayyal, 1995; Tang et al., 2010a). As suction arises, tensile stresses are produced in the soil, with fracturing occurring once the tensile stresses reach the tensile strength of the material (Corte & Higashi, 1960). Peron et al. (2009) suggested that the crack initiation was directly related to the moment at which the air entry value of the soil was reached. Shin & Santamarina (2011) assumed something similar, linking the air intrusion into the pores to crack initiation. Scherer (1990) hinted that an analogous phenomenon takes place during the drying of gels. These observations lead to the conclusion that there is a direct association between the tensile strength and the water retention properties of the soil. Laboratory experiments performed on evaporating clay samples have shown that crack initiation and intensity are dependent on several factors, such as soil thickness, drying speed and initial water content (Corte & Higashi, 1960; Kodikara et al., 2000; Nahlawi & Kodikara, 2006; Tang et al., 2008, 2010a; Costa et al., 2013). Tang et al. (2008, 2010a) and Costa et al. (2013) were able to quantify the influence of the desiccation rate on the amount of cracks produced by drying layers of equal thickness at different rates, with layers under faster drying exhibiting more fractures than the ones under a slow drying regime.

These investigations show that there is a drying and shrinkage rate dependency

in the ripening and cracking of shrinking soils. However, there is still not enough understanding regarding the role played by each time dependent variable on the overall response of a desiccating layer. Probably the most recognizable time dependent factor is the (non-uniform) change in water content with depth due to evaporation. This aspect also influences the time and water content dependent evolution of suction, stiffness and strength. A less well-defined feature is the potential rate dependency of the clay properties. To the author's knowledge this element has seldom been studied in the context of ripening soils. Analyzing the behavior of the time dependent hydro-mechanical response of a rate dependent material is not straightforward, as the material rate dependency and the time dependent state, which change with water evaporation, overlap in the response. Moreover, cracking is a localized process which breaks any homogeneity in the response as soon as it is triggered.
This investigation aimed at examining the effects of rate dependency in desiccation and cracking by means of a combination of various laboratory tests on small physical models. The tests were also utilized to evaluate their representativeness in the description of the material behavior.

1.2. Research Objectives

The key objectives of this thesis were as follows:

- Investigate the effects of boundary conditions and geometrical constraints on the inception and propagation of desiccation cracks in a typical clay;
- Analyze the conditions for fracture propagation (in a consolidating layer), investigating the role of stress changes with depth;
- Evaluate the relationship between water content, strain rate and tensile strength and stiffness of the soil;
- Characterize the drying behavior of the soil under different evaporative regimes and initial conditions, and analyze their effects on the suction development;
- Assess rate dependency of the factors involved in the fracture generation and propagation process.

1.3. Thesis Organization

Chapter 1 outlines the problem and the research objectives.
Chapter 2 presents the open evaporation experiments performed on clay boards under different material and boundary conditions.
Chapter 3 reports the assessment completed to evaluate the effects of strain rate and water content on the tensile strength and stiffness of a clay.
Chapter 4 describes the tests carried out to study the effects of evaporation rate and initial conditions on soil desiccation and suction development.
Chapter 5 introduces a basic mechanical model that employs several hypotheses to try to explain fracture development in soil based on the observations made during

the laboratory experiments.
Chapter 6 summarizes the conclusions of this research.

2

Observations on the Desiccation and Cracking of Clay Layers

The power of accurate observation is commonly called cynicism by those who have not got it.

George Bernard Shaw

This chapter is based on a paper submitted and reviewed in Engineering Geology Tollenaar et al. (2017b).

2.1. Introduction

Much investigation has already been carried out in geotechnical engineering on desiccation cracks. Kindle (1917) performed the first qualitative experiments looking into the formation of soil cracks. Nevertheless, it was not until Corte & Higashi (1960) that detailed and comprehensive studies into the subject were carried out. They analized the behavior of clay layers prepared in rectangular containers of two sizes (60 x 84 cm and 87 x 122 cm) under different conditions. Their investigation was performed using a glacial clay prepared as a slurry with a 60% initial water content for all their tests, and with thicknesses between 2 and 50 mm. The clay had a plastic limit and plasticity index of 13.8% and 17.5%, respectively. They also studied the frictional effects of the container's bottom by utilizing smooth plywood, plywood soaked in grease, glass and a sand layer. Among their findings are the dependence of the cell size, fracture length and cracking water content on the evaporating soil layer thickness, with thick layers exhibiting larger cells, longer fractures and higher cracking water contents than thin ones. They assessed the effects of the adhesion of the soil to the bottom of the container on the amount of fractures generated, and observed that the more adhesive the bottom material, the more cracks were generated. It was determined that the cracking water content was also related to the desiccation speed, with faster speeds having lower cracking water contents. Based on these observations, Corte & Higashi (1960) developed geometrical and mechanical interpretations of the phenomenon. These outcomes have been later corroborated by other researchers, such as Kodikara et al. (2000) who analysed the data of Corte & Higashi (1960) and Lau (1987), Nahlawi & Kodikara (2006), Lakshmikantha et al. (2006) and Costa et al. (2013). Tang et al. (2008), Tang et al. (2010a) and Costa et al. (2013) were able to show that there was an influence of the desiccation rate in the amount of cracks produced. Rodríguez et al. (2007) observed that the effects of soil thickness on the cracking water content were not noticeable for very thin soil layers. Peron et al. (2009) looked at free and constrained desiccation, and crack patterns. They studied the boundary constraints necessary for cracking, the stages of soil deformation during drying, the relationship between the crack initiation point and the saturation of the material, and crack patterns.

Several theoretical frameworks have been developed to describe the previous experimental observations on fracture initiation and propagation. Some authors have tried to explain the cracking processes using linear elastic fracture mechanics (LEFM), including Morris et al. (1992), Morris et al. (1994), Hallett et al. (1995) and Konrad & Ayad (1997). Hallett & Newson (2005) incorporated the crack-tip opening angle into their LEFM framework, and Prat et al. (2008) took into account the results of fracture toughness and tensile tests in their LEFM model. Abu-Hejleh & Znidarčić (1995) described the cracking process in terms of the consolidation and shrinkage of the desiccating material. Rodríguez et al. (2007) presented a general approach, introducing coupled hydro-mechanical behavior of the soil in unsaturated conditions to simulate the cracking in their laboratory experiments on mine tailings. Shin & Santamarina (2011) utilized an effective stress approach and explained the crack initiation process using the evolution of the air-water interface membrane as the

soil dries.
It is generally assumed that soil cracks produced by evaporation start at the surface and propagate downwards. Nonetheless, these assumptions are not corroborated by all the experimental results. Already Corte & Higashi (1960) postulated that propagation occurs towards the surface or the bottom from the center of the layer. Alternatively and based on field observations, Weinberger (2001) assumed that the most common propagation direction is upwards, starting from the bottom of the layer. Lakshmikantha et al. (2013) noticed during their experiments that cracks started at the bottom of the specimens, propagating vertically upwards and then horizontally.
Both the inception and propagation of desiccation cracks are the result of a combination of material properties, and boundary and internal constraints. These factors are interrelated and it is challenging to clearly distinguish between the respective influences. In this chapter a series of tests were carried out to try to separately evaluate the role of material properties and that of boundary conditions on the initiation and development of cracks in drying clay. This included varying the initial layer thickness, the initial water content, the surface area of the set-up and the container material type. Emphasis is given to the conditions of fracture initiation and propagation, particularly looking at what occurs vertically across the soil layer.

2.2. Materials and Methods

The investigation was carried out using a commercially available river clay (Ve-Ka, K-10000) from blocks having an original water content of 34 ± 2%. An analysis done using a combination of X-ray diffraction and X-ray fluorescence showed that the clay was composed (by mass) of 50.2% quartz, 21% vermiculite, 16.2% muscovite, 6.8% anorthite and 5.8% calcite approximately. The physical properties of the clay are shown on Table 2.1.

Table 2.1: Physical properties of the clay.

Property		Value
Specific Gravity		2.74
Consistency		
	Liquid Limit	57%
	Plasticity Index	33%
	Shrinkage Limit	12%
Soil Classification		CH
Grain Size Analysis		
	Sand	3.1%
	Silt	54.9%
	Clay	42%

This same material will be used in all the subsequent chapters of the thesis.
All the tests were performed in a climate controlled room with temperature and relative humidity at 19.0 ± 1 ºC and 65 ± 6%, respectively. Open water evaporation

measurements carried out in parallel to the experiments indicated that the average daily evaporation was approximately 2.5 mm/day. The air circulation in the room was provided by the air conditioning system, which blew diffused air at several points in the ceiling. To try to achieve the most homogeneous air flow conditions for the experiments, all containers were placed on the floor of the room, providing a distance of at least 3 m from the air diffusers.

Haliburton (1978) presented guidelines regarding the storage and desiccation of fine grained dredged materials. He indicated that the end of the free water decant phase (called by him "decant point") was around 1.8 times the liquid limit. According to him, after this point the evaporation from the soil is governed by the capillary resupply potential of the soil. This investigation focused on the desiccation of dredged material, therefore the initial water content for the experiments was varied between two and three times the liquid limit (a water content of 114 and 170% respectively). This provided a minimum water decant phase, while also allowing the comparison between different initial conditions.

The experiments were mainly carried out using square wooden containers of diverse sizes, with clay layer thickness that varied between 20, 50 and 100 mm. In order to evaluate the effect of the frictional resistance and adherence to the boundaries, additional tests were carried out using plastic and metal containers. Table 2.2 shows the full list of performed tests.

Table 2.2: Summary of the experiments carried out.

Dimensions (m) W x L	Initial Clay Thickness (mm)	Container Material	Moisture Content (x Liquid Limit)
0.3 x 0.3	20	Wood	3
0.3 x 0.3	50	Wood	2
0.3 x 0.3	50	Wood	3
0.3 x 0.3	100	Wood	2
0.5 x 0.5	20	Wood	3
0.5 x 0.5	50	Wood	3
0.5 x 0.5	100	Wood	2
1 x 1	20	Wood	3
1 x 1	50	Wood	3
1 x 1	100	Wood	2
0.4 x 0.4	40	Metal	2
0.4 x 0.4	40	Metal	3
0.35 x 0.5	50	Plastic	2
0.35 x 0.5	50	Plastic	3

Before preparing the clay for the boxes, samples for water content determination were taken from each of the bags containing the clay. Afterwards, clay directly out of the bag was cut into small blocks (each piece averaging approx. 20 mm^3), which were placed in a steel container. Tap water was added until the desired water content was achieved (tap water was employed in order not to drastically change

the chemistry of the river clay). Subsequently, the steel container was set in a Hobart A200N mixer for 45 minutes at a mixing speed of 200 rpm. The resultant paste was deposited in a plastic container, where it was sealed and left for at least 24 hours to further homogenize. At this point samples of the clay mixture were obtained to test for water content.
The wooden containers were filled with water for at least 48 hours before placing any clay in them. This allowed for the wood to completely saturate before pouring the mud in the boxes to the desired thickness. Even though great care was taken, some air was trapped during the pouring of the mud.
All tests were carried out until the clay was seen to be completely dry, which in practice represented a water content of 6 ± 1%. During the tests the mass change in time was not measured. Due to the large overall mass of most of the experiments, it was not possible to find weigh scales with an accuracy high enough to make proper measurements. Additionally, measuring the overall mass change in time provides only information of the average water content on the entire test, but not on the specific situation at the fracture location. Therefore, during the experiments, clay samples were obtained in close proximity to the cracks from some of the tests for water content determination. The soil was extracted using a small spoon or a small auger and then it was placed in an oven for 24 hours.
Pictures of the samples were taken using a Canon 400D camera at 8 megapixels. The pictures were used to measure the approximate cell area, crack length and crack with at the end of the experiments. To correct for perspective the software Perspective Image Correction (Schroeder, 2017) was employed. Digimizer (MedCalc, 2016) was used for the measurement of areas and lengths.

2.3. Results and Discussion

2.3.1. General Observations

Table 2.3 summarizes the results of the experiments.

Figures 2.1 and 2.2 present picture sequences of the evolution of cracks in the clay under different conditions at approximately the beginning, the midpoint and the end of fracturing. Figure 2.1 compares the evolution of cracks in containers of the same size, but with different initial clay thicknesses. Figure 2.2 shows fracture progression in containers of different size, but with the same initial clay thickness.
It is clear from Figure 2.1 that thicker clay layers displayed less cracks, larger intact areas and wider fractures than the thinner ones. This outcome that can be partly explained the different desiccation speeds (e.g. the thinner the layer, the faster the drying) affecting cracking. Scherer (1990) and Scherer & Smith (1995) pointed out that the drying front tends to be more irregular during fast drying, contributing to the presence of more flaws, which lead to the generation of more fractures.
Figure 2.2 illustrates the impact that the size of the container can have in the fracture generation. The clay in the 0.3 x 0.3 m and 0.5 x 0.5 m containers produced few and relatively short fractures that did not manage to generate any substantial breakage (i.e. cells). At the end of those tests it was noticed that the dry clay

Table 2.3: Summary of the test results including the approximate cell areas, length and width of cracks.

Dim. (m) W x L	Initial Clay Thk. (mm)	Container Material	Initial Water Cont. (%)	Amt. of Cells	Total Cell Area (m^2)	Avg. Cell Area (m^2)	Amt. of Cracks	Avg. Crack Length (mm)	Avg. Crack Width (mm)	Days to First Crack	Total Test Length (Days)
0.3 x 0.3	20	Wood	170	1	0.070	0.070	6	63	2	30	37
0.3 x 0.3	50	Wood	114	2	0.078	0.039	1	299	21	15	59
0.3 x 0.3	50	Wood	170	7	0.060	0.009	8	152	14	29	69
0.3 x 0.3*	100	Wood	114	-	-	-	-	-	-	12	-
0.5 x 0.5	20	Wood	170	1	0.203	0.203	10	122	5	26	37
0.5 x 0.5	50	Wood	170	9	0.181	0.020	11	192	26	37	85
0.5 x 0.5	100	Wood	114	4	0.169	0.042	3	317	36	24	92
1 x 1	20	Wood	170	26	0.841	0.032	62	167	15	40	60
1 x 1	50	Wood	170	22	0.686	0.031	23	255	29	49	102
1 x 1	100	Wood	114	9	0.595	0.066	11	387	39	28	118
0.4 x 0.4	40	Metal	114	1	0.126	0.126	6	144	9	32	49
0.4 x 0.4	40	Metal	170	9	0.119	0.013	11	147	15	42	62
0.35 x 0.5	50	Plastic	114	9	0.118	0.013	10	134	14	33	79
0.35 x 0.5	50	Plastic	170	13	0.114	0.009	13	130	15	35	88

*Sacrificial test.

was detached from the bottom of the container, something that did not happen in the 1 x 1 m one. The detachment from the bottom allowed for the relatively free shrinkage of the clay, reducing the magnitude of the tensile forces developed. Because in the 1 x 1 m container the surface of the clay was larger, there was also a larger constraint, allowing for the tensile forces to build up leading to the eventual fracturing of the clay. The situation exposed in Figures 2.1 and 2.2 highlights some of the relevant factors that need to be taken into consideration during soil cracking experiments when upscaling results from the laboratory to the field and when downscaling field samples to the laboratory. Such factors include the ratio between the area of the setup and the thickness of the soil, the friction provided by the surface of the container, initial water content and the atmospheric conditions.

A variation in cracking was also noted in clay boards with same area and initial thickness, but different initial water content. In the cases with low initial water contents, the final amount of fractures was lower than in the boards with high initial water contents. Figure 2.3 and 2.4 compare the difference in cracking in 0.3 x 0.3 m boards with 50 mm initial thickness at similar stages of drying (i.e. water content).

Additionally there were differences seen in the quantity of cracks that originated in containers of different materials. Most of the fractures in the plastic containers were caused by boundary effects related to the walls. Discarding those fractures, the containers with starting water content of 114% and 170% had a total of one cell with three cracks and two cells with five cracks, respectively. The amount of fractures and cells were lower than in comparable tests using wooden containers, because the plastic provided less friction than the wood. It is known that the base material influences the generation of fractures (Corte & Higashi, 1960; Groisman & Kaplan, 1994; Weinberger, 1999; Peron et al., 2009), given that the tensile forces responsible for cracking originate in part from the resistance of the bottom friction to the shrinkage of the material. The metal container with clay at an initial water content of 114% exhibited fewer cracks with shorter length than similar tests on wood containers. The fractures were not long enough to produce the breakage of the clay into cells. Nevertheless, the other metal container with clay at an initial water content of 170% produced more cracks that were wider, which broke the clay into nine cells. The amount and size of cells were comparable to the 0.5 x 0.5 test on the wooden container with an initial thickness of 50 mm.

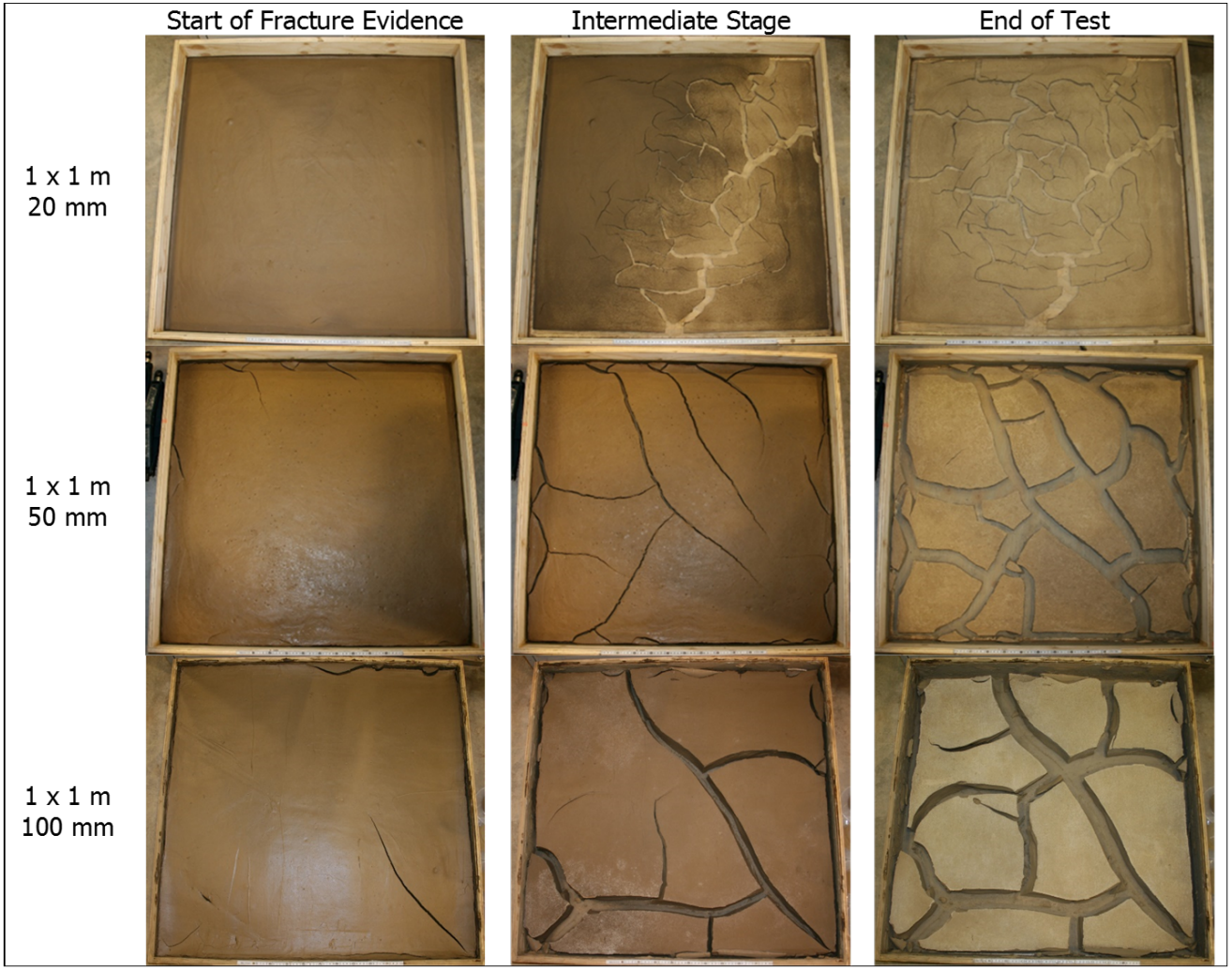

Figure 2.1: Comparison of the evolution of cracks in containers of the same size, but with different initial clay thicknesses. The general description of each test is located on the left column.

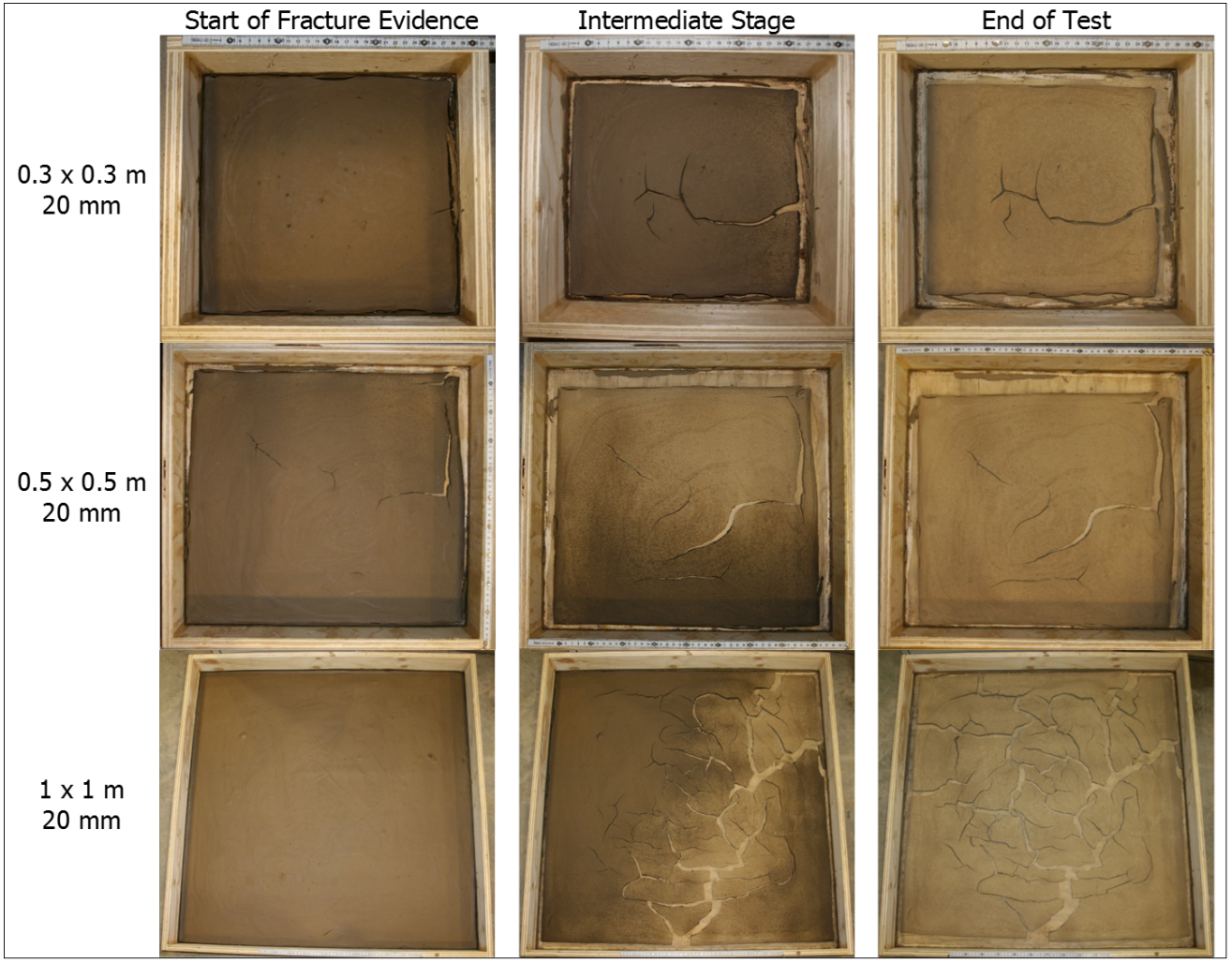

Figure 2.2: Comparison of the evolution of cracks in containers with the same initial clay thickness, but of different size. The general description of each test is located on the left column.

Figure 2.3: Cracking in 0.3 x 0.3 m board with 50 mm initial thickness and an initial water content of three times liquid limit approx. (170%).

Figure 2.4: Cracking in 0.3 x 0.3 m board with 50 mm initial thickness and an initial water content of twice the liquid limit approx. (114%).

Concerning the overall deformations noted through the desiccation of the slurries, at least five distinct deformation stages were observed:

- Stage one: the deformations of the soil were limited to the vertical direction, due mostly to the consolidation of the material;
- Stage two: horizontal deformations, attributable to the shrinkage of the material, complemented the ones observed in phase one. The horizontal deformations were noticeable only after the soil started partially detaching from the walls for the containers;
- Stage three: release of the tensile forces through fracture initiation and propagation;
- Stage four: continued shrinkage (related to the residual shrinkage defined by Bronswijk (1988));
- Stage five: drying without visible shrinkage.

The stages correlate to the phases depicted in the shrinkage curve by Haines (1923) and Bronswijk (1988), and they are similar to the ones described by Abu-Hejleh & Znidarčić (1995). Peron et al. (2009) also defined the deformations during the drying process, but they grouped all in just two steps. In practice, the greatest amount of deformation ensues during the first three stages. The partition between the different stages is difficult to define, since they tend to overlap and more than one of the stages can be taken place at the same time in different sections of the sample.

2.3.2. Fracture Development and Intersections

In few instances, it was detected that fractures started at locations where a small air bubble trapped in the mud, or an uneven surface was present. The effects on crack initiation of surface defects causing stress concentrations, such as the presence of coarse material, debris, or uneven surfaces, were also observed by Groisman & Kaplan (1994), Zabat et al. (1997), Weinberger (1999) and Tang et al. (2011). The influence of the surface defects was mainly noticeable in the plastic and metal containers. In these two cases, most of the fractures started close to the centre of the board, or parallel to the walls of the container as a result of the tensile forces produced by the settlement of the soil.

As a general feature in most of the tests, the first fracture started appearing in the clay itself at the interface between the wall of the container and the clay (e.g. Figures 2.1 and 2.2). The separation of the clay from the container wall was not considered a fracture, as it was a boundary effect. The soil close to the walls generally showed less settlement due to the adherence and frictional resistance of the mud to the wall of the container.

The different constraints in the two orthogonal horizontal directions resulted in the cracks generally starting to propagate at angles around 30° from the walls of the container, and in few cases at angles of 45°. The fractures that opened near the corners of the boxes displayed angles of approximately 45°. All the angles other than 90° with respect to the theoretical principal stress direction (i.e. parallel to the edge of the clay) denoted the influence of shear forces at least during the initial stages

of the cracking process. The shear forces arose from non-symmetrical boundary conditions imposed by the container, e.g. only partial detachment from the wall, differences in drying, settlement and adhesion to the bottom, etc. Nonetheless, the fractures that propagated through the clay and eventually reached the edge of the board, did so at an angle of 90° with respect to the border of the clay. The reason for this orientation and tensile crack regime was the lack of constraints provided by the wall of the container, since by that stage the clay was fully detached from it.
The initial cracks generally propagated inwards through the clay. This fractures were the ones that tended to be the widest. After the initial fractures were mostly developed, a second set of cracks appeared, especially in the large boards (1 x 1 m in area). This typically occurred in the boards with an initial thickness of 50 and 100 mm (Figure 2.1). In the boards the board with an initial thickness of 20 mm, the first and second set of fractures usually developed in parallel (Figures 2.2). When the cracks formed cells in the 50 and 100 mm thick boards, they were mostly of regular shapes with four to five sides. In the 20 mm thick experiments that managed to form cells, they were very irregular in shape and with many sides (Figures 2.1 and 2.2).
The tests with initial thicknesses of 50 and 100 mm showed patterns with fractures repeatedly intersecting each other at 90° (Figure 2.1). Conversely, the boards with 20 mm initial thickness exhibited fracture intersections at both 90° and 120° approximately (Figure 2.2). The observations showed that the fracture mode was also affected by the thickness of the soil layer. Analogous observations were made by Groisman & Kaplan (1994) during their model desiccation experiments with coffee-water mixtures. Fractures intersecting at 90° and 120° point out to the major influence of tensile and shear forces respectively. Angles of 120° were not observed in the 50 and 100 mm thick layers because the shear forces were relatively small in comparison with the tensile forces produced. Vogel et al. (2005) and Peron et al. (2009) also saw mostly fractures intersecting at 90° and 120°. They both came to similar conclusions relating the 120° junctions to the branching of a crack and the 90° junctions to the coalescence of two fractures, both cases corresponding to the most efficient way of energy dissipation for their particular situation.

2.3.3. Fracture Initiation and Water Content

The thickness of the material is known to have an effect on the cracking water content. To assess the average water content of the clay at which the cracks started appearing, soil samples of the entire layer thickness were taken from the crack tips, as soon as fracturing was visible. Soil was taken of tests with an initial thicknesses of 20 and 50 mm, with a starting water content of approximately three times liquid limit (170%) and placed in wooden containers. The measurements indicated that in the 20 mm thick layer the first crack became visible after 26 days at an average water content of 48.4%, compared to 61% for the 50 mm layer after 37 days. A second set of samples was obtained from layers having initial thicknesses of 50 and 100 mm, and a starting water content of approximately twice the liquid limit (114%). The average water content at which the first cracks became visible was approximately 65.6% at 15 days and 83.4% at 12 days, respectively. Nahlawi

& Kodikara (2006) indicated that the reduction of cracking water content with the decrease of layer thickness was affected by the increase in desiccation speed. From the measurements it is also evident that the average cracking water content can be above or below the value at the liquid limit, suggesting that this reference does not provide relevant information on the fracture onset.

To evaluate the development of the water content profile in time in relation to fracture initiation and propagation, samples were taken from a 0.3 x 0.3 m clay board with a starting water content of approximately twice the liquid limit (114%) and an initial thickness of 100 mm. The samples were obtained by removing soil at three different moments in 10 mm intervals for the entire thickness of the layer, beginning when the fracture was first observed and finishing when it crossed the entire board. The material was extracted in close proximity to the location of the fracture tip at the time, and all measurements were made at enough distance from each other, so as to minimize the chances of influence between them. The results are outlined in Table 2.4. The first crack appeared 12 days after the test was started, and two additional sample sets were obtained at 20 and 30 days.

Table 2.4: Water content in percentage (%) with depth, measured at 12 (fracture initiation), 20 and 30 days after the start of the test. The 0.3 x 0.3 m clay board contained soil at an initial water content of approximately twice the liquid limit (114%) and a starting thickness of 100 mm (sacrificial board described in Table 2.3).

Height from Layer Bottom (mm)	Water Content (%)		
70-80	76.1	61.4	
60-70	81.9	66.6	52.8
50-60	83.5	68.5	55.7
40-50	84	69.9	59
30-40	85.7	71.3	59.6
20-30	84.3	72.5	58.7
10-20	86.4	70.7	60
0-10	84.9	67.6*	59
Average	83.4	68.6	57.8

*sample not from a full 10 mm interval

The effect of the evaporation front was reflected in a lower water content in the upper 10 mm. Below this level the water content remained relatively constant. The maximum water content was located in the bottom quarter to the bottom third of the layer approximately. Due to the small differences in the water content values, average water content could be used to reasonably represent the state of the entire layer.

2.3.4. Observations on Fracture Propagation

During the drying process, linear depressions were observed also on the surface of the clay. As the soil continued drying, these depressions developed into cracks and continued appearing ahead of the opening fracture (Figure 2.5). It

was then evident that the depressions were the surface expression of a fracture advancing horizontally and under the surface, before emerging at the surface.

Figure 2.5: Surface depression on the clay surface ahead of a crack.

The depressions noticed ahead of the cracks were not isolated occurrences during this investigation. They appeared in all the boxes, regardless of their dimensions, bottom material, initial soil thickness and water content. As it is exemplified in Figure 2.6, they took place in almost every single crack propagating through the soil. However, they were less visible in the 20 mm thick experiments and in the metal container test with an initial water content of twice the liquid limit. During the last stage of drying, the surface depressions stopped appearing ahead of the fractures, probably due to an increase of stiffness in the upper section of the clay.

Drainage through the bottom of the trays was also not a cause for them, since there was no drainage possible from the plastic and metal containers. Moreover, tests were done with the wooden containers submerged in water, in order to evaluate the permeability of the wood. No perceptible water flow through the wood was seen.

These depressions can also be noticed in the work of Müller & Dahm (2000), Tang et al. (2010b) (Figure 2.7) and Lakshmikantha et al. (2013). However only Müller & Dahm (2000) and Lakshmikantha et al. (2013) described them, with Müller & Dahm (2000) suggesting that they might be the expression of the fracture propagating under the surface.

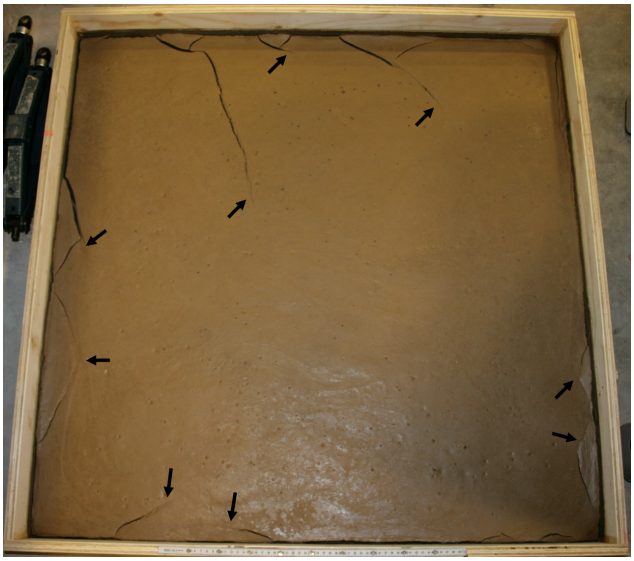

Figure 2.6: Depressions on the clay indicated with black arrows for a 1 m^2 container with a 50 mm (initial thickness) soil layer and an initial water content of 170%.

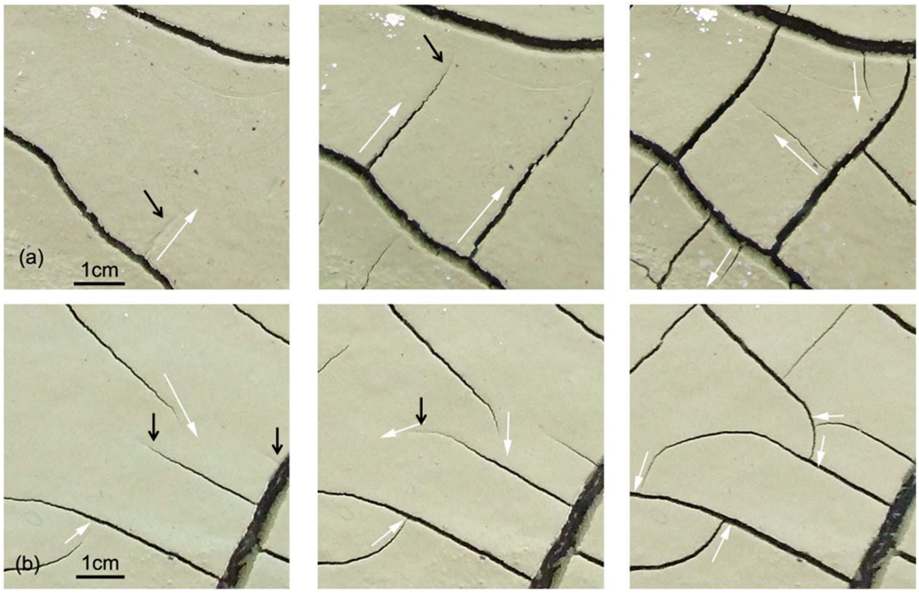

Figure 2.7: Black arrows pointing to the depressions ahead of the fractures in other experiments (modified from Tang et al. (2010b)).

Similar depressions were observed in the field and were not related to any boundary constraints. Figure 2.8 shows this phenomenon occurring in a sediment depot in the Wormer- and Jisperveld area in The Netherlands.

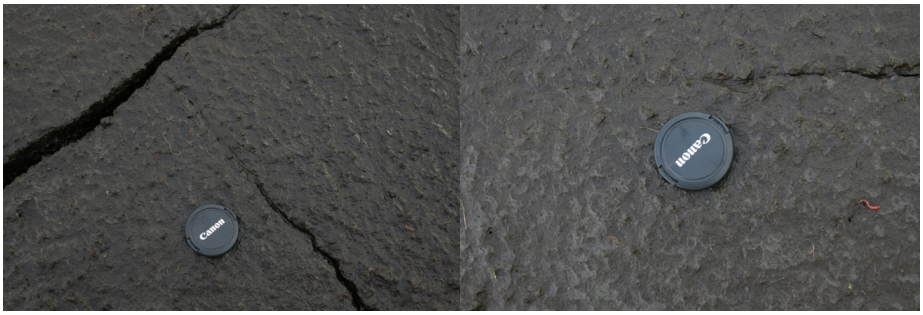

Figure 2.8: Depressions observed in the field.

After the clay fully dried, the walls of the sections or cells formed by the fractures were inspected. Unlike Nahlawi & Kodikara (2002), Kodikara et al. (2004), Peron et al. (2009) and Zielinski et al. (2014), only slight curling of the clay cells in the experiments with 20 mm initial thickness was noticed. In that case, the curling can be attributed to the differential drying between the top and bottom of the sample, as explained by Scherer (1990) and Zielinski et al. (2014). A curvature of the clay surface close to the walls of the containers was detected in most of the tests, but this was a result of boundary effects (differential settlement) and not curling (see also Figure 2.13).
Evidence of plumose structures was observed in the cracks from all the containers, no matter what size, tray material, thickness of soil, or initial water content in the tests (Figures 2.9, 2.10 and 2.11).

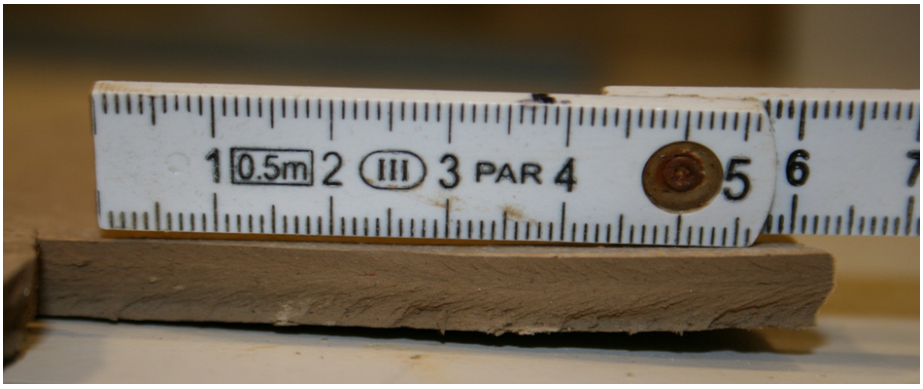

Figure 2.9: Plumose structures in fractures from container with a 20 mm initial clay thickness.

Plumose fractures were first described by Woodworth (1895, 1896), who observed them in closely spaced parallel joints in argillites. Plumose fractures have

Figure 2.10: Plumose structures in fractures from container with a 50 mm initial clay thickness.

Figure 2.11: Plumose structures in fractures from container with a 100 mm initial clay thickness.

also been noted before in lab experiments, such as the ones carried out in soil by Corte & Higashi (1960), cellulose acetate by Kies et al. (1950), by Müller & Dahm (2000) in starch-water mixtures and by Kitsunezaki (2009) in calcium carbonate. Furthermore, they have been seen in clays dried in the field (Weinberger, 1999, 2001; Knight, 2005). These provide information about the direction and mode of failure, with the hackles indicating the overall and local propagation directions of the fracture. The morphology of the plumose structure also shows how the crack front line progressed as the fracture advanced (Figure 2.12).

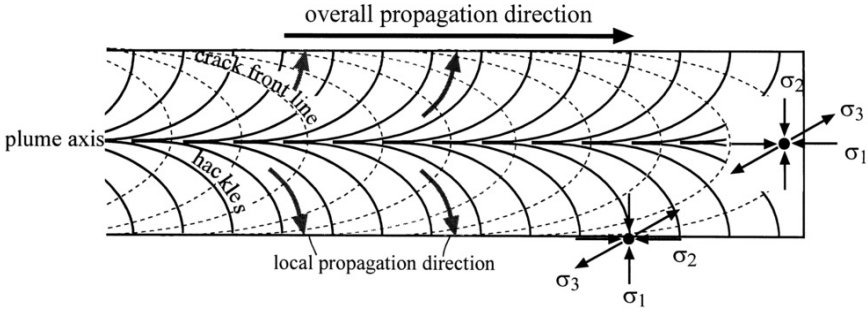

Figure 2.12: Schematic illustration of a symmetric plumose fracture (Weinberger, 1999).

The experiments with initial thickness of 20 mm displayed quasi-symmetric plumose structures. However, in the tests where thicker layers were used (50 and 100 mm initial thickness), the structures started becoming asymmetric.
In the case of the tests completed, the location of the plume axis and the crack front line, in addition to the surface depressions observed in front of the cracks, gave a strong indication that the overall propagation of the fractures happened under the surface. This differs from the common understanding of crack propagation, which is as starting from the surface of the drying soil and advancing vertically downwards. Nonetheless, the local propagation direction might still evolve from sub-horizontal to vertical, as the hackles begin to migrate upwards and downward with fracture propagation.
Corte & Higashi (1960) referred to the plumose fracture description made by Kies et al. (1950). They hypothesized that the cracks started at the centre of the soil layer and propagated either to the surface or to the bottom. This is certainly the case at a local scale, but the overall propagation direction and the crack front line do not necessarily follow the same path. Müller & Dahm (2000) recognized that the majority of the fractures in their starch experiments started at the surface, but there were instances where they began at the bottom or at some mid-layer location. Based on his field observations, Weinberger (2001) assumed that most cracks start at or close to the bottom of the layer, propagate upwards and then horizontally. Something similar was noticed by Lakshmikantha et al. (2013) during their experiments. Peron et al. (2009) could not determine, if fractures started at the top or the bottom of the layer in their clay slab tests. However, Kitsunezaki (2009), Shin & Santamarina (2011) and (Tang et al., 2010b, 2011) described how cracks always

start at the surface of the layer.
What was observed during the experiments in this study is that the fractures might start anywhere along the depth of the layer (Figure 2.13). The exact location of initiation would be very difficult to establish, since it would require detailed knowledge of all the forces at every single point in the clay. Yet the general area where the fracture might originate can be deduced, and it is consistent with locations of local stress concentration (e.g. the edge of the clay board, or a surface disturbance). And unlike it was proposed by Corte & Higashi (1960), it was evident (in the case of these experiments) that the crack front line advanced under the surface.

Figure 2.13: Example of a fracture starting at the bottom left corner of the layer and advancing under the surface towards the right.

Based on the observations related to the surface depressions, plumose fractures and water content with depth, it can be established that the fracture propagation in the tests did not occur in the areas of the layer with the lower water contents. The depth of propagation approximately followed the zone at which the water content was represented by its average value. As it was noted, layers under different starting conditions displayed different cracking water contents. Therefore, water content is not the unique dominant factor in fracture propagation, with the rate of water content change also governing soil behavior.

3

Experimental Evaluation of the Effects of Pull Rate on the Tensile Behavior of a Clay

When a man does not know what harbour he is making for,
no wind is the right wind.

Lucius Annaeus Seneca

This chapter is based on a paper accepted in Applied Clay Science Tollenaar et al. (2017a).

3.1. Introduction

Several laboratory studies have been carried out to examine the tensile strength of soils. Most of this research has been performed in clays, or in clay, silt and sand mixtures. The methods employed in the investigations can be divided into two kinds: indirect and direct tests. Indirect methods generate tension indirectly by applying other forces. The results are evaluated and interpreted relying on assumptions of the stress distributions to obtain the resultant tensile forces. The most common indirect tests used are the Brazilian test (Blazejczak et al., 1995; Hallett et al., 1995; De Souza Villar et al., 2009; Beckett et al., 2015), the three point bend test (Haberfield & Johnston, 1989; Hallett & Newson, 2001; Wang et al., 2007; Yoshida & Hallett, 2008), the four point bend test (Hallett & Newson, 2005; Wang et al., 2007), the modified double punch test (Fang & Chen, 1972; Kim et al., 2007) and the split tensile test (Fang & Chen, 1972). Other indirect tests include flexural tests (Farrell et al., 1967; Briones & Uehara, 1977), the unconfined penetration test developed by modifying the double punch test (Fang & Fernandez, 1981), the pneumatic method (Snyder & Miller, 1985) and the modified unconfined penetration test (Kim et al., 2007, 2012). Direct methods subject the soil in fact to tensile forces, making it possible to measure them immediately. Among the direct methods are the "dog bone" shaped horizontal pulling tests and similar devices (Tschebotarioff et al., 1953; Hasegawa & Ikeuti, 1966; Leavell & Peters, 1987; Mikulitsch & Gudehus, 1995; Nahlawi et al., 2004; Tamrakar et al., 2005, 2007; Rodríguez, 2006; Rodríguez et al., 2007; Prat et al., 2008; Lakshmikantha et al., 2012; Trabelsi et al., 2012; Murray et al., 2014; Stirling et al., 2015), the hanging "dog bone" tests (Ajaz & Parry, 1974; Towner, 1987), cylindrical acrylic cell tests (Nearing et al., 1988, 1991), pulling tests on hourglass shaped samples (Ibarra et al., 2005), tensile tests in the centrifuge (Vomocil et al., 1961), uniaxially loaded soil cores (Farrell et al., 1967) and hanging cylinders (Heibrock et al., 2005). Tests on the resistance to fracture performed by measuring the fracture toughness were also done by Chandler (1984); Lee et al. (1988); Harison et al. (1994) and Prat et al. (2008).

Notwithstanding the many studies focusing on the tensile strength, a relatively small number of investigations have been carried out using different pull rates to estimate the rate dependency of the tensile strength of soil. Table 3.1 provides a brief summary of these studies. Fang & Chen (1972) reported that the tensile strength was not sensitive to loading rates. The observation was later confirmed by Kim et al. (2007), who detected no definite trends in tensile strength variation for different loading rates. Heibrock et al. (2005) also mentioned that pull velocities did not result in any change in the measured tensile strength in their experimental tests. Tamrakar et al. (2005) employed various constant pull rates, but they made no remark regarding their influence on the tensile strength. Nevertheless, Tamrakar et al. (2007) did address the subject by examining the tensile strengths attained with different pull rates. They noticed in their experiments that there was a variation in the tensile strength. The lowest strength values were achieved for rates between 0.1 and 0.34 mm/min, with increasing strengths for rates above and below that pull rate range. After an examination of their results, the trends and magnitude of the changes described by Tamrakar et al. (2007) do not seem to support their conclusion

to a large extent. On the contrary, they seemed to confirm the conclusions by Fang & Chen (1972); Heibrock et al. (2005) and Kim et al. (2007).

Table 3.1: Summary of studies using different pull rates to determine the tensile strength.

Authors	Pull Rate	Soil Type
Fang & Chen (1972)	between 0.03 and 2 in/min (0.762 and 50.8 mm/min)	Silty clay
Heibrock et al. (2005)	below 0.06 mm/min	Clay
Tamrakar et al. (2005)	0.174, 0.342 and 0.882 mm/min	Clay/sand, silt/sand mixtures
Kim et al. (2007)	between 0.1 and 1 %/min (between 0.113 and 1.13 mm/min)	Sand/bentonite mixtures
Tamrakar et al. (2007)	between 0.09 and 1.75 mm/min	Clay/silt, clay/sand, silt/sand mixtures

Most of the previous investigations on tensile strength were performed on clayey soils at water contents below the liquid limit. However, as it was shown on Chapter 2, fractures can start above the liquid limit, making it crucial to reconsider the behavior of the soil in tension at high water contents.
In this chapter, the tensile strength of a clay was investigated in the laboratory by means of strain controlled direct pull tests. The intent was to further examine the relationship between strain rate and tensile strength at water contents below and above the liquid limit. The combined effect of initial water content and pull rate was evaluated to support the understanding of cracking soils under different evaporative regimes.

3.2. Methodology

The clay was cut into small blocks (each piece averaging approx. 20 mm^3), which were deposited in a steel container. Tap water was added until the necessary amount to achieve the desired water content was reached. Tap water was employed in order not to drastically change the chemistry of the river clay. Subsequently, the steel container was placed in a Hobart A200N mixer for 45 minutes, at a mixing speed of 200 rpm. The resultant slurry was put in a plastic container, where it was sealed and left for at least 24 hours to further homogenize. The samples were prepared at initial average water contents of 36, 50, 62 and 77±0.5 %. In this study, each of the clay sample sets was tested at five different pull rates: 1, 0.1, 0.0089, 0.0015 and 0.0005 mm/min. The choice of pull speeds was based on the available range for the equipment. However, the pull rates investigated were also in the range of the expected development of tensile stresses during evaporation processes in natural conditions (typically few mm per day).

3.2.1. Set-up

Considering the requirements of this investigation, a horizontal dog-bone type device was selected. Several geometries and configurations were examined, among them the ones used by Nahlawi et al. (2004); Ibarra et al. (2005); Tamrakar et al. (2005, 2007); Rodríguez (2002); Rodríguez et al. (2007) and Lakshmikantha et al. (2012). It was decided that the most suitable geometry was the one employed by Rodríguez (2002); Rodríguez et al. (2007); Lakshmikantha et al. (2012) and Trabelsi et al. (2012), which was derived from the apparatus utilized by Mikulitsch & Gudehus (1995). Their device was easier to adapt for the testing of clays at the water content range of interest in this study. The apparatus was replicated with small modifications, such as the pulling mechanism, and the location of the load cell and LVDT (Figure 3.1 and 3.2).

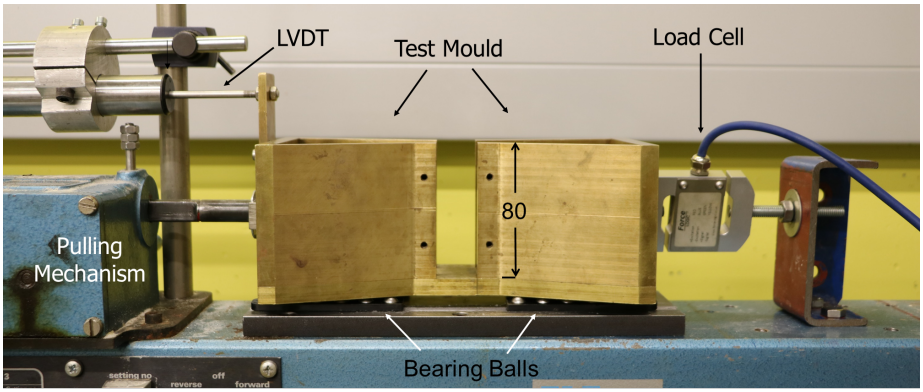

Figure 3.1: Side view of the test setup. Removable plates in the center section are not present. All the indicated dimensions are in mm.

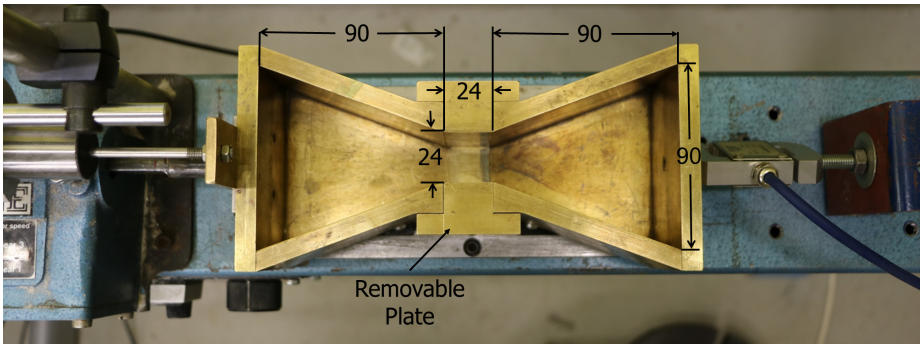

Figure 3.2: Top view of the test setup (dimensions in mm).

The mould consists of two trapezoid shaped ends joined together by a central square section. Both ends are free to slide with respect to each other. The square section has two removable plates acting as side walls. The whole device rested

on bearing balls on top of an ELE-Intertest frame (typically used for direct shear tests), allowing for the utilization of several different pulling speeds. One side of the equipment was connected to the frame through a Force Logic FBB-01 S-beam load cell (100 ± 0.02 N) and the other section was attached to the pulling mechanism. Horizontal displacement was measured using a Schlumberger AC100 LVDT (100 ± 0.02 mm).
In order to assess the horizontal strains produced, pictures were taken from the top of the apparatus during some of the tests. For this purpose a Canon 70D camera mounted on top of the test set up was employed. The pictures were taken at eight megapixels with the area of interest having a resolution of 72 x 72 dpi. The evaluation of the pictures was done using the particle image velocimetry (PIV) software GeoPIV-RG (White et al., 2003; Stanier et al., 2015).

3.2.2. Device Preparation

The rectangular plates holding the two trapezoidal sections together were coated on the inside with Vaseline. This was done to reduce the adhesion of the clay, as well as to minimize the disturbance on the soil when the blocks were removed before starting the pulling test. Before placing the soil in the apparatus, the plates were screwed to both trapezoidal sections. Next, a 40 mm thick layer of clay was spread inside the device using a spatula. The air bubble entrapment was minimized by applying thin layers of clay, while exerting enough pressure with the spatula to drive the air bubbles out. After the clay was placed to the desired thickness, the container was weighed. Vaseline was then sprayed over the surface of the soil to minimize evaporation during the test as much as possible, after which the apparatus was weighed again. Subsequently, the device was mounted on the frame, the LVDT and load cell were connected, and the rectangular plates joining the two trapezoidal sections were removed. Before starting the test, the desired pull speed was set and the recording of the force and displacement were started. All the tests were carried out at a temperature of 21 ± 3°C and a relative humidity of 35 ± 3%. The final water contents were calculated by weighing the device full of soil before and after the test. To confirm the final water content values, samples were taken from each of the trapezoidal ends at the end of each test and placed in the oven. No samples could be extracted from the central section, since the Vaseline could not be effectively separated from the soil.
In spite of the care taken to avoid water loss as much as possible, the samples experienced a small change in water content. Based on the initial and final water contents, an average evaporation rate of 2.0×10^{-2} g/m^{2}s was calculated for the longest tests (where the water content varied the most). Tests on parallel samples showed that without Vaseline, under the same temperature but higher relative humidity, the evaporation rate was on average four times higher. This proves that the Vaseline was effective in limiting the evaporation during the tests.

3.3. Results and Discussion

Table 3.2 summarizes the relevant data and results of the tests. The water contents at which the maximum value of tensile stress was reached were calculated by assuming a linear decrease in the water content with time from the beginning to the end of the test. This assumption was based on the relatively constant external conditions imposed in the laboratory on the saturated samples.

The initial bulk density was estimated based on the initial soil mass employed in the test and the volume of the apparatus, assuming a perfectly flat upper surface. The calculated bulk density varied slightly within the test sets, which was a result of small changes in the water content and the approximation on the constant height of the sample. There were also small differences in the bulk density between the tests sets, but Favaretti (1995), Tamrakar et al. (2005), Rodríguez (2006) and Prat et al. (2008) indicated that the influence of the density on the tensile strength was small when the soil was close or at full saturation.

The tensile stresses were calculated by dividing the measured force by the nominal cross sectional area of the central section. The maximum tensile stress can be assumed to be the tensile strength of the soil for the given conditions.

Table 3.2: Summary of the results for the four sets of tensile tests.

Test Set Name	Test Name	Initial Water Content (%)	Final Water Content (%)	Pull Rate (mm/min)	Approx. Bulk Density (g/m^3)	Max. Force (N)	Max. Tensile Stress (kPa)	Displacement at Max. Tensile Stress (mm)	Approx. Water Content at Max Tensile Stress (%)
35	35A	35.9	35.9	1	1.94	12.13	12.64	1.1	35.9
	35B	35.9	35.7	0.1	1.91	8.15	8.49	0.2	35.9
	35C	35.9	35.3	0.0089	1.93	8.35	8.70	0.3	35.8
	35D	35.9	33.8	0.0015	1.94	8.10	8.43	0.4	35.2
	35E	35.9	33.3	0.0005	1.91	8.40	11.36	0.1	35.2
50	50A	50.2	49.8	1	1.73	1.34	1.40	2.9	50.1
	50B	50.2	49.6	0.1	1.72	1.26	1.31	1.3	50.0
	50C	50.2	48.6	0.0089	1.76	1.30	1.36	0.5	50.0
	50D	50.2	46.8	0.0015	1.73	1.01	1.05	0.3	49.4
	50E	50.2	45.0	0.0005	1.73	1.55	1.61	0.3	48.5
65	65A	62.2	62.0	1	1.64	0.43	0.45	1.5	62.2
	65B	62.2	61.5	0.1	1.63	0.31	0.32	1.4	62.1
	65C	62.2	58.8	0.0089	1.64	0.66	0.68	0.9	61.4
	65D	62.2	55.5	0.0015	1.67	0.58	0.61	0.5	60.7
	65E	62.2	54.9	0.0005	1.65	0.99	1.13	0.3	59.2
80	80A	77.4	76.9	1	1.59	0.22	0.23	5.9	77.3
	80B	77.4	76.4	0.1	1.56	0.15	0.18	3.6	77.1
	80C	77.4	72.8	0.0089	1.58	0.31	0.33	2.1	75.8
	80D	77.4	70.7	0.0015	1.58	0.16	0.18	0.6	74.4
	80E	77.4	66.1	0.0005	1.56	0.19	0.20	0.4	69.7

3.3.1. Analysis of Fracture Development

Figure 3.3 and 3.4 show the force/displacement diagrams for test sets 35 and 50 (values referring approximately to the initial water content), each one including an assessment of the clay under two sample pull rates. They exemplify what was observed in the test sets. There was a clear difference in the behavior of the clay under different pull rates, with slow pull rates causing a stiffer and more brittle response in the soil than the fast ones. This was reflected in maximum force being achieved with a smaller displacement in the test with the lower pull rate, and post peak force decreasing much faster. The observations imply that under tension, the stiffness response of the soil is not only dependent on the water content, but is also directly affected by the pull rate.

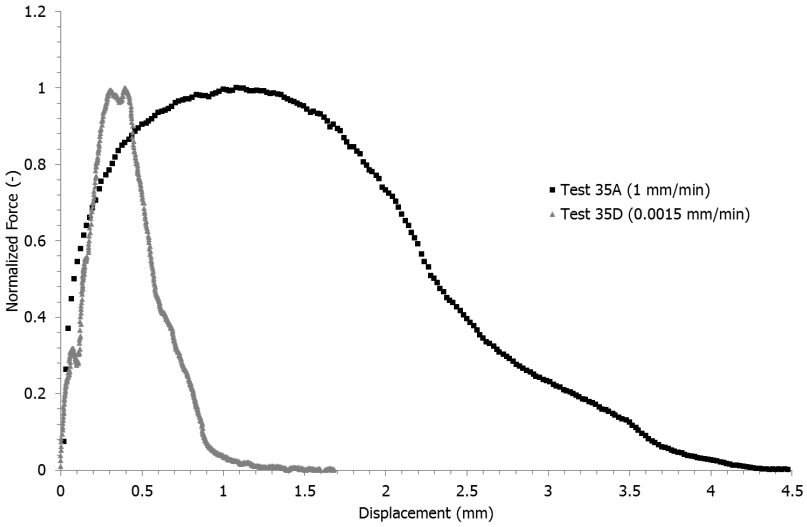

Figure 3.3: Comparison between the normalized forces of Tests 35A and 35D (tests with approx. 35% water content and a 1 and 0.0015 mm/min pull rate, respectively).

The force/displacement diagrams obtained in the tests were very similar to the ones described by Hallett & Newson (2005), who observed comparable force/displacement curves in their studies of tensile behavior of soils using a four-point bend test apparatus. Hallett & Newson (2005) extended to their soil tests the elastic-plastic theory developed by Turner & Kolednik (1994, 1997) to interpret their tests on highly ductile metals. This allowed them to distinguish between different stages in the fracture progression when they analyzed the force/strain diagrams obtained during their tests. They suggested that at the start of loading, the linear relationship between the applied force and the strain indicated the ”elastic range” of the material. After passing the yield point, the material enters its ”plastic range” which they called the crack opening stage. During this phase, the increasing force applied produces sufficient energy buildup to break the inter-particle bonds, leading to the generation of a fracture. Once the fracture opens, there is a marked

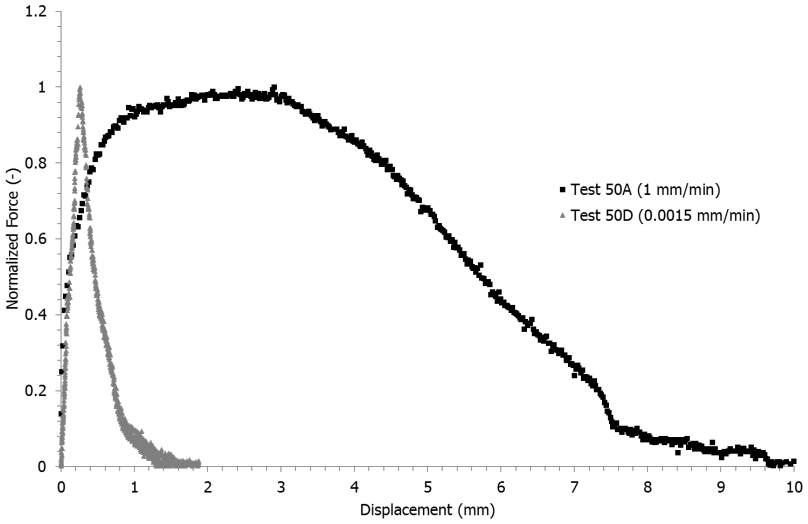

Figure 3.4: Comparison between the normalized forces of Tests 50A and 50D (tests with approx. 50% water content and a 1 and 0.0015 mm/min pull rate, respectively).

drop in the force and crack propagation starts. At this point the force necessary to continue the deformation begins to drop, until the fracture reaches the stable ductile crack growth stage under an almost constant force. All the stages described by Hallett & Newson (2005) were observed during the tests in this analysis and in their corresponding force/displacement diagrams, although the tensile force tended asymptotically to zero in all the tests performed. It can be inferred that the "inter-particle" bonds were mostly provided by the suction while the soft soil remains in a saturated state (Peron et al., 2009; Shin & Santamarina, 2011). The propagation stage would correspond to the progressive desaturation in the vicinity of the crack, once the air entry value is surpassed.

The load/displacement diagrams for tests 50A (1 mm/min) and 50D (0.0015 min/min) were analyzed following the descriptions provided by Hallett & Newson (2005) (Figures 3.5 and 3.6). Besides measuring the loads and displacements during the tests, the samples were also monitored visually to help assessing the fracture initiation and propagation. No physical measurements of the cracks was carried out, because no way could be devised to perform them accurately without disturbing the tests. The figures confirm that the "crack opening" and "crack propagation" stages are much shorter for the slow pull rate than for the fast one. As theorized by Hallett & Newson (2005), during the "crack opening" stage the plastic processes occurring in the soil cause the matric potential to become more negative at the location where the fracture will happen. The potential continues to build up (due to the increasing force being applied) until the fracture starts propagating, producing a drop in the registered force. It is reasonable to assume that during the crack opening stage the combination of reduction in surface and suction increase is still able to provide

resistance to the pulling force, which reaches its maximum at the instant just before the advent of the crack. The theory implies that the tensile strength of the soil will depend on the maximum matric potential which can be generated in the pores before cavitation leads to soil particle separation (i.e. continuous crack growth). From this premise it could be inferred that the tensile strength of the soil is dependent on its intrinsic properties and the water content, but not much on the loading rate. Nevertheless, the stiffness response of the clay is clearly dependent on how the matric potential develops. This result might indicate the possibility of the influence of different drainage constraints on the soil response under the different pull rates.

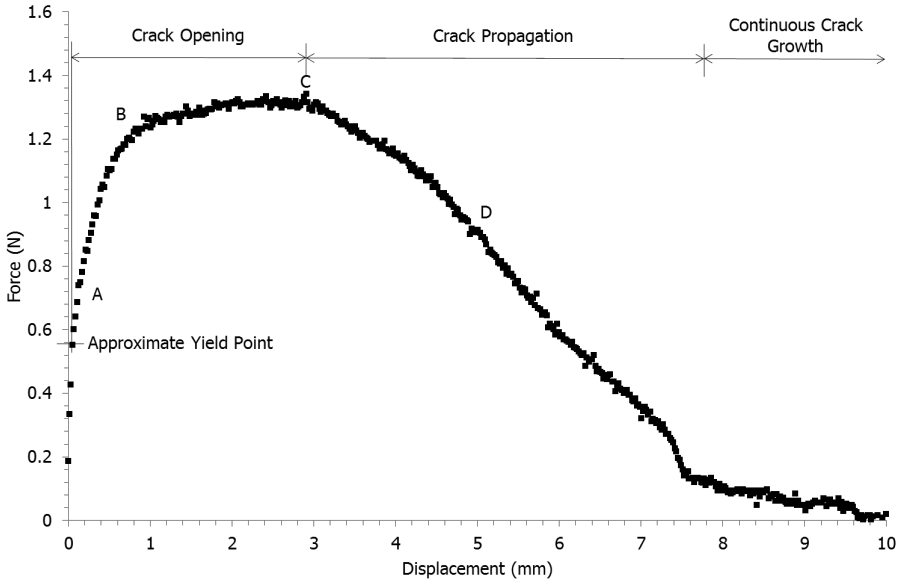

Figure 3.5: Force/displacement diagram for Test 50A (approx. 50% initial water content and a 1 mm/min pull rate) with its fracture development stages.

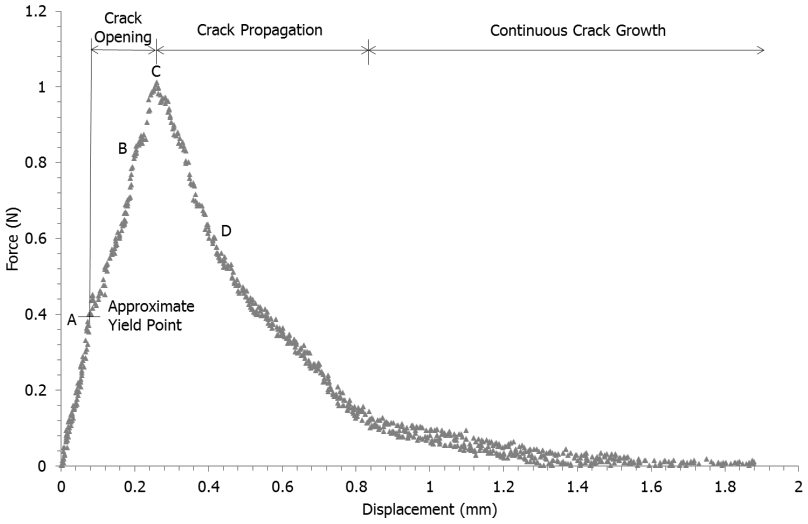

Figure 3.6: Force/displacement diagram for Test 50D (approx. 50% initial water content and a 0.0015 mm/min pull rate) with its fracture development stages.

3.3.2. Tensile Strength and Displacement Rates

The tensile strength reached in the tests exhibited a strong correlation with the water content, but little to no sensitivity to the pull rate (Figure 3.7). The tensile strength diminished with increasing water content following an exponential trend. The same trend was observed by Hasegawa & Ikeuti (1966), Farrell et al. (1967), Towner (1987), Nahlawi et al. (2004), Ibarra et al. (2005), Trabelsi et al. (2012) and Stirling et al. (2015), on natural and compacted soils.

To assist with the data interpretation, four water retention curves starting at different water contents obtained from evaporation tests performed with the HYPROP testing equipment (UMS, 2012, 2015) are presented in Figure 3.8. The tensile strength values from Figure 3.7 were also added for comparison. The values for tensile strength plot in the vicinity of the area where the air entry value for the relevant water content would be expected. This substantiates the correlation between the tensile strength and the moment in which cavitation occurs in the soil, as previously hypothesized.

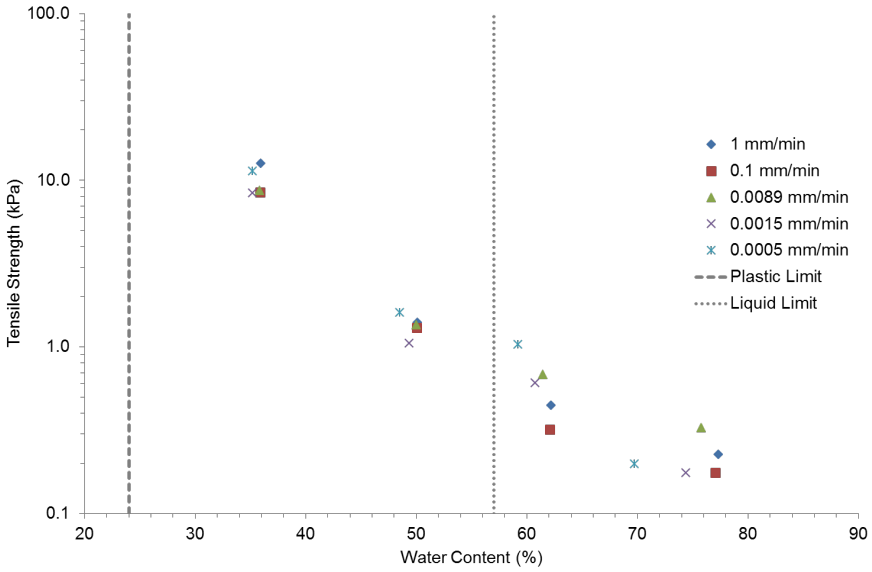

Figure 3.7: Tensile strength reached at different water contents with different pull rates.

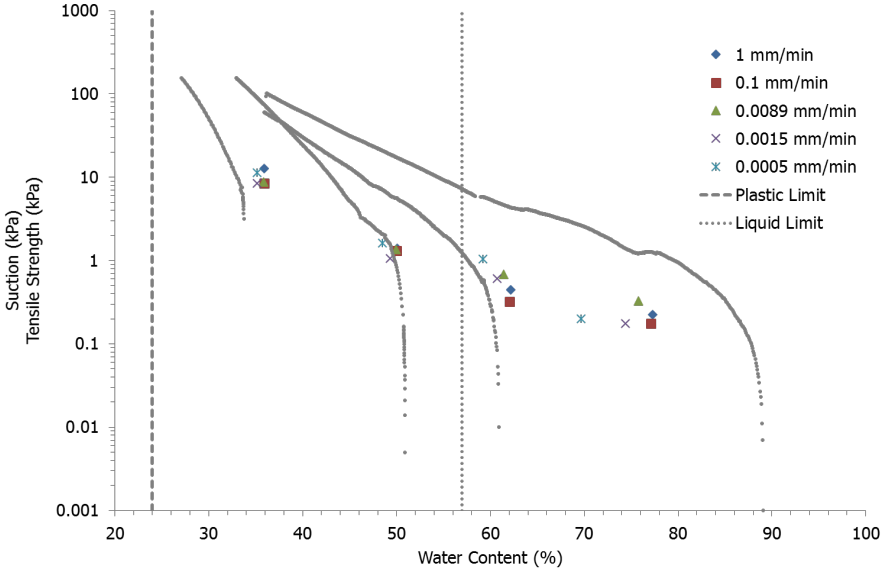

Figure 3.8: Water retention curves for the clay starting at four different initial water contents combined with the tensile strength values reached at different water contents with different pull rates.

Figure 3.9 presents the tensile strength at different pull rates for each clay set. Differences in the values for each particular set are visible, nevertheless no clear trend for any of the sets can be detected. The scatter in the values for each set can be attributed to the inherent variability in the sample preparation and testing, and the fact that the results are displayed ignoring the exact water content at which the tensile strengths occurred. The observations of Figures 3.7 and 3.9 seem to confirm the remarks made by Fang & Chen (1972), Heibrock et al. (2005) and Kim et al. (2007), in regards to the apparent lack of sensitivity of the tensile strength to the pull rate.

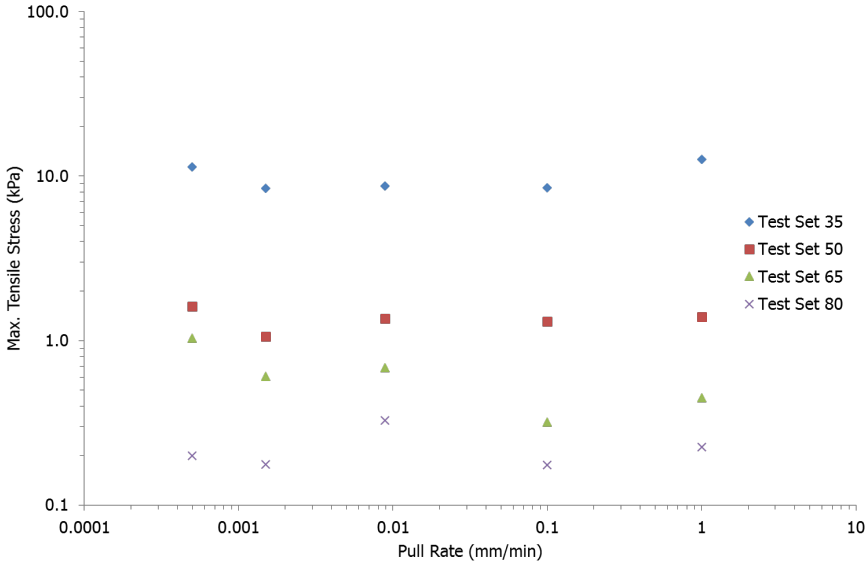

Figure 3.9: Tensile strength as function of pull rate for the different test sets.

The axial displacement at the maximum tensile stress varied exponentially with increasing water content for all pull rates (Figure 3.10). Hasegawa & Ikeuti (1966) also found an exponential relationship between maximum strain and water content in their controlled stress tests. Farrell et al. (1967) described a similar trend, even though they plotted axial strain at failure against different water contents for a single pull rate.
Figure 3.10 shows that the average stiffness of the soil, which is reflected in the value of the axial displacement at maximum tensile stress, depends on the pull rate and the water content, being this last factor the most significant one. However, it also appears that the sensitivity to the pull rate increases together with the pull rate itself.

To obtain information on the material, not depending on the size of the sample nor on the specific experimental device, in Figure 3.11 the data were processed

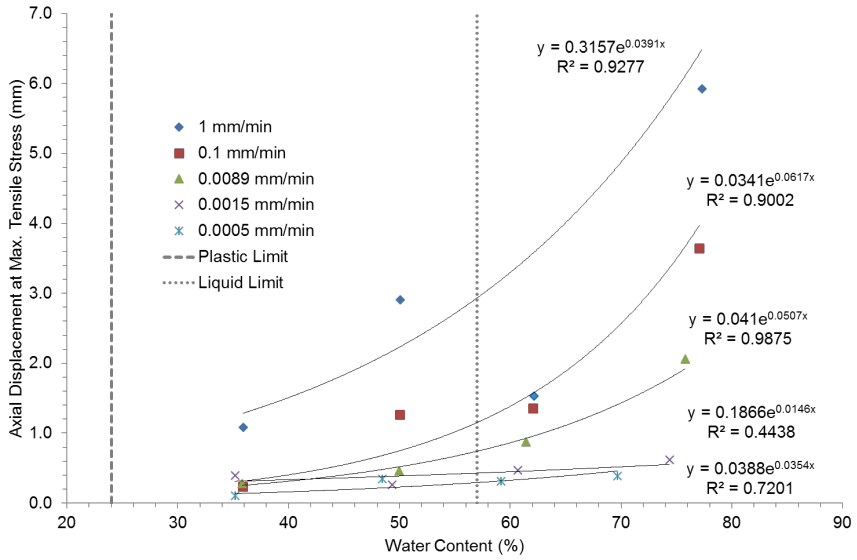

Figure 3.10: Axial displacement at maximum tensile stress with different water contents for varying pull rates with approximate trends fitted to each of the curves.

to obtain an indication of the average stiffness of the samples as a function of water content and axial strain rate. The secant modulus was calculated based on the maximum tensile stress recorded for each test. The strain was determined by assuming an area of influence during the deformations of approximately three times the length of the central section of the device (24 mm to each side of the central section, equivalent to a total of 72 mm). The assumption was based on the results from the GeoPIV analysis presented in the next section. The secant modulus was plotted against the strain rate for each of the test series.
The experimental data in Figure 3.10 can be reasonably approximated by a function of the type:

$$E^{Secant} = E_{Ref}^{Secant}(w^{-C_1})(\dot{\epsilon}_a^{-C_2}) \tag{3.1}$$

where E^{Secant} is the secant modulus, w is the water content (-) and $\dot{\epsilon}_a$ is the axial strain rate (day^{-1}). E_{Ref}^{Secant} is the reference secant modulus and equals 0.4 kPa (for $w = 1$ and $\dot{\epsilon}_a = 1$). C_1 and C_2 have values of 6.8 and 0.32, respectively.

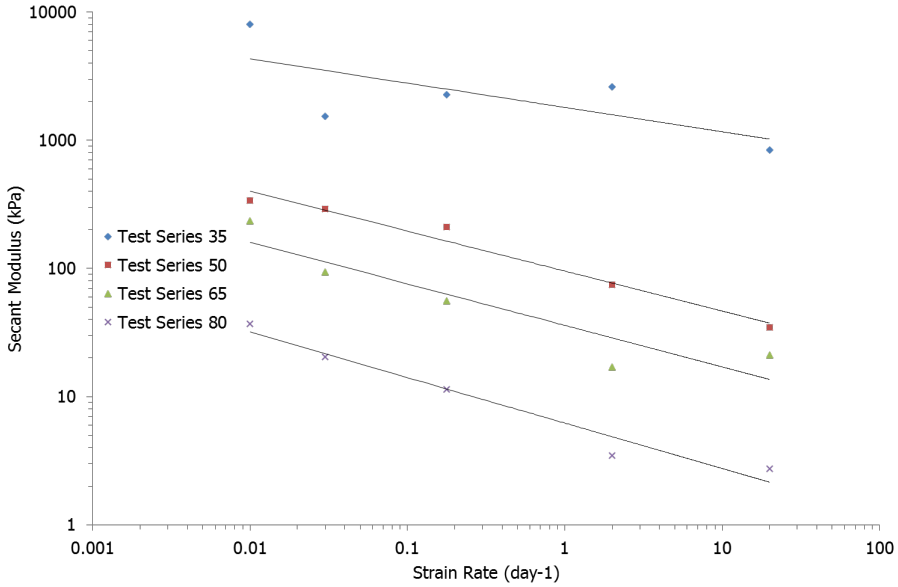

Figure 3.11: Secant modulus at different strain rates for each test series.

3.3.3. Particle Image Velocimetry Analysis

A two dimensional (horizontal plane) assessment of the strains generated during the pull tests was carried out on the pictures taken during the tests. The qualitative evaluation was performed using GeoPIV-RG (White et al., 2003; Stanier et al., 2015). The results of the assessments on test 50A and 50D are presented in Figures 3.12 and 3.13 respectively, and they are related to the force/displacement diagrams of each test (Figures 3.5 and 3.6). The analysis was done to evaluate the strains that took place in the samples, between selected points on the force/displacement diagrams. These points were then related to their corresponding images. The evaluation was divided into volumetric strain (the sum of the x-axis and y-axis strains, hence not the true volumetric strain), x-axis strain (strain parallel to the applied force) and y axis strain (strain perpendicular to the applied force). No photogrammetric target was used when the pictures were taken. Instead several fixed locations on the equipment were employed as reference points. The shortcoming of this method was that the quantitative representativeness of the results is somehow limited. The patch sizes for evaluation were optimized manually, trying to have the minimum amount of wild vectors while keeping the highest precision possible. The standard errors were estimated to be 0.0075 and 0.005 pixel for the analysis of test 50A and 50D, respectively. The strains were plotted in a ± 5% range, with positive values representing compression (shrinking) and the negative values denoting extension (stretching).

In Figure 3.12, Image Set A registered the strains between the start of the test and slightly passed yield point of the soil. The strain along the x-axis was mainly

tensile with concentrations of up to -2%, particularly in the areas were the central section of the equipment joins the trapezoidal pieces. This was consistent with the location where the fracture developed. Along the y-axis the strains were compressive with values of approximately 1%, especially concentrated in the upper corners of the central section. Image Set B refers to a state well into the crack opening domain. As expected, the fracture could not be clearly distinguished yet, but the x-axis strains were higher than -5% around the area where the fracture was going to appear, displaying a well-defined area of stress concentrations. Immediately to the left and right a relaxation zone could be observed. The rest of the central section displayed a higher magnitude of tensile strains, but still below -1%. As in the previous set, the y-axis strains continued to be compressive, concentrating mainly in the upper corners of the central section. However, the area affected by the strains increased in size, with a magnitude of around 1.5%, and the entire central section started exhibiting some small compressive strains (below 1%). Overall, the general deformations in the x- and y-axis were very similar to the previous set. Image Set C corresponded to the maximum force recorded and it was on the border between the crack opening and crack initiation stages. At this point the fracture was already visible, showing tensile strains higher than -5% along the x-axis on the area immediate to it. The area of relaxation directly to the right and to the left of the fracture expanded, but now there was a noticeable zone of compression with a strain magnitude of up to 1%. Along the y-axis, the upper extreme of the fracture continued to undergo compressive strains of a similar magnitude as before. Nevertheless, the tensile strains of at least -5% emerged in the lower end of the crack. Image Set D was well into the crack initiation domain and it showed deformations largely similar to Image Set C, but with a higher magnitude.

Overall during the progression of the test, the central section tended to elongate along the x-axis. The exception was the zone immediately around the fracture, which displayed some compression. The y-axis strains appeared to be mostly compressive. The volumetric strain of the central section of the sample remained relatively small during the entire test. An effect of the corners of the trapezoidal sections could be appreciated, which were reflected in some concentrations of strains around those particular locations, but as a whole the stresses appear evenly distributed across the section of the sample.

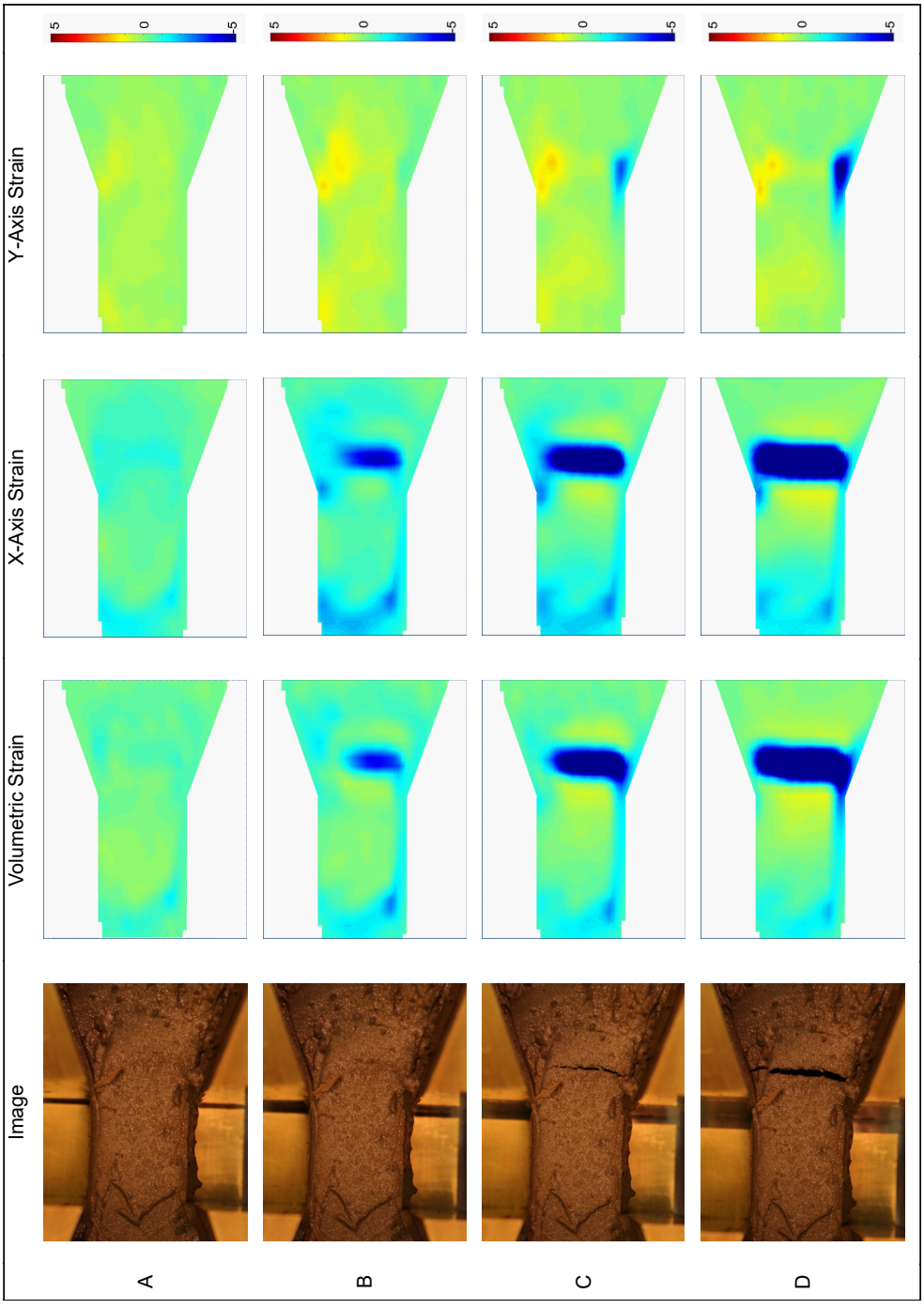

Figure 3.12: Image sets with the GeoPIV-RG strain analysis results for Test 50A. The location of each of the points assessed can be found in Figure 3.5. Strains were plotted in a ± 5% range.

The images in Figure 3.13 refer to the sample subjected to a controlled pull rate of 0.0015 mm/min. Image Set A presents the strains which occurred between the start of the test and the approximate yield point. Tensile strains in the x-axis of up to -2% were detected in the location where the fracture was going to appear. There were not evenly distributed, concentrating mainly in the lower right corner of the central section. Differently from Test 50A, the predominant strains in the x and y-axis indicated compression in the rest of the central section of the device, being particularly evident in the y-axis with strain magnitudes of up to 2.5%. Image Set B was situated directly in the crack opening stage. The picture displayed the emergence of the fracture, which was characterized in the PIV analysis by a zone of tensile strains around its location. The strains were mainly concentrated in the upper and lower ends of the crack, with a magnitude of -2%. The x- and y- axis compressive strains in the central section were even more pronounced than in the previous set, displaying a larger affected area with strains of approximately 2%. As in Test 50A, there was a zone of relaxation of strains in the x-axis to the left and to the right of the location of the fracture. At the point of the maximum force (Image Set C), the crack was already visible, with a clear and defined x-axis tensile strain zone around it. As predicted by the strain concentrations in the previous sets, the crack started in the lower right corner of the central section and it progressed upwards. An area of relaxation next to the fracture was again evident, represented by a zone with almost no strains to the right and left of it. The compressive regime of the central section in both axes continued, predominantly in the y-axis, where it reached strains of 4%. Tensile strains in the y-axis emerged in the vicinity of the upper and lower edges of the right trapezoidal section. During the crack initiation stage (Image Set D) the fracture was very noticeable, as well as its effects on the surrounding strains. However, in this stage the x-axis tensile strains were more homogeneously distributed along the entire fracture and of a greater magnitude (larger than -5%). The areas with no strains to the right and left of the crack were still present. In y-axis were again compressive in the central section and near the fracture. The tensile strains near the upper and lower corners of the right trapezoidal section were still visible, with strains of up to -1%. In general, the overall deformation mode remained similar to the previous stage.

Throughout the entire test it was clear that there were marked compressive strains in the central segment of the device, which can be interpreted as a loss in total volume in that area. The loss can be partly attributed to the soil evaporation during the test. As with the analysis of Test 50A, there was not a homogenous distribution of the stresses across the failure area and the fracture did not develop perfectly perpendicular to the applied load (shear forces were probably generated). Some of the factors contributing to these problems were the boundary effects produced by shape of the device and the preparation of the specimen.

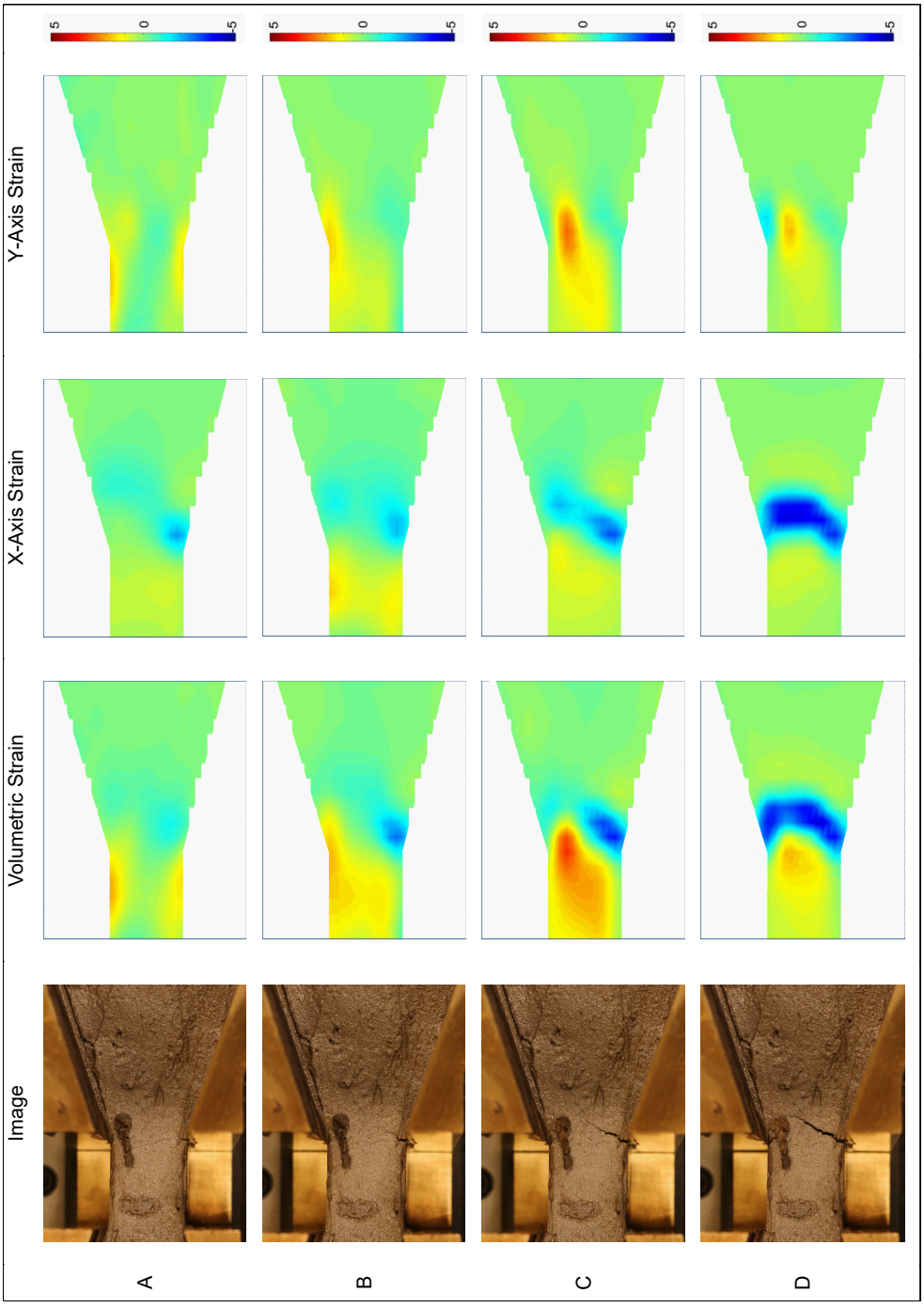

Figure 3.13: Image sets with the GeoPIV-RG strain analysis results for Test 50D. The location of each of the points assessed can be found in Figure 3.6. Strains were plotted in a ± 5% range.

Following the analysis of the soil behavior completed with GeoPIV-RG, the response under different pull rates could be partly justified by different drainage conditions. As the soil was pulled at a high rate, it deformed in response to the tension imposed by elongating in a direction parallel to the force applied. This resulted in a contraction of the soil in the plane perpendicular to the tension applied, compensating for the elongation occurring normal to that plane. Due to nearly undrained conditions, even as the soil underwent distortion, it tended to hold an approximate constant volume. All this allowed the soil to sustain a relatively large deformation before failure, permitting it to respond as a material with a relatively low stiffness. The slow pull rate was low enough to allow for excess pore water pressures to partially or totally dissipate and the total volume of the sample did not remain constant. The change in volume occurred due to the contribution of the evaporation and to the probable rearrangement of the soil particles to accommodate the changes in pore pressure. The outcome of this process was that the soil responded in a stiffer manner to the load applied.

Overall, the experimental data confirmed that the strain rate has a major effect on the global stiffness of the soil does not substantially affect its tensile strength.

4

Small Scale Evaporation Tests on a Clay: Influence of Drying Rate on a Clay Layer

Better by far to embrace the hard truth
than a reassuring fable.

Carl Sagan

This chapter is based on a paper submitted and reviewed in Canadian Geotechnical Journal Tollenaar et al. (2017c).

4.1. Introduction

The impact of evaporation in soils has been extensively studied regarding its effects on shallow foundations (Sattler & Fredlund, 1989; Silvestri et al., 1990; Cui & Zornberg, 2008; Corti et al., 2011; Al Qadad et al., 2012), as well as its influence on soil covers and liners for mining, industrial and municipal waste (Wilson et al., 1994, 1997; Yanful & Choo, 1997; Yang & Yanful, 2002; Yanful et al., 2003; Blight, 2002, 2009; Cui & Zornberg, 2008). In most of these applications desiccation fracturing of the soil is one of the main issues that needs to be addressed during the lifetime of the earth structure. Cracks not only affect the hydraulic and mechanical properties of the soil, but also have a detrimental effect on the integrity of earthworks.

The evaporation rate has been recognized to play an important role in the fracture generation. For instance, high evaporation rates produce more fractures than low ones (Corte & Higashi, 1960; Tang et al., 2008, 2010a; Costa et al., 2013). Moreover, the desiccation rate has been related to the sample thickness, the cracking water content and the type of cracking patterns produced (Corte & Higashi, 1960; Lau, 1987; Kodikara et al., 2000; Nahlawi & Kodikara, 2006; Tang et al., 2008, 2010a; Costa et al., 2013).

Several laboratory investigations have been conducted to study characteristics of evaporation in soil. Wilson et al. (1994) performed controlled evaporation experiments to compare the results with the predictions of their soil-atmosphere model. The tests were carried out using sand columns, which were instrumented with thermocouples and included sampling ports. This allowed them to measure the evaporation rate, the temperature and water content profiles in the soil. Wilson et al. (1997) studied the evaporation behavior of different soil types using thin soil sections on evaporation pans. They concluded that suction and evaporation from soil have a direct relationship, which is independent of the soil properties and time. Garnier et al. (1997) employed soil cylinders instrumented with tensiometers and laser sensors. They proposed a method to simultaneously estimate the shrinkage curve, the water retention curve and the hydraulic conductivity curve. Yanful & Choo (1997) performed laboratory tests under controlled conditions with instrumented columns. They used TDR probes and thermocouples to measure the evaporation rates and behavior of clay, fine sand, coarse sand and top soil. Yang & Yanful (2002) and Yanful et al. (2003) utilized soil columns with TDR, thermocouples and a controlled water supply to study the effects of drainage, using constant and changing water tables respectively. They determined that lowering the water level affects the evaporation from soil by limiting the water supply through drainage and the generation of suction. Song (2014) and Song et al. (2016) made use of an environmental chamber to study evaporation from sand and clay. Their measurements revealed that the soil temperature is strongly affected by the air conditions (temperature), the evaporation rate (less evaporation, more energy available for heating the soil) and the desiccation cracks (increase in evaporative surface).

The objective of this investigation is to examine the effects of the evaporation conditions and the initial water content on the desiccation and suction development in clay. The study was carried out by assessing the drying behavior of a clay from

two different starting conditions (high and low water contents), under fast and slow evaporation. At the same time the influence of the different evaporative regimes on the development of suction in the soil was explored. Some aspects of the rate dependent process were highlighted and tentatively discussed.

4.2. Methodology

For the study of evaporation, it was decided to use the HYPROP apparatus (UMS, 2012). The device was originally designed to determine the hydraulic conductivity and water retention characteristics of soil samples using the evaporation method (UMS, 2012). Instead, in this investigation the data was elaborated by treating the samples as a small physical model, since it permitted the downscaling of the atmospheric drying process, while allowing for the continuous acquisition of measurements of suction and mass loss.

The HYPROP consists of a main sensor unit comprising of two tensiometers of different length. An 80 mm stainless steel ring with a 50 mm height is used for containing the soil sample that is placed on the sensor unit (Figure 4.1). The entire set up sits on top of a weigh scale. The air entry value of the ceramic tips is 880 kPa, but as the water in shaft cavitates earlier, the maximum suction that can be measured is approximately 100 kPa. However, careful saturation can temporarily delay cavitation and extend the measurement range to around 150 kPa.

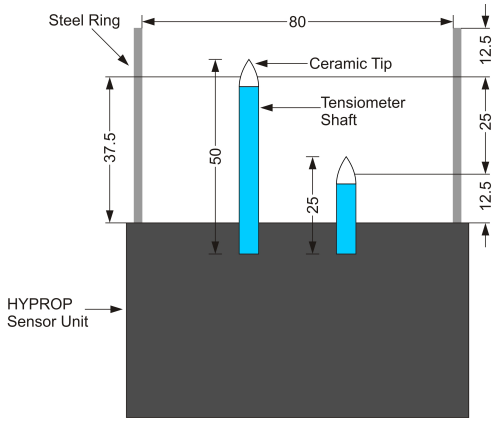

Figure 4.1: Schematic diagram showing the internal dimensions in mm of the HYPROP.

The measurements were performed in a controlled climate room at two different evaporation conditions. The tests were also conducted with the clay at two different initial water contents: one in a plastic state with a water content slightly higher than the plastic limit; and another one in liquid state with a water content of approximately twice the liquid limit. Details about the test settings are outlined in Table 4.1.

The set-up of the HYPROP was carried out following the method described in the manual (UMS, 2015). The inner side of the steel rings from the HYPROP were

Table 4.1: Description of the tests.

Test Name*	Test Type	Initial Water Content (%)	Initial Mass (g)	Room Air Temp. (ºC)	R.H. of Air (%)	Air Recirc. Volume (L/min)
FL	Fast Evap.	118.5	358.4	19.4 ± 0.3	65 ± 6	200
FP	Fast Evap.	37.6	463.1	19.4 ± 0.3	65 ± 6	200
SL	Slow Evap.	116	356.1	10.9 ± 0.4	84 ± 5	nil
SP	Slow Evap.	35.2	471.5	10.9 ± 0.4	84 ± 5	nil

*F: fast evaporation; S: slow evaporation; L: sample prepared in state of liquid consistency; P: sample with consistency in the plastic regime.

coated with a thin layer of silicone oil before being used to minimize the adhesion of the clay during the drying process. There were two deviations from the standard procedure: the saturation of the tips; and the preparation of the soil samples for testing.

The tips were saturated by putting them in a container with de-aired and demineralized water at approximately 50 ºC. The vessel was then subjected a vacuum of approximately -90 kPa in order to make the water with the tips boil. The process was repeated at least three times, or until there were no air bubbles observed in the acrylic tubes containing the ceramic tips. This technique proved to be as good as the procedure recommended by UMS and it managed to saturate the tips faster.

For all the tests with slurry only the short tensiometer was used, because preliminary tests showed that the long tensiometer shaft could be bent and damaged as the clay shrunk. Therefore, the corresponding suction was measured locally at approximately 12.5 mm from the bottom of the sample. For the plastic clay the long tensiometer was utilized in one case where only limited shrinkage was expected.

The samples with plastic consistency were prepared by pushing one of the provided metal rings directly into the clay block. The top and bottom were trimmed, and the holes for the tensiometers were drilled using the small hand auger supplied by UMS. Measurements of water content and bulk density indicated that the material was in a saturated state at the beginning of the tests.

A different method was employed for the preparation of the soils with a liquid consistency. The slurries were made by cutting the clay blocks into small pieces, which were then deposited in a steel container. Tap water was added until the desired water content was achieved. Subsequently, the clay-water mixture was stirred for 45 minutes in a Hobart A200N mixer at 200 rpm. The resultant slurry was put in a plastic container, where it was sealed and left for at least 24 hours to further homogenize. Then the HYPROP sensor unit was prepared with the short tensiometer and the ring was clamped on to it. The slurry was poured in the device all the way to the top of the ring and the measurement was started immediately afterwards.

After each test was finished, the soil sample with the ring were placed in a 105 ºC oven for 24 hours to determine the final water content.

The typical test set up used during the measurements is shown in Figure 4.2. The

experiments were run employing three HYPROPs at the same time: two with soil samples and one with water to measure the potential open water evaporation. During preliminary tests of the set-up, it was noticed that air recirculation above the samples increased the drying rate (phenomenon also observed and described by Blight (2002)). This can partly attributed to the elimination of the layer of stagnant air building up right above the soil surface. To encourage evaporation, air was recirculated in the fast evaporation tests using air pumps. The air recirculation was not employed in the slow evaporation tests. The air pumping system employed during the fast evaporation tests was capable of supplying 200 L/min of air to each HYPROP. The air was delivered directly through hoses with an internal diameter of 4 mm. The ends of the hoses were positioned 100 mm above the samples, ensuring that the air stream was aimed to the center of the sample in a direction normal to the surface of it. It was assumed that the temperature and relative humidity of the pumped air was the same as in the climate room. All the data generated by the HYPROPs and their weigh scales was recorded using tensioVIEW (UMS, 2013), which was installed in an adjacent computer. The temperature and relative humidity were recorded during the entire test by means of a data logger positioned beside the equipment.

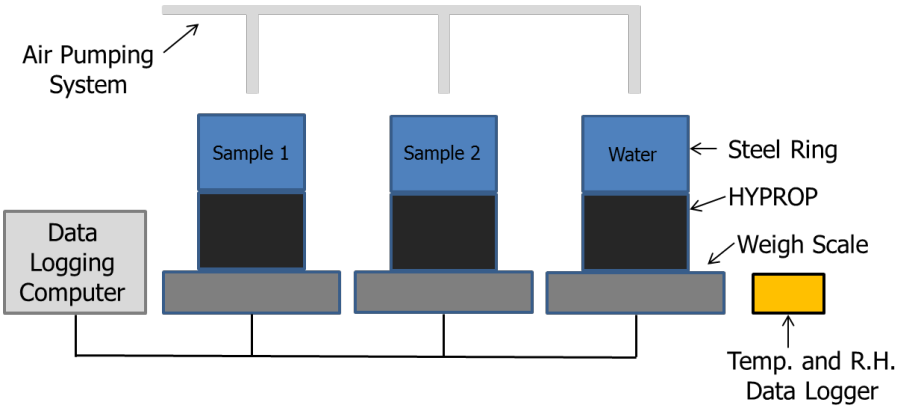

Figure 4.2: Schematic diagram of the typical equipment set up during the measurements (figure not to scale).

All tests were stopped shortly after the air entry point of ceramic in the tensiometer was reached (approx. 880 kPa).

4.3. Results and Discussion

4.3.1. Observations on Evaporation Rate

The total test duration and the final water contents of the samples are shown in Table 4.2.

Table 4.2: Conditions at the end of the tests.

Test Name	Test Length (Days)	Average Water Content at Air Entry Point of Ceramic Tip (%)	Average Water Content at End of Test (%)
FL	5.4	16.7	13.5
FP	2.1	22.2	20
SL	98.9	15.3	7.8
SP	24.8	15.9	15

Figures 4.3 and 4.4 show the cumulative mass loss in time of the clay slurry tests (FL, SL), in both cases compared to the cumulative mass loss of open water. As expected, in both instances water exhibited a relatively constant evaporation rate, reflected in the constant rate of mass loss.

The evaporation rate of the slurry in Test FL was similar to that of water, but at the beginning of the test the rate of mass loss in the clay was slightly higher than that of water (Figure 4.3). The larger mass loss rate of the soil continued only until the second day. From day two until the end of day four, the rate of mass loss of the soil and the water remained approximately constant and approximately equal. At the end of day four the mass loss rate in the clay decreased and became smaller than the one of the water. The correspondent average water content of the sample when 880 kPa of suction were reached was slightly above the shrinkage limit.

Analogous observations are valid for Test SL (Figure 4.4). Nevertheless, in this test the differences in mass loss rate were more accentuated, especially at the beginning, with the soil displaying a higher mass loss rate than the water. The mass loss rate of the clay decreased slightly after approximately day 15, but continued being higher than the one of water until around day 75. After this point it started decreasing significantly until becoming nearly zero on day 90, signaling the absence of any water available for evaporation. The state at which the mass loss almost stopped coincided with an average water content of approximately 8%, corresponding to a value 4% below the shrinkage limit of the soil.

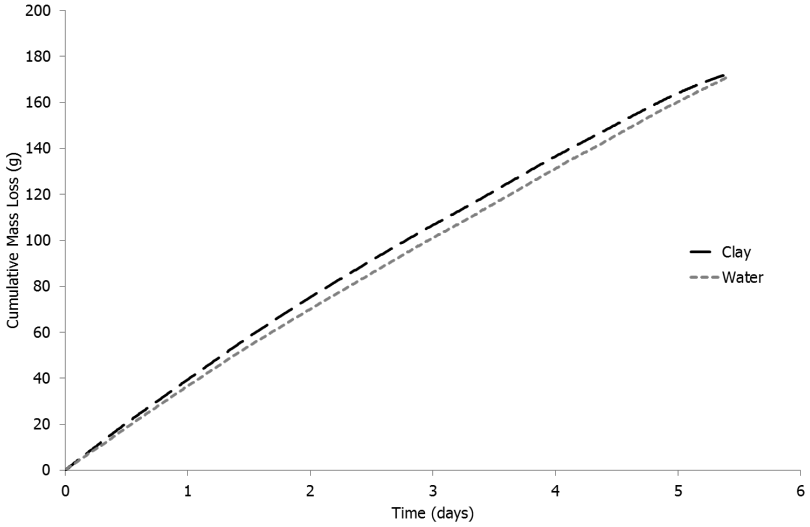

Figure 4.3: Cumulative mass loss in time between the clay sample and open water for Test FL.

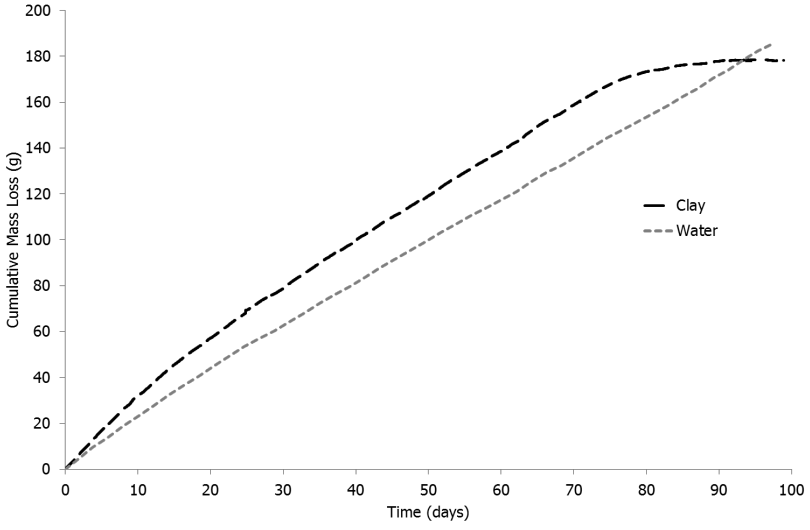

Figure 4.4: Cumulative mass loss in time between the clay sample and open water for Test SL.

Figures 4.5 and 4.6 show the cumulative mass loss in time of the plastic clay tests (FP, SP), in both cases compared to the cumulative mass loss of open water. A similar phenomenon as observed in Tests FL and SL was noted in Tests FP and SP, regarding the rates of mass loss in the clay compared to the ones in water. In Test FP, the clay initially lost mass faster than the water (Figure 4.5). After approximately 0.9 days, the rate became the same and then it started decreasing. The decline in the rate may be related to the reduction in the availability of water, which in Test FP became more accentuated because of the higher evaporation rate.
In the case of Test SP, the difference in evaporation rates was the most noticeable of all in the range of water contents investigated (Figure 4.6). The clay lost mass faster than the water during the entire test, even though the rate displayed a slight decrease with time. However, towards the end of the test, the evaporation rate from the soil started becoming similar to the one in water.

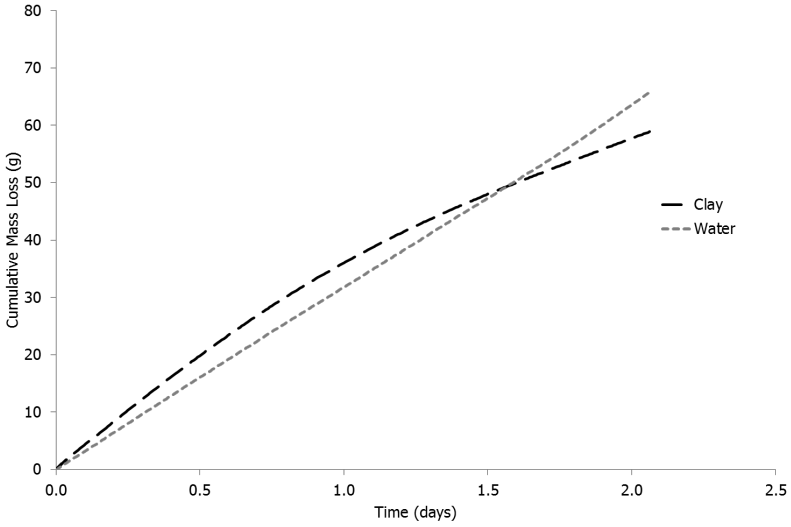

Figure 4.5: Cumulative mass loss in time between the clay sample and open water for Test FP.

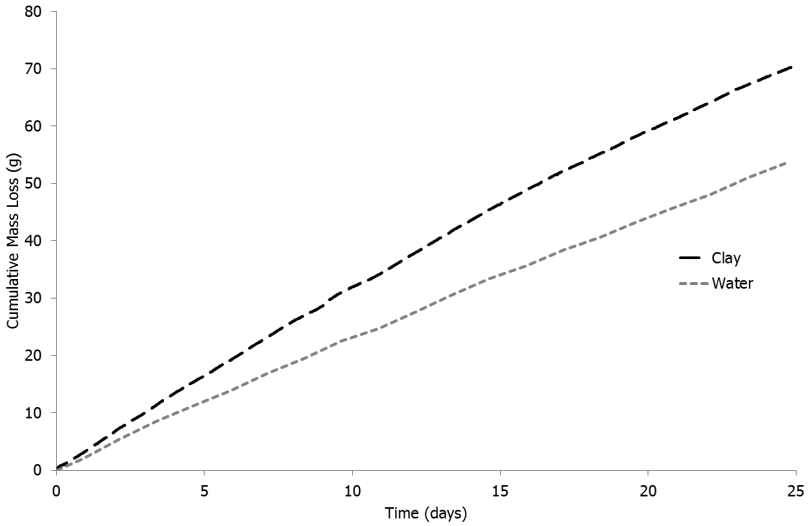

Figure 4.6: Cumulative mass loss in time between the clay sample and open water for Test SP.

4.3.2. Comparison between Potential and Actual Evaporation Rates

At the beginning of all tests, the rate of mass loss of the soil was higher than that of the water. The mass loss then decreased in rate at different velocities, all depending on the initial state of the material and the evaporation conditions. The implications of this observation are that under certain conditions the potential evaporation rate (PE) can be lower than the actual evaporation rate (AE), which contradicts the common assumption that the maximum evaporation is achieved on an open water surface.

Already Penman (1941) hinted that during his isothermal laboratory experiments there was a higher evaporation rate in the soil than in the water. He assumed that this occurred because the temperature of the soil was higher than the temperature of the water, although he made no mention about temperature measurements having been made on the materials during his experiments. Taking this difference in temperature into account, and considering the same vapor pressure difference, he estimated that the evaporation of the soil was between 0.8 and 0.9 times that of the water. Based on his outdoor experiments and on the outdoor tests performed by White (1932), Penman (1948) stated that the evaporation from a freshly wetted soil was 0.9 times that of an open water surface exposed to the same weather conditions in all seasons. However, he admitted that a more detailed study was needed, since aspects such as the mean surface temperature and its daily amplitude were not well understood. Holmes (1961) indirectly assumed that the AE could only be as high as the PE, as he considered that the ratio between AE and PE could only be as high as one. Wilson et al. (1994) employed similar assumptions. Outdoor experiments carried out by Hellwig (1973) to study the evaporation of water from sand

also showed that during parts of the day the evaporation from the sand was greater than in open water. The evaporation from the water exceeded that from the sand only after midnight and in the morning. During this period the surface temperature of the water was far larger than that of the sand helping explain the difference in evaporation. He attributed the temperature difference to the ability of the water to store more energy than the sand, creating a larger temperature gradient between the surface of the water and the air than between the surface of the sand and the air. No explanation was given for the higher evaporation rates observed in the sand during the day. Blight (2002) and Blight (2009) observed a similar phenomenon and came to analogous conclusions. No direct explanation for the higher evaporation rates in soil was given by him either. Wilson et al. (1997) also observed a higher AE than PE in their laboratory experiments, which was reflected in the ratio between the two values being greater than one. They attributed this phenomenon to slight variations in aerodynamic resistance in the air spaces above the water and soil evaporation pans, and differences in the surface temperatures during the tests. They identified that the AE relative to the PE was a function of water availability, soil texture and drying rate.

In the case of the tests covered in this investigation, the solar radiation (which Penman (1948), Hellwig (1973) and Blight (2009) claimed to be partly responsible for the observed differences in evaporation between soil and water) cannot explain the difference in evaporation rates, since all the experiments were carried out in laboratory conditions. In general, evaporation from an open water surface is dependent on the water temperature, the air velocity above the surface, and the air temperature and humidity. The only one from these factors that was not known was the water temperature, which together with the temperature of the soil, were not recorded. Based on the analysis of evaporation in soils carried out by Philip (1957), Blight (2002) and Bittelli et al. (2008), it can be speculated that a contributing factor in the higher AE than PE were differences in heat fluxes between the saturated soil and the water, promoting a higher evaporation in the former than in the latter. An additional factor that could have had an influence is the greater evaporative surface present in the soil. As illustrated in Figure 4.7, the water is equivalent to a flat surface, analogous to a single large meniscus. In contrast, the surface of the soil is comprised of the surface from the exposed soil particles and the surface coming from the formation and presence of many small menisci. Moreover, the roughness of the soil surface might have induced turbulent flow at the evaporative surface, also contributing to the difference.

Figures 4.8 and 4.9 display the ratio of actual evaporation and potential evaporation (AE/PE) against time for all tests. This was presented in the same manner as Wilson et al. (1997), who modified a similar curve provided by Holmes (1961). It is worth noting that on average, in the initial stages of the tests and in both the fast and slow evaporation tests, the AE/PE ratio was lower for the liquid clay than for the plastic sample. The exception was Test SP in which the two first points were below Test SL, but the situation reverted at the tests progressed. The faster evaporation rate may be attributed to the greater roughness present on the surface of the solid clay compared to the clay in slurry state, increasing the amount of surface available

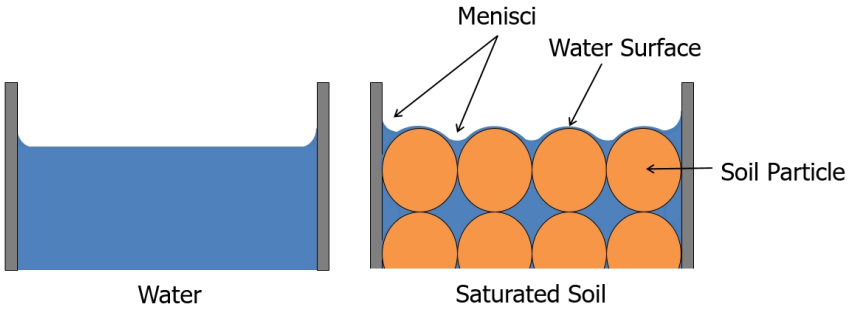

Figure 4.7: Schematic illustration comparing the surface conditions during the evaporation test of open water and a saturated soil.

for evaporation. In the plastic clay there could also be an earlier contribution from the menisci near the surface, which in the early stages is not so pronounced in the slurry due to the water availability on the surface of the soil.

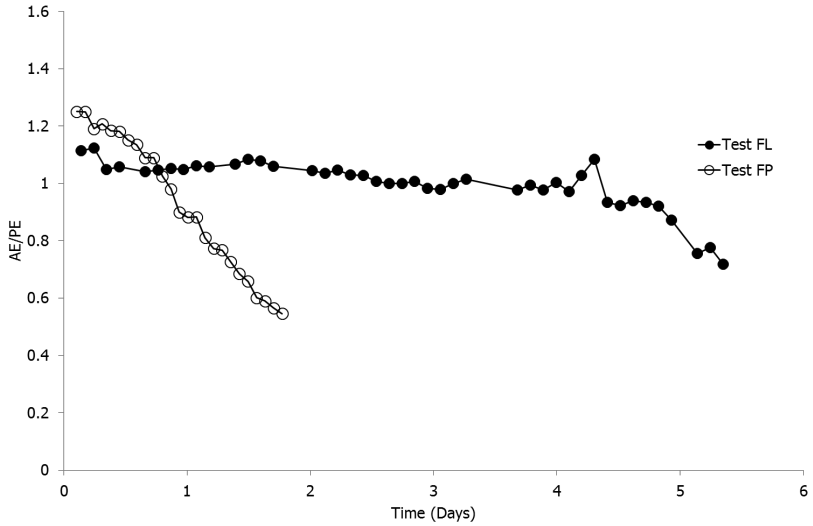

Figure 4.8: Variation of the ratio of actual evaporation and potential evaporation in time for Tests FL and FP.

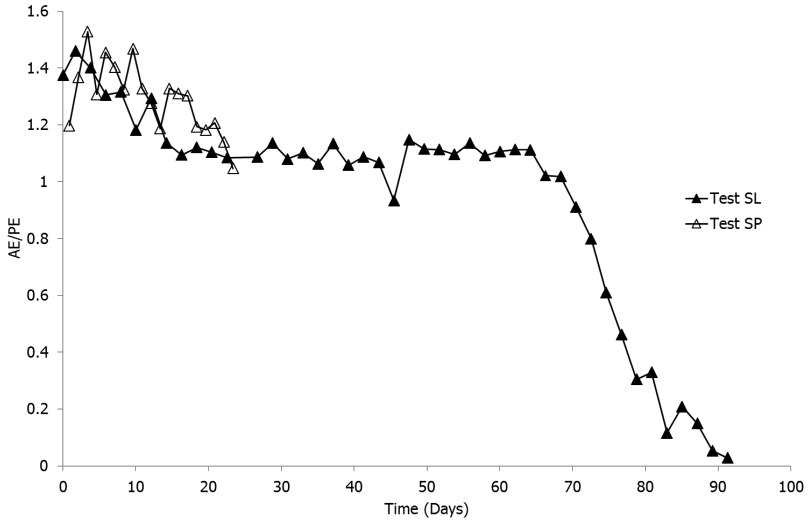

Figure 4.9: Variation of the ratio of actual evaporation and potential evaporation in time for Tests SL and SP.

Figure 4.10 presents the evolution of the AE/PE ratio with average water content for all tests. In addition to what was seen in Figures 4.8 and 4.9, tests that were subject to slow evaporation presented on average higher AE/PE values than the tests under fast evaporation. The tests with slurries showed an evaporation rate above or near an AE/PE ratio of one until an average water content of approximately 25% (a value very close to the plastic limit of the material). This stage can be correlated to the constant-rate stage described by Hillel (1980), where the soil surface remains fully saturated or close to full saturation. The soil also stays conductive enough to supply sufficient water to meet the evaporative demand. During this stage evaporation rate is limited and controlled by the environmental conditions.
After an average water content of around 25%, there was a marked decline in the AE/PE ratio for the tests with slurries. This may indicate that at this moment the suction development and reduction in hydraulic conductivity reached a point where they could impose a substantial constraint on the evaporation, decreasing the availability of water at the surface. This phase is associated with the falling-rate stage Hillel (1980), where there is not enough flow of water to the surface of the soil to maintain the maximum evaporation.
The behavior in the tests with clay in a "plastic" state was not the same as with the slurries, due to the different starting water content and soil structure. For Test SP, the AE/PE ratio also displayed a decline around an average water content of 25%, but the ratio remained higher than one for the duration of the measurements. In the case of Test FP, the decline in the AE/PE ratio seemed to begin from the start of the test (average water content of 35% approx.). It is possible that due to the high evaporation rate, large differentials in water content with depth were produced.

This led to the generation of a dry upper layer effectively blocking the evaporation from the lower sections. Therefore, for Test FP the average water content was probably not representative of what was happening on the surface of the sample. The differences between Tests SL and FL can be probably attributed to a similar phenomenon.

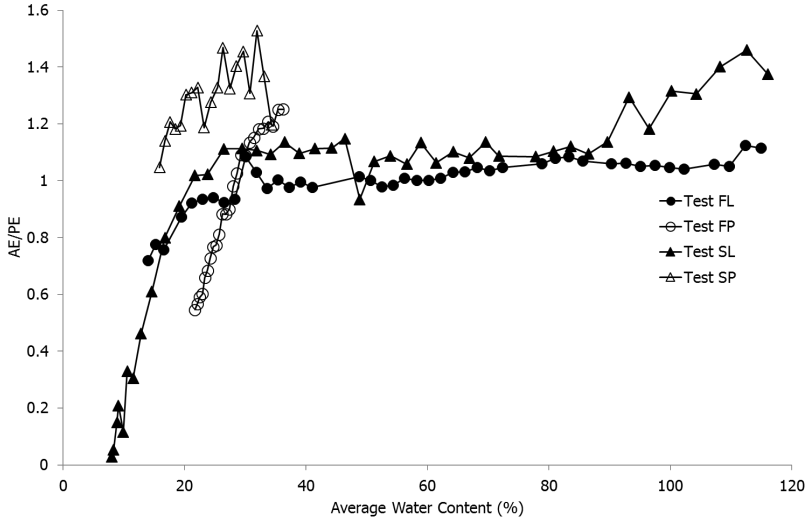

Figure 4.10: Variation of the ratio of actual evaporation and potential evaporation with average water content for all tests.

4.3.3. Suction Development

Total suctions were compared in the tests with similar initial water content. The data is reported starting from the moment in which positive suction was first detected and until cavitation of the tensiometer shaft was reached.
As it is revealed in Figures 4.11 to 4.12, there was a difference between the curves that originated from clays in liquid and plastic state. This can be justified by the influence of the different fabric in the liquid and plastic samples. A clear difference can also be appreciated in the suctions measured corresponding to the same average water content in the samples subjected to fast and slow evaporation. Considering that the suction could only be measured at a single point (located at a height of approximately 12.5 mm from the bottom) and that the measurements of mass just reflect the average water content of the sample, the differences in suction can be explained by two occurrences: an influence of different water content gradients generated within the sample under the drying regimes; and/or a dependence of the suction on the drying rate.

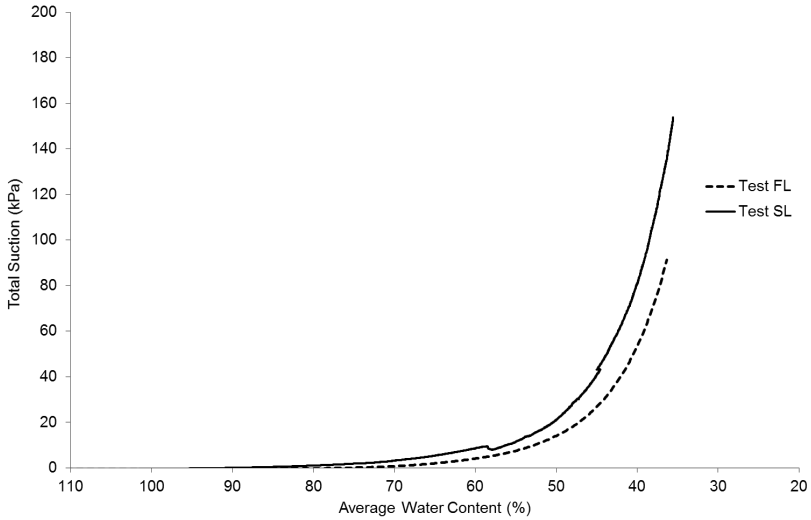

Figure 4.11: Comparison of the total suctions measured with respect to the average water content in the sample for Tests FL and SL.

In order to establish how the water content profiles evolved in time as the soil dried, a second series of experiments was performed under the analyzed conditions. The setup described in Figure 4.2 was used to dry four soil samples at the same conditions as Test FP and another four at same settings as Test SP. Each sample was removed once a predetermined average water content was reached. Then they were dissected in 10 mm layers, which were subsequently placed in the oven for water content determination. For each of the new tests, the four rings containing the samples were named A, B, C and D, with ring A being the first one that was removed and ring D the last one.

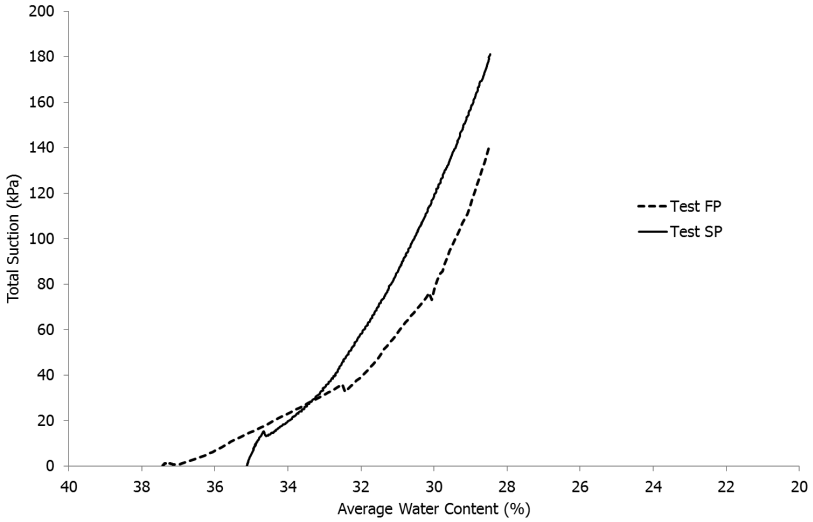

Figure 4.12: Comparison of the total suctions measured with respect to the average water content in the sample for Tests FP and SP.

Figure 4.13 and 4.14 confirm the strong impact of the evaporation rate in the water content profiles that develop with depth for a given average water content. If the evaporation rate is low, there is likely enough time for the water content to equalize throughout the sample. As a result, a nearly homogeneous water content with depth can be seen, similar to the observed average one (Figure 4.13). With a high evaporation rate, for a given average water content, higher water content gradients can are observed along the vertical soil profile (Figure 4.14). In general, a reduction of water content also implies a decrease in the permeability, either due to a decrease in the void ratio or a reduction in the degree of saturation. A smaller water content on the top layer will result in a faster decrease in permeability which will further slowdown the evaporation rate. The results shown in Figure 4.13 and 4.14 validate the explanations put forward for the soil behavior observed in Figure 4.10.

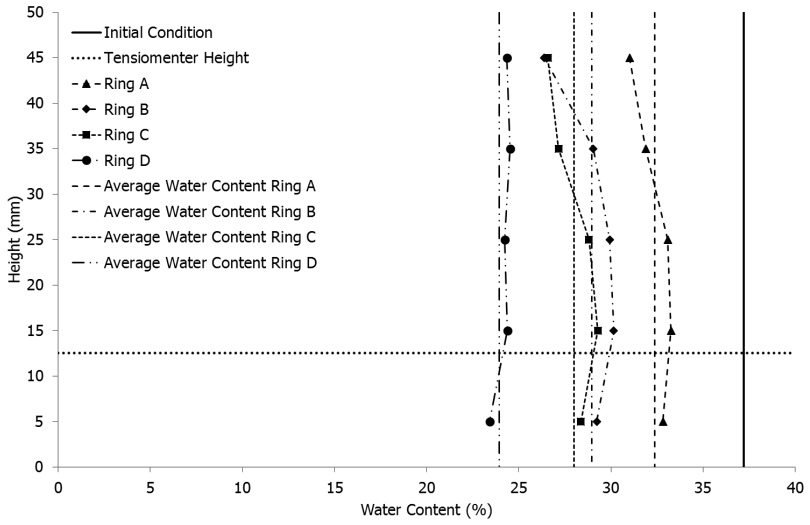

Figure 4.13: Results for the slow evaporation sequence of samples. The water content values for every 10 mm layer are displayed as dots and the average water content for the entire sample is presented as a line.

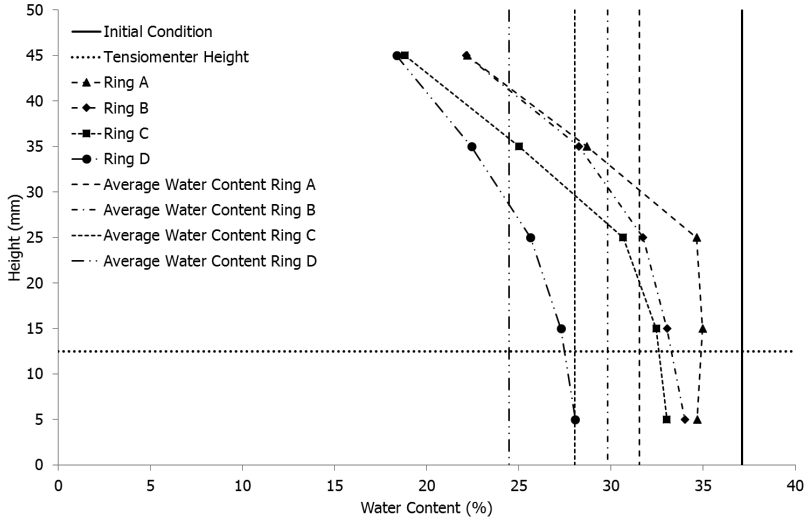

Figure 4.14: Results for the fast evaporation sequence of samples. The water content values for every 10 mm layer are displayed as dots and the average water content for the entire sample is presented as a line.

The results of the test exposed a discrepancy between the values of the average water content and the water content at the point of suction measurement (Figures 4.13 and 4.14). Therefore, it was decided to re-evaluate the suction values from tests FP and SP. The average water contents for these tests were correlated with the results of the rings A to D for the fast and slow evaporation. This allowed to relate the average water content for the entire sample to the actual water content present at the tensiometer tip (at an elevation of approximately 12.5 mm from the bottom). The suction values were back calculated by assigning the suction measured for a given average water content to the corresponding local water content at the tensiometer tip elevation. An additional high suction value for each curve was obtained by extrapolating the curves of Tests FP and SP with the cavitation point of the ceramic tip. The results are presented in Figure 4.15.
While there was a clear impact of the water content gradient with depth in the measurements, there was equally a dependence of the measured suction on the drying rate, with higher suctions measured for the same water content at higher evaporation rates. The dynamic effects in the soil water retention curve have already been noticed in several laboratory studies, for example Davidson et al. (1966), Topp et al. (1967), Watson & Whisler (1968), Smiles et al. (1971), Elzeftawy & Mansell (1975), Wana-Etyem (1984), Schultze et al. (1997) and Wildenschild et al. (2001). In general it was stated that the larger the time rate change in boundary suction or water content, the larger the dynamic effect. The majority of these investigations show the same type of variation in the soil water retention curves with change in boundary suction. Referring to Figure 4.15 to exemplify this variation, for the same change in water content, there is a larger increase in suction for the sample subjected to the high evaporation rate and vice versa. The size of the dynamic effects are reported to depend on factors such as the grain size distribution, porosity and permeability of the soil, and also on the fluid properties (Hassanizadeh et al., 2002). Wildenschild et al. (2001) attributed the phenomenon to a number of physical processes, such as the entrapment of water, pore water blockage, air entrapment, the air-entry value effect and the dynamic contact angle effect, which are all explained in detail in their investigation. However, these results refer mostly to non-deformable soils, in the absence of relevant changes in void ratio and fabric during evaporation.

Based on the description of the changes in clay structure behavior with drying made by Kodikara et al. (1999), Tripathy et al. (2010) and Tripathy et al. (2014), it is also possible that part of the dynamic effects can be caused by the distinctive response of the soil structure to the differences in boundary suction produced by the evaporation rates. The suction imposed on the soil can be interpreted as a stress which causes the material to shrink. In the case of a slow evaporation rate, the stress change of the soil is going to be similarly slow. That would allow for the particles to associate and rearrange as suction develops, reducing the size of the pores and thus delaying suction build up. On the other hand, if the evaporation is fast, the soil particles would not be allowed to accommodate as they associate. In this case, the particles would quickly lock in place, producing pores with larger size and allowing an earlier build-up of suction.
In an attempt to further investigate the effects of the evaporation rate on the suc-

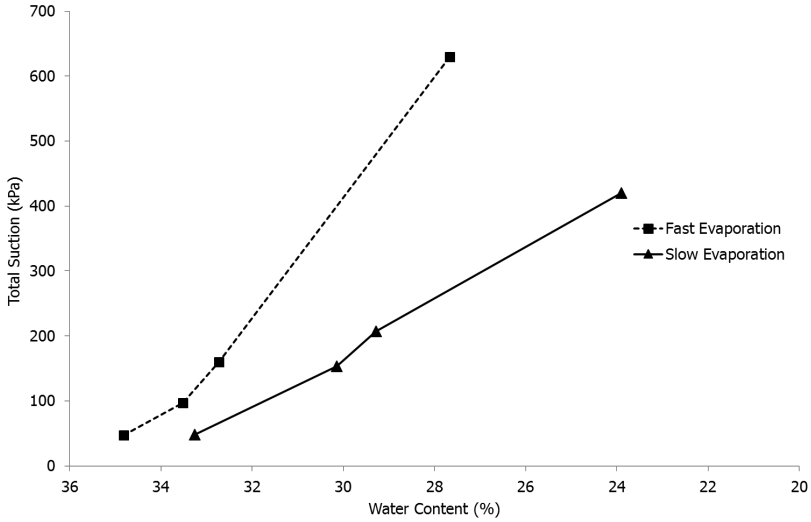

Figure 4.15: Re-evaluated the suction values from Tests FP and SP, based on correlating the water content values obtained for each ring in the tests described Figure 4.13 and 4.14 at the elevation of the tensiometer tip (12.5 mm from the bottom), and correlating them to the average water contents for Tests FP and SP to obtain the new suctions. The high suction values were found by extrapolating the curves of Tests FP and SP with the cavitation point of the ceramic tip.

tion build up, a new FP test was completed. This time the suction was allowed to build up for approximately 2.5 hours and then the soil was covered with plastic to stop any further evaporation. For the New Test FP, the two tensiometers of different length were utilized, in order to evaluate the possibility of any water migration and changes in suction with depth in the sample. Since the drying and shrinkage of the sample were very limited, the use of the two tensiometers presented no problem. The suction in the sample was allowed to reach steady-state conditions before it was removed and dissected in the same way as the tests shown in Figures 4.13 and 4.14. The results of the new test are presented in Figures 4.16 and 4.17.

In Figure 4.16 it was observed that the response of the upper tensiometer to the fast evaporation was a sharp increase in suction. The lower tensiometer exhibited a slower response, which was expected. After stopping the evaporation, the suction in the upper tensiometer dropped abruptly, while in the lower tensiometer continued rising at a slow pace. It took close to 2.5 days for the suction to go from a transient to a steady state. The suction continued to slowly increase for both tensiometers until the end of the test, due to the very small evaporation that took place in spite of the plastic cover.

When looking at the water content profile at the end of the New Test FP (Figure 4.17), and comparing it to the suction evolution, it seems that there was some degree of water content equalization with depth. The increase of suction in the lower tensiometer can be attributed to a reduction of the water content around the tensiometer tip after the evaporation was stopped. The exact opposite is valid

for the upper tensiometer. Nevertheless, it was clear that at steady state there were two different water content values (for the upper and lower tensiometers) corresponding to a single suction. The existence of one suction value for two water contents can be explained by the fact that after the evaporation was stopped, the soil surrounding the upper tensiometer underwent a process of rewetting. This meant that the upper and lower tensiometers were following different water retention curve paths (a wetting and a drying path, respectively).
In Figure 4.17 there is a comparison between the water content profile of the New Test FP and a similar profile from Figure 4.13. Both profiles were almost identical with the exception of the top 15 mm. This section was affected by the fast evaporation to which the New Test FP was exposed, producing irreversible changes in the structure of the soil.
What was evident from the test is that the sample under slow evaporation obeyed a behavior that resembled a steady state condition, whereas the fast evaporation represented a transient state. It is reasonable to think that the suction at which the New Test FP reached the steady state was equal to the suction that would have been developed under slow evaporation for that particular average water content. This results can be interpreted as a time dependent hydraulic phenomenon. But if there was a permanent time dependent effect on the water retention behavior is still undetermined.

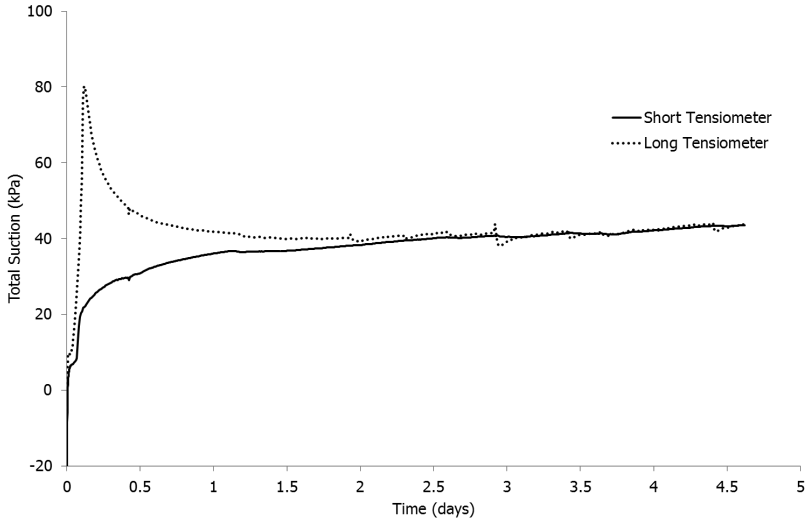

Figure 4.16: Suction development with time for the entire New Test FP.

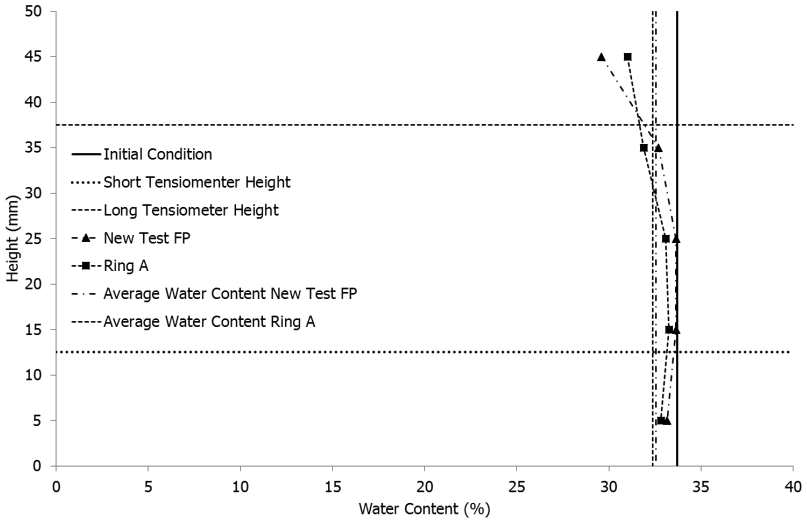

Figure 4.17: Water content values for every 10 mm layer for the New Test FP, compared to the results of Ring A in the experiment shown in Figure 4.13.

5

Modelling Desiccation Cracking in a Homogenous Clay Layer: Comparison Between Different Hypotheses

The greatest enemy of knowledge is not ignorance.
It is the illusion of knowledge.

Daniel J. Boorstin

This chapter is based on a paper published in the E-UNSAT 2016 Conference, Jommi et al. (2016).

5.1. Introduction

It is generally believed that fractures in soil start at the surface and then they propagate downwards. Weinberger (2001) described that under laboratory conditions, the initiation of fractures commonly happens at the surface of the desiccating layer. However, as it was pointed out in Chapter 2, that it is not always the case. In the tests described in that chapter, it was observed that the fractures can initiate and propagate under the surface.

Several simplified models have been created to simulate the generation of cracks in soil (Morris et al., 1992; Abu-Hejleh & Znidarčić, 1995; Konrad & Ayad, 1997; Peron et al., 2007), but all of them are based on the hypothesis that the fracture initially starts at the top of the desiccating layer. The assumption is reasonable given that the dryer section in the soil profile is at the top, where the largest amount of suction is potentially developed. These simplified models tackle the drying process as a weakly coupled, nearly steady-state process. They use a unique relationship between the water content and the relevant variables playing a part in the mechanics of the system, and they cannot simulate cracks beginning below the surface.

It has been established experimentally that under the same environmental and initial conditions, thin clay layers dry faster than thick ones. The latter also exhibit less cracks, larger intact areas and wider fractures (Corte & Higashi, 1960; Kodikara et al., 2000; Nahlawi & Kodikara, 2006; Tang et al., 2008, 2010a; Costa et al., 2013). The phenomenon has been attributed to the difference between desiccation rates. This premise has been confirmed by studies performed by Tang et al. (2008, 2010a) and Costa et al. (2013). Corte & Higashi (1960) also observed that the average water contents at the onset of cracking decreased as the drying speed increased.

As experimental evidence shows, there is a clear rate dependency of the stresses involved during soil drying and cracking.

The experimental results presented in Chapter 3 indicate that the tensile strength depends strongly on the water content, but there is no significant variation in the tensile strength with different pulling rates. The observations are in agreement with the conclusions of Fang & Chen (1972); Heibrock et al. (2005) and Kim et al. (2007). On the contrary, the dependence of the tensile stiffness on the water ratio and tensile strain rate is noticeable. In Chapter 4 evidence is also provided indicating some dependence of the soil water retention curve (SWRC) on the evaporation speed. Moreover, the air entry value upon drying was shown to depend on the initial water content, hence confirming the important role played by the soil fabric. These suggests that the key factor to predict crack onset below the surface must be looked for among the other hydro-mechanical properties governing the response of the compressible soil upon drying. This chapter presents an exercise aimed at analyzing the consequences of different hypotheses about the material behavior on the theoretical prediction of crack initiation in a homogenous soil layer. The goal is to provide an insight into the role of different factors on the onset of cracking, and their dependence on both the water content and the water content change rate.

5.2. Description of the Crack Initiation Model

A simple 1-D model is used to describe the behavior of a homogenous isotropic deformable clay layer undergoing evaporation from the top surface. Up until the first crack appears, the layer can be described by a one-dimensional system with all relevant quantities varying only with depth, z. If the soil layer is initially saturated, previous research and the results from this experimental investigation suggest that the first crack appears during the saturated state. Accepting this hypothesis, the water ratio $e_w = V_w/V_s$, where V_w is the volume of water and V_s is the reference volume of solids, is sufficient to describe the distribution of void ratio and water content throughout the soil profile before cracking occurs.

The water ratio profile changes in time and depth due to the evaporative flux at the top surface of the layer, and it was chosen as the driving variable of the simple hydromechanical model. The mechanical behavior of the soil was described by the simplest allowable laws suggested by the experimental evidence. This was carried out to highlight the role played by different hypotheses in the response of the soil layer to the evaporation process. The hydraulic fluxes are not explicitly accounted for in the formulation, as the current water ratio distribution is sufficient for the suction profile to be calculated from the drying branch of the SWRC. In the formulation, compression stresses and strains are assumed positive. The change rate in the variables is designated by a superscript dot. The vertical and horizontal components of stress, σ, and strain, ϵ, are designated by subscripts z and h, respectively.

5.2.1. Relevant Assumptions

The soil is assumed to be homogenous, isotropic and saturated until the first crack occurs. If the variation of water content with depth and time is known, the current water ratio and water ratio rate can be calculated at any depth, serving as the input of the model.

A simple incremental hypo-elastic model is assumed to describe the material stiffness:

$$\begin{bmatrix} \dot{p}' \\ \dot{q} \end{bmatrix} = \begin{bmatrix} K & 0 \\ 0 & 3G \end{bmatrix} \begin{bmatrix} \dot{\epsilon}_{vol} \\ \dot{\epsilon}_d \end{bmatrix} \tag{5.1}$$

where K is the bulk modulus and G is the shear modulus. The stress and strain variables are defined as:

$$p' = \frac{1}{3}\left(\sigma'_z + 2\sigma'_h\right) \tag{5.2}$$

$$q = \left(\sigma'_z - \sigma'_h\right) \tag{5.3}$$

$$\epsilon_{vol} = \left(\epsilon_z + 2\epsilon_h\right) \tag{5.4}$$

$$\epsilon_d = \frac{2}{3}\left(\epsilon_z - \epsilon_h\right) \tag{5.5}$$

In principle, the stiffness moduli can depend on the water ratio and on the water ratio rate. In the following sections different hypotheses are evaluated and their consequences analyzed.
The volumetric (shrinkage) strain rate is given by:

$$\dot{\epsilon}_{vol} = -\frac{\dot{e}_w}{1 + e_w} \tag{5.6}$$

where e_w represents the water ratio:

$$e_w = wG_s \tag{5.7}$$

The volumetric (shrinkage) strain is assumed to be entirely due to a change in effective stress acting on the soil element:

$$\dot{\epsilon}_{vol} = \frac{1}{K}\dot{p}' = \frac{1}{K}(\dot{p} - \dot{u}_w) = \frac{1}{K}(\dot{p} + \dot{s}) \tag{5.8}$$

where u_w is the pore water pressure and s is the suction. Under saturated conditions, $s = -u_w$.
If the soil element is free to deform, no shear strains and consequently no shear stresses are developed. Under a 1-D constraint, when only vertical deformation is allowed, a shear strain must accompany the volumetric strain, so that the following lateral constraint is complied with:

$$\dot{\epsilon}_h = 0 \tag{5.9}$$

Using the pseudo-elastic law, the lateral effective stress can be obtained from the previous assumptions in the form:

$$\dot{\sigma}'_h = \dot{s} - \frac{2}{3}G\dot{\epsilon}_{vol} = \dot{s} + \frac{2}{3}G\frac{\dot{e}_w}{1 + e_w} \tag{5.10}$$

It is worth noting that the change in total stress due to the water mass change during evaporation is disregarded in the formulation. The choice is justified by the fact that the latter term is two orders of magnitude smaller than the corresponding changes in suction. The total horizontal stress increment is given by:

$$\dot{\sigma}_h = \dot{\sigma}'_h - \dot{s} = \frac{2}{3}G\frac{\dot{e}_w}{1 + e_w} \tag{5.11}$$

During evaporation, the horizontal stress decreases as tensile stresses are developed. In the absence of weak spots, the idealized crack initiation condition can be defined as the moment when the total tensile stress attains the same value as the tensile strength:

$$|\sigma_h| = |\sigma^T| \tag{5.12}$$

The choice for an assessment in terms of total stresses is justified by the available experimental data on tensile strength, which is expressed in terms of the total stress

needed to trigger tensile failure.
In the saturated range the bulk modulus can be obtained as the derivative of the SWRC:

$$K = -(1 + e_w)\frac{\delta s}{\delta e_w} \tag{5.13}$$

To evaluate the shear modulus, two different paths were considered. The simplest method is to derive it from K:

$$G = \frac{3(1 - 2\nu)}{2(1 + \nu)}K \tag{5.14}$$

assuming a convenient value for the Poisson's ratio. This could be the choice in the absence of any other information.
The second method relies on the tensile tests performed in Chapter 3, as shown in section 5.3.3.

5.2.2. Constitutive Assumptions

The response of the soil to a given change in water ratio in the simplified 1-D model depends on: (i) tensile strength, (ii) tensile stiffness, and (iii) soil water retention properties, which link the water ratio to the suction.
The response of the soil layer is analyzed first at an elementary level (Model I), assuming constant values for the soil stiffness and strength. This approach has been used in previous models that have focused exclusively on the crack onset (Morris et al., 1992; Peron et al., 2007). In the second analysis (Model II), the stiffness is assumed to depend on the strain rate, which is in accordance with the evidence of the experimental results in Chapter 3. In the last study, a dependence of the stiffness and water retention curve on the drying rate was considered, as well (Model III). It is worth reminding that no attempt was made to formalize the constitutive laws in a comprehensive thermo-mechanical framework. Instead, non-linear hypo-elastic laws were used, interpolating the experimental information.
Based on the results obtained in Chapter 3, the tensile strength was given a power law of the type:

$$\sigma^T = c e_w^{-d} \tag{5.15}$$

The water retention curve was described by a standard van Genuchten's equation (van Genuchten, 1980) with two independent parameters, assuming m = 1 – 1/n. The determination of the parameters was based on the water retention curves presented in Chapter 3 (Figure 3.8). The bulk modulus K(e_w) was calculated with Eq.(5.13) from the retention curve.

5.3. Model Predictions and Discussion

5.3.1. The Benchmark Problem

A homogenous soil layer, 0.1 m thick, was assigned the initial state which characterized the 0.1 m thick test described in Chapter 2, section 2.3.3. The water

ratio profile was constant at the beginning of the tests, with a value of e_{w_0} = 2.55. A final water content profile was assigned, based on laboratory measurements made after two weeks of drying. To simplify the analysis, a constant drying rate at each depth was assumed between the initial and final states. This allowed to define a set of water content values between the initial and final water content profiles, resulting in the water ratio evolution history in Figure 5.1 plotted as a function of the original height. The water ratio rate varied from 0.03 to 0.01 day^{-1} with depth. Table 5.1 summarizes the values of the parameters used in the simulations to describe the tensile strength (Eq. 5.15).

Table 5.1: Parameters used to describe tensile strength (Eq.5.14).

Variable	**MODEL I Depending on e_w**	**MODEL II and III Depending on e_w, $\dot{e}_w$**
$\|\sigma^T\|$ (kPa)	c = 6.5 kPa d = 3.65	c = 6.5 kPa d = 3.65

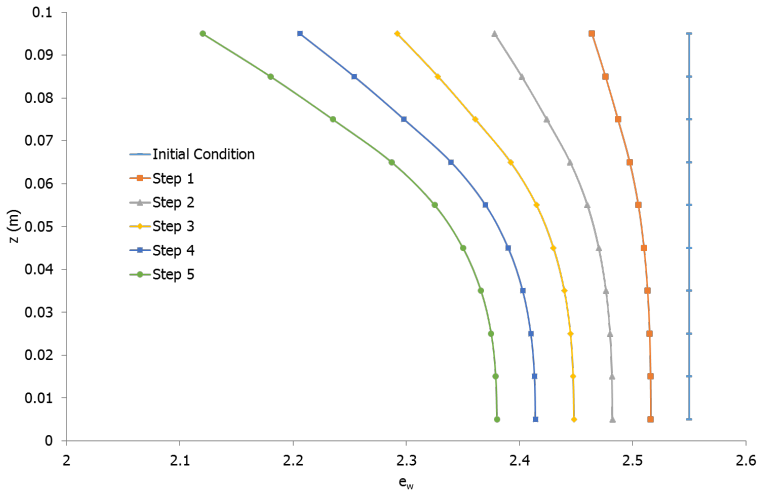

Figure 5.1: Water ratio profiles given as input to the 1-D model.

5.3.2. Results for Model I

In Figure 5.2, the evolution of the suction profile is reported for Model I, showing an increase of the suction with time and attaining the maximum values at the top of the soil layer. The horizontal tensile stress and tensile strength also increase, reaching the highest value at the top of the layer (Figure 5.3). A constant value of $\nu = 0.3$ was used in the simulations.

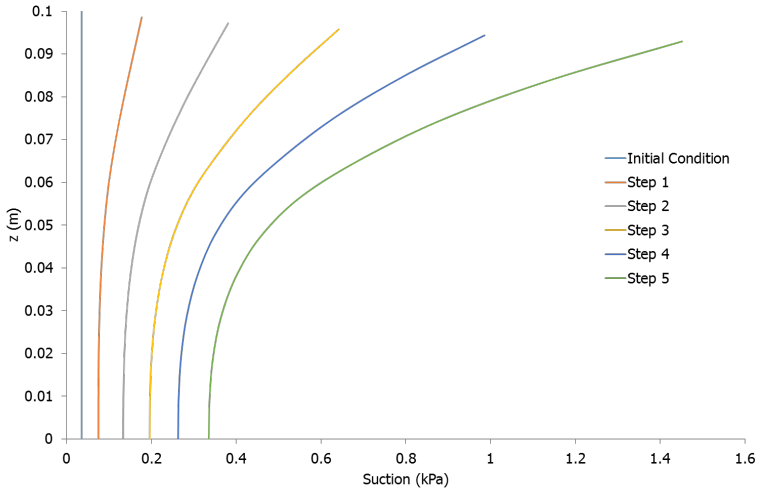

Figure 5.2: Suction profiles predicted by Model I.

As depicted in Figure 5.4, the maximum tensile stress approaches the tensile strength and eventually reaches it (step 2 in the case of Figure 5.4). For Model I, the tensile strength is attained at the top of the layer before than at any other depth. This result is not due to the particular values assumed for the parameters, but it is a consequence of the shape of the curves, all having a similar dependence on the water ratio. If the tensile strength were to increase faster, no tensile crack would be predicted. On the contrary, if the condition for crack onset is met (Eq. 5.9), it would initially occur at the surface of the layer.

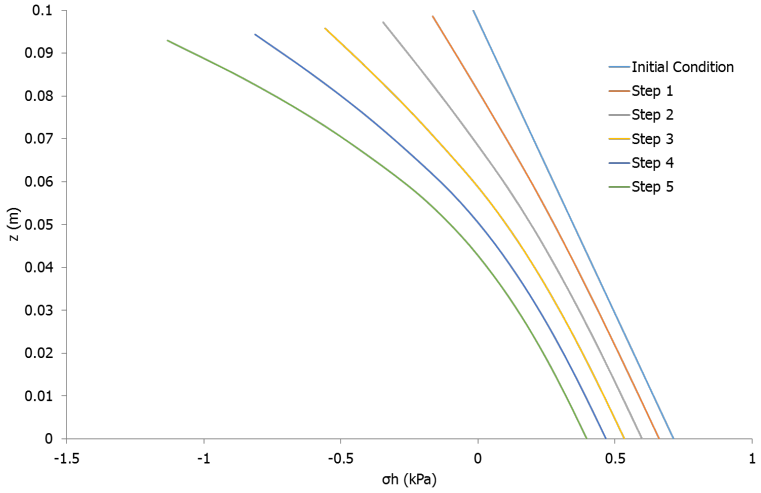

Figure 5.3: Horizontal total stress profile predicted by Model I.

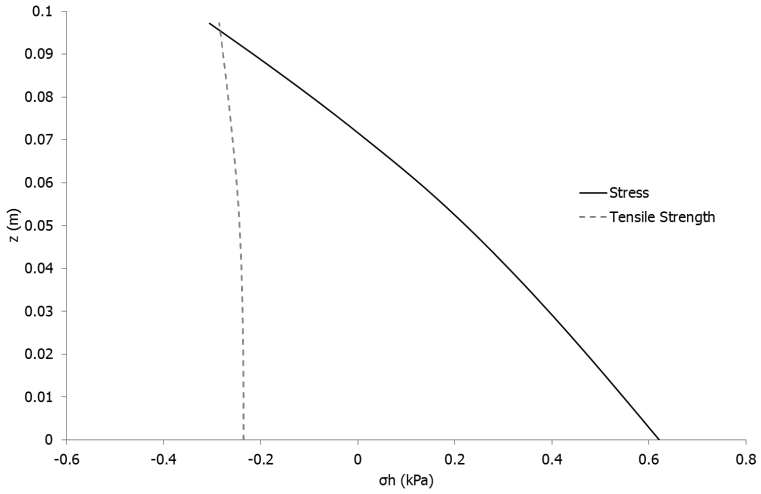

Figure 5.4: Comparison between the horizontal stress at step 2 and the tensile strength defined for Model I.

5.3.3. Dependence of the Stiffness on the Pull Rate

Th experimental data collected in Chapter 3 suggests that the stiffness might also depend on the strain rate (in addition to the water ratio). Nonetheless, while the strain rate is relevant for the stiffness, the tensile strength is almost insensitive to it.

During the tensile tests in Chapter 3 the deformation was predominantly axial and the secant modulus estimated for each of the tests was employed to model the tensile stiffness dependence on the strain rate. The estimations of the modulus were done by employing the maximum tensile (axial) stress and an estimated axial strain, assuming an area of influence of approximately three times the length of central area of the test device (equivalent to 72 mm).

If the isotropic soil was free to deform during drying, the lateral horizontal strain would be:

$$\dot{\epsilon}_x = \frac{1}{3}\dot{\epsilon}_{vol} = -\frac{1}{3}\frac{\dot{e}_w}{1+e_w} = -\frac{1}{3}\frac{\dot{e}_w}{1+e_{w0}} \tag{5.16}$$

assuming that the initial water content is approximately the same as the final one. During one dimensional drying no lateral strain can occur until the onset of cracking. Therefore, it is assumed that an equal and opposite lateral strain generated by the raising tensile stress counteracts the soil's tendency to shrink. Using the inverse of equation 5.16, the evaporation rate can be linked to the strain rate in the form:

$$\dot{e}_w = -3\,(1+e_{w0})\,\dot{\epsilon}_x \tag{5.17}$$

and this allows expressing the data in Chapter 3 in terms of water ratio and water ratio rate:

$$E = \gamma(e_w^{-\delta})(\dot{e}_w^{-\beta}) \tag{5.18}$$

with γ, δ and β having values of 2000, 6.8 and 0.32, respectively.

The shear modulus and Poisson's ratio can be therefore evaluated as:

$$G = \frac{3}{2}\frac{3KE}{9K-E} \tag{5.19}$$

$$\nu = \frac{E-2G}{2G} \tag{5.20}$$

The evolution of G and ν for the same drying history as before are presented in Figures 5.5 and 5.6. The resulting values of ν are around 0.3 for the analyzed drying rate. It is also shown that the faster the drying rate, the higher the resulting Poisson's ratio. It is worthwhile highlighting that in this case, ν is calculated based on completely independent experimental information. The values obtained suggest that the simplifying assumptions seem to be reasonable as a first approximation.

In spite of E evolving differently than before, the tensile stresses develop faster close to the surface of the layer in the same manner as in Model I. The same is valid for the tensile strength, but the tensile stresses develop at a higher rate. As consequence, the tensile stress surpasses the tensile strength during drying step 4 (Figure 5.7).

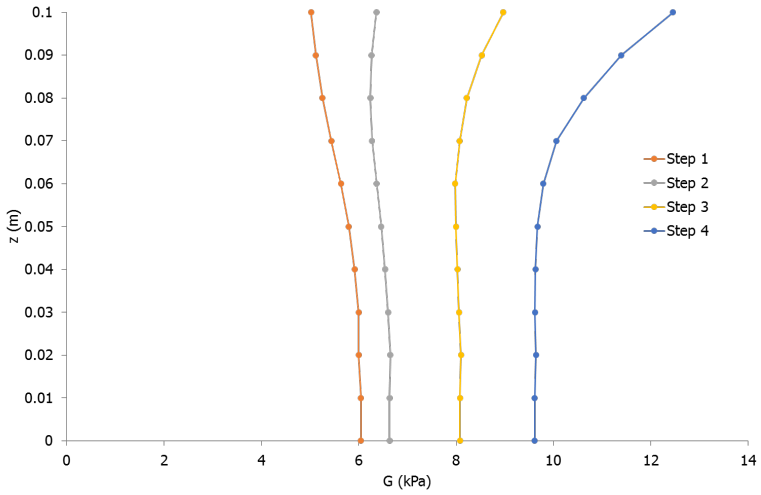

Figure 5.5: Shear modulus predicted for the first four steps in Model II.

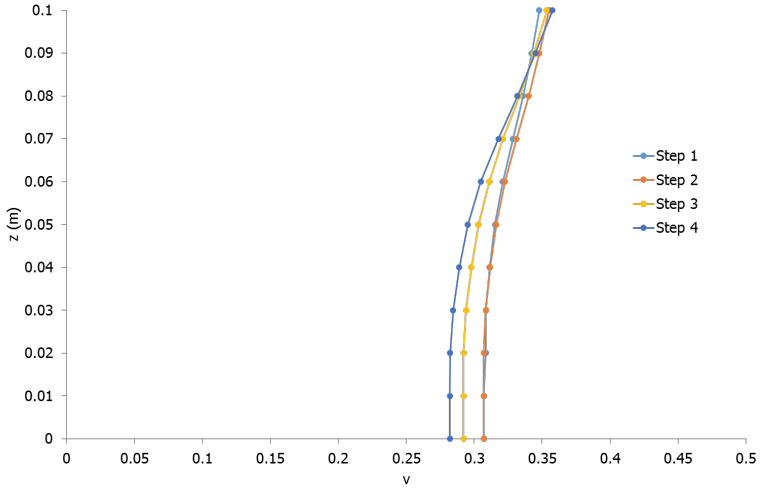

Figure 5.6: Poisson's ratio predicted for the first four steps in Model II.

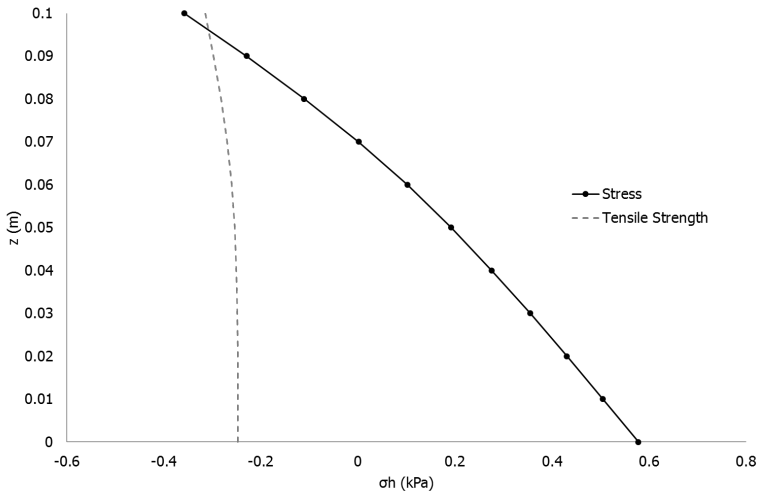

Figure 5.7: Comparison between the horizontal stress and the tensile strength defined for Model II at step 4.

5.3.4. Dependence on the Rate of Water Ratio

The results shown in Figure 5.4 and 5.7 indicated that the dependence of the stiffness on the water ratio and strain rate, as calibrated on the experimental results, was not enough to justify the occurrence of first cracks below the surface of the clay layer. Therefore, the crack initiation below the surface must be the result of some previously unaccounted factors.

Sensitivity analyzes showed that the suction can be a dominant factor in the shape of the horizontal stress with depth. To allow for the shape of the horizontal stress to change, the dependence of the water retention curve on the water ratio rate can be explored. Although this is not a common assumption, some previous work has already highlighted that this dependence may exist, either from a theoretical standpoint, or from experimental observations.

Experimental observations in Chapter 3 on the dependence of the tensile stiffness on the drying rate suggested that an intrinsic time scale characterizes the response of the soil fabric to water content changes. A decrease in tensile stiffness at increasing drying rate can be justified by the development of lower suction values. These lower suction values for a given water content could be justified by fast drying tending to maintain an open fabric with larger pores. If drying is slow enough for the fabric to rearrange, a more massive fabric with smaller pores can develop as a consequence. Based on this hypothesis, the water retention curve was made dependent on the rate of water ratio, by assuming a shape parameter n of the form:

$$n = \bar{n} + \bar{\eta}\dot{e}_w \tag{5.21}$$

The resulting curves are represented in Figure 5.8. The parameters used for

the water retention curve are summarized in Table 5.2. In the range of drying rates analyzed, n is always higher than 1. The corresponding tangent bulk moduli are shown in Figure 5.9.

Table 5.2: Parameters for the SWRC for Models I and II.

Parameter	MODEL I and II Constant	MODEL II Depending on e_w, $\dot{e}_w$
α (kPa^{-1})	1.0	1.0
n	1.04	$\bar{n}$=0.96
		$\bar{\eta}$ = 5.04 (d)

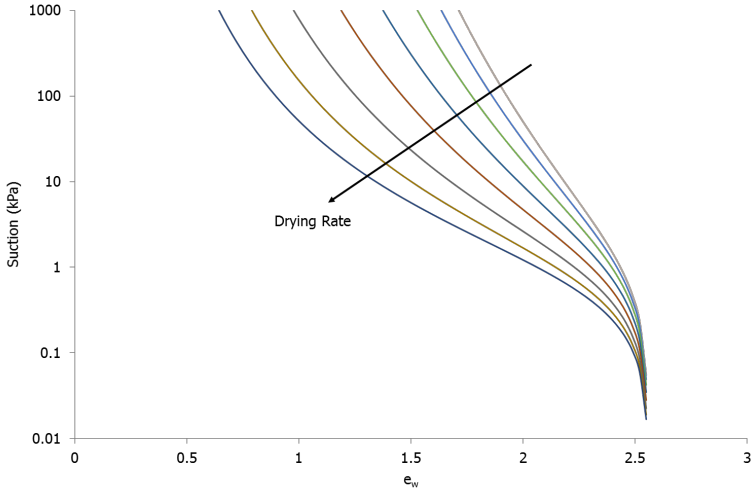

Figure 5.8: Suction vs water ratio and water ratio rate.

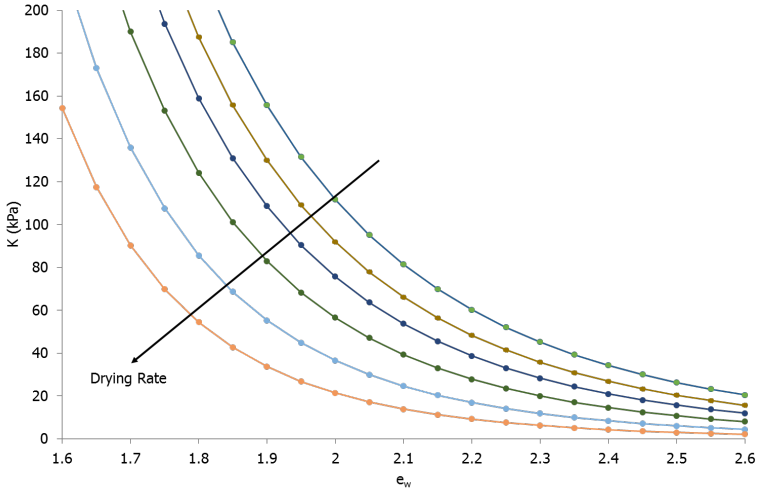

Figure 5.9: Bulk modulus vs water ratio and water ratio rate.

The drying rate dependence of the suction developed for a given water ratio yields a suction increase rate which is different for each depth. The implications are evident from the results of the simulation completed with Model III (Figure 5.10).

The different rates at the different depths change the shape of the suction profile in time. As a result, the horizontal stress profile varies with depth, and the horizontal stresses at the top of the layer can increase less rapidly than at depth. As observed in Figure 5.10, the onset of cracking is predicted for a water ratio profile occurring during step 5. The critical depth is not on the surface anymore. On the contrary, the horizontal stress can reach the values of tensile strength at different depths below the surface, or even near to the bottom of the layer.

The results of this numerical simulation suggest that there might be a theoretical justification for the development of cracks below the surface which were actually observed in the laboratory on the physical models. However, the results described in Chapter 4 show that the development of suction in a drying layer (at the depths at which it was measured) is a complicated time dependent process, which also depends on the hydraulic conductivity of the soil.

Although no definite conclusions can be drawn at this stage, the hypotheses put forward in this chapter are meant to define a path for future research.

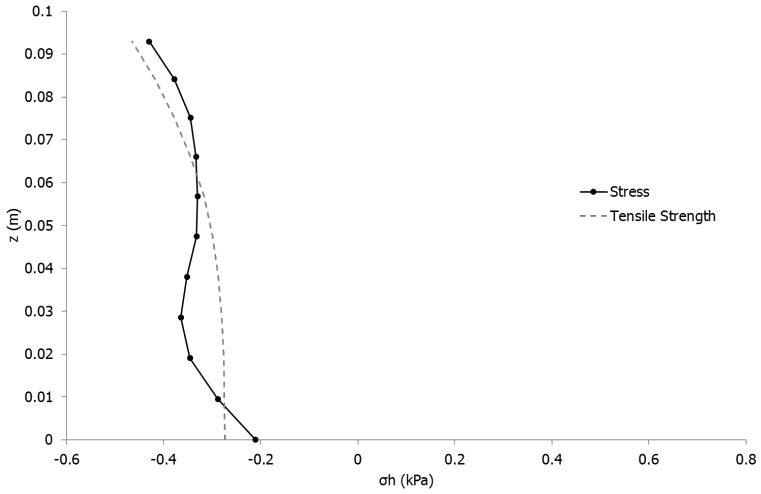

Figure 5.10: Comparison between the horizontal stress and the tensile strength at step 5 predicted by Model III.

6

Conclusions and Recommendations

He who knows all the answers
has not been asked all the questions.

Confucius

6.1. Observations and Conclusions

As stated in Chapter 1, the main objectives of this thesis were to (1) investigate the effects of boundary conditions and material properties on the inception and propagation of desiccation cracks; (2) analyze the conditions for fracture propagation (in a consolidating layer), investigating the role of stress changes with depth; (3) evaluate the relationship between water content, strain rate and tensile strength and stiffness of the soil; (4) characterize the drying behavior of the soil under different evaporative regimes and initial conditions, and analyze their effects on the suction development; and (5) assess rate dependency of the factors involved in the fracture generation and propagation process. An experimental approach was adopted to try to answer the questions, on a series of complementary small scale laboratory models.

6.1.1. Conditions of Fracture Propagation, Effects of Boundary Conditions and Material Properties

A series of tests was carried out in a controlled environment on model samples to study the crack formation in desiccating clay under different initial and boundary conditions, including initial water content, layer thickness, set-up size and material. For the same initial and atmospheric conditions, the thickness of the soil layer significantly influenced the water content at which cracking began. The thicker the layer, the higher the water content at which the crack started. The amount and aperture of the fractures generated were affected by the layer thickness, as well. Thinner layers exhibited more fractures than the thick ones.

The material at the base of the soil samples affected the amount of fractures produced. The lower the friction of the base material, the lower the amount of cracks generated.

From the water content measurements it was also evident that the average cracking water content could be above or below the value of the liquid limit, suggesting that this reference did not provide relevant information on the fracture onset. Water content was similarly not the unique dominant factor in fracture propagation, with the rate of water content change also governing soil behavior.

As a result of evaporation, the water content decreased continuously in time, but the differences in the water content measured with depth during the tests were relatively small (except for the top and bottom few millimeters where the water content was lower than average). Consequently, the average water content seemed to reasonably represent the water content of the entire layer.

Based on the observations related to the surface depressions, plumose fractures and water content with depth, it can be established that the fracture propagation in the tests happened under the surface. The propagation did not occur in the areas of the layer with the lowest water contents.

During the drying of the experiments, it was observed that the angles of the initial fractures that were other than 90° with respect to the theoretical principal stress directions, denoted the influence of shear forces arising from non-symmetrical boundary conditions. The angles between fracture intersections were affected by the

thickness of the soil layer. Thin layers presented fractures intersecting at 90° and 120°, highlighting the influence tensile and shear forces, respectively. As the layer thickness increased, only fractures intersecting at 90° were observed.
Factors such as the ratio between the area of the setup and the thickness of the soil, the friction provided by the surface of the container, initial water content and the atmospheric conditions need to be taken into consideration during soil cracking experiments when upscaling results from the laboratory to the field and when downscaling field samples to the laboratory.

6.1.2. Relationship between Water Content, Strain Rate and Tensile Strength of the Soil

The effects of pull rate and water content on the tensile strength of a clay were investigated by means of direct tensile tests with a specially designed device. Further analysis of the tests was carried out by using PIV techniques.
The tensile strength of the soil was mainly dependent on the water content. The pull rate had a negligible influence on it. However, the pull rate did have an impact in the stiffness response of the soil.
The soil showed almost undrained behavior at high pull rates, characterized by low stiffness. At lower pull rates the soil experienced volume changes, which can be the cause for the material to display a stiffer response. High pull rates could be recommended to limit the effects of evaporation during the test. Nonetheless, as mentioned before, a partially undrained response is expected at high pull rates, which limit the interpretation of the data to total stresses.
In principle, slow pull rate tests seem to allow for conditions closer to steady state. However, the interpretation is complicated by the effects of evaporation which can become relevant, if significant variations of water content occur.

6.1.3. Drying Rate and Suction Development in the Soil

Tests were carried out on clay samples at two different initial water contents corresponding to different states (i.e. liquid and plastic), to determine their behavior under two distinct evaporation conditions. The aim of the investigation was to provide insight on how evaporation rates affect the drying of a compressible material, as well as their influence on the suction development.
It was found that the actual evaporation could be larger than the potential evaporation, i.e. the evaporation of an open water surface is not always the highest that can be achieved. The surface texture and the influence of the pore structure in a soil played a major role in the evaporation rate.
The evaporation rate had an impact in the final water distributions within the soil. If the evaporation is stopped, there can be internal drying-wetting cycles that take place in the soil layer. The evaporation rate to which the soil was exposed directly affected the suction development in time. This suggested that there was not a unique soil water retention curve describing suction generation. Dynamic effects in the soil water retention curve were especially noticeable at high evaporation rates.

6.1.4. Insight from Simple Mechanical Models

Simple one dimensional models were set up to assist in the interpretation of the data, without pretending to develop of a comprehensive numerical and constitutive framework for the drying and cracking soil layers. They were conceived to explore the consequences of various material behavior assumptions on the response of a deformable clay layer to atmospheric desiccation. Different hypotheses were tested to try to investigate the necessary requirements for cracks to start at depth in shrinking clay, assuming the absence of weak spots and with a limited influence of external constraints. The attempts at simulating fractures appearing below the surface with the assumptions used were either unsuccessful, or not totally convincing. There are additional unknown factors involved in the generation and propagation of fractures under the surface, besides the dependence of the stiffness on the shrinkage rate and the water ratio rate. Nonetheless, the examples showed that the role of time dependency is crucial and should be addressed in the future.

6.2. Recommendations for Further Work

Some of the recommendations for further study include extending the physical modeling performed in this thesis to include the effects of soil drainage on the desiccation and fracturing of soil. An additional step would be to incorporate the influence of changing water table levels, as well as rewetting cycles.

In order to obtain better results during the tensile tests, it is suggested to find ways of stopping or slowing down the evaporation from the soil. This could be done by designing a cover system, or performing the tests in a high humidity climate chamber. Extra insight could be gained by conducting experiments to evaluate the effects of a vertical load on the tensile strength of the soil. The influence of size effects on the tensile strength could similarly be studied by changing the dimensions of the samples tested.

As observed in the evaporation tests, it is also important to investigate the internal rewetting and drying cycles in a soil layer. This is essential for understanding the effects of diurnal cycles on the suction development and evaporation of a soil. Additional work can be carried out to analyze the impact of different drying rates alternated with rewetting cycles.

None of the hypotheses put forward to attempt to capture the propagation of fractures under the surface were able to replicate the phenomenon in a convincing way. In this aspect further efforts need to made to find a suitable mechanical framework, or to improve on the suggested hypotheses. Nevertheless, the results of this work can be used as guideline for advanced modelling purposes.

A

Appendix

A

A.1. Assessing the water retention properties of shrinking soils with high initial water content using the HYPROP device.

A.1.1. Introduction

The HYPROP is a relatively new device used for determining the water retention and hydraulic conductivity properties of soils. The system is based on the evaporation method, first introduced by Wind (1966) and later modified into the simplified evaporation method by Schindler (1980).
The HYPROP device consists of a main sensor unit containing two tensiometers of different length. Suction is measured at two heights within a soil sample, while the mass of the sample is simultaneously measured at defined time intervals. From the initial water content, measured weight loss and specific gravity, the volumetric water content is calculated and plotted against the mean suction value to obtain the drying branch of the Soil Water Retention Curve (SWRC).
The difference between the suction values and the distance between the tensiometers are then used to calculate the average hydraulic gradient. The hydraulic conductivity is calculated with the following equation (Schindler & Müller, 2006):

$$K(\psi) = \frac{\Delta V}{2A \cdot \Delta t \cdot i_m} \tag{A.1}$$

where ψ is the mean suction between the upper and lower tensiometer, A is the cross sectional area of the sample, ΔV is the evaporated water volume, Δt is the reference time interval and i_m is the mean hydraulic gradient in the interval, defined as:

$$i_m = \frac{1}{2}\left(\frac{\psi_{t_1,upper} - \psi_{t_1,lower}}{\Delta z} + \frac{\psi_{t_2,upper} - \psi_{t_2,lower}}{\Delta z}\right) - 1 \tag{A.2}$$

where $\psi_{t,upper,lower}$ are the values of the tension head at the upper and lower tensiometer at times t_1 and t_2, and Δz is the vertical distance of the tensiometer positions.
It is not clear the reason why the hydraulic conductivity equation is multiplied by 1/2 (equation A.1).
As described in detail by Schindler (1980) and Schindler et al. (2010), the simplified evaporation method relies on two assumptions: quasi steady state conditions, assuming that the flux and hydraulic gradient are approximately constant over the time interval; and a linear distribution of water content and suction over the sample height during each time interval. According to Schindler (1980) and Schindler & Müller (2006) these assumptions should hold for sand, silt, loam and peat soils. Despite water content and tension being nonlinear, taking short time intervals can make the non-linearity insignificant. Peters & Durner (2008) looked at the errors arising from the linearization assumptions in the simplified evaporation method.

They found them to be very small, in particular regarding the determination of the water retention curve.
Even though the HYPROP was not originally designed to be used for shrinking soils, its application has been extended to them by using a rubber membrane around the sample (Schindler & Mueller, 2013; Schindler et al., 2015). However, there seems to be no case in the literature where the HYPROP has been used with slurries. Maček et al. (2013) performed tests using high and low plasticity clays. They started with samples having water contents as high as 91%, but no mention was made of the plastic or liquid limits. Dolinar (2015) examined montmorillonite, calcium-montmorillonite and illite, utilizing initial water contents slightly over the liquid limit. The other experimental investigations found on the literature (Schindler et al., 2010; Campbell et al., 2012; Schindler et al., 2012; Maček et al., 2013; Schelle et al., 2013a; Schindler & Mueller, 2013; Eibisch et al., 2015; Schindler et al., 2015) seem to have been performed on samples starting from water contents below the liquid limit, based on the test description.
In this section adjustments to the prescribed test procedure and data interpretation of the HYPROP tests are proposed, in order to extend its use to the determination of the water retention properties of fine grained soils having initial consistency well above their liquid limit, and therefore showing significant shrinkage during drying.

A.1.2. Methodology

The HYPROP tests were performed in a climate controlled room with a relative humidity of 34% (± 6%) and a temperature of 24 ºC (± 1 ºC). They were conducted with the clay at five different initial conditions: two below and three above liquid limit (Table A.1). Additionally a test was carried out on water.

Table A.1: Initial conditions for the HYPROP tests.

Sample Name	Initial Water Fraction (m_w/m_t) (%)	Initial Water Content (m_w/m_s) (%)	Initial Water Ratio ($(m_w/m_s)*G_s$) (-)	Liquidity Index (-)
A	25	34	0.93	0,30
B	34	51	1.4	0.82
C	42	71	1.94	1.42
D	53	113	3.1	2.7
E	57	138	3.77	3.45
F	100	-	-	-

With respect to the standard test preparation techniques (UMS, 2012), special care was put in saturating the tips. They were saturated by putting them in a container with de-aired and demineralized water at approximately 50 ºC. The vessel was then subjected a vacuum of approximately -90 kPa in order to make the water with the tips boil. The process was repeated at least three times, or until there were no air bubbles observed in the acrylic tubes containing the ceramic tips. This technique proved to be as good as the procedure recommended by UMS and it managed to saturate the tips faster.

Some preliminary tests with slurry were performed using both tensiometers (data not reported here). Based on the observations done during those tests, it was decided to use only the short tensiometer shaft. The reasoning behind this choice is explained in the next section. In test A, the sample was prepared by pushing one of the provided metal rings directly into the clay block, conforming to the standard sampling procedure. For test B, the metal ring was carefully filled with a previously prepared clay paste by means of a spatula. Care was taken to minimize the inclusion of air pockets during the filling procedure. In both test A and B, the top and bottom were trimmed, and the holes for the tensiometers were drilled using the small hand auger supplied by UMS, as indicated in the HYPROP manual (UMS, 2012). Based on the measurement of water content and bulk density, it was found that the material was already in a saturated state.

A different method was employed for the preparation of the soil samples with water contents above liquid limit. The slurries were made by cutting the clay blocks into small pieces, which were then put in a steel container. Tap water was added until the desired water content was achieved. The clay-water mixture was stirred for 45 minutes in a Hobart A200N mixer at 200 rpm. The resultant slurry was deposited in a plastic container, where it was sealed and left for at least 24 hours to further homogenize. Then the HYPROP sensor unit was prepared with the short tensiometer shaft, and the ring was clamped on to it. Immediately afterwards, the slurry was poured in the device all the way to the top of the ring and the measurement was started. At the end of each test, the soil sample with the ring were placed in an oven for 24 hours at 105 ºC to determine the water content.

The data was recorded using TensioVIEW (UMS, 2013). Tension is assumed to be positive. Therefore, water pressure above the atmospheric value is indicated with negative values.

To assist with the interpretation of the data, additional tests were carried out in which the sensor unit was placed in a micro-CT-Scanner at regular time intervals (General Electric, Phoenix, Nanotom S). CT-scan analysis was performed on a clay slurry sample with an initial water content of 95%. In order to enable the X-rays to penetrate the soil sample, the steel ring was replaced by a PVC ring of the same dimensions. A voxel size of 0.065 mm was used for all images. The pictures were initially exported to VGStudio MAX (VolumeGraphics, 2013) and then they were processed with Avizo (FEI, 2013).

A.1.3. Results and Discussion

Preliminary Tests

During the preliminary tests, where the standard HYPROP procedure was followed using two tensiometers, it was observed that the tensiometer shafts created noticeable disturbances during the drying process. For the samples with high initial water contents, the long tensiometer shaft emerged above the surface of soil during the initial consolidation period. This rendered any tension measurements from the long tensiometer beyond that point meaningless.

The soil shrinkage also caused the tensiometer shafts to bend and get damaged. This was especially the case for the long tensiometer shaft, which in several occa-

sions was left permanently deformed. Since both shafts are fixed to the bottom of the sensor unit, their resistance against the shrinkage of the soil also resulted in the formation and propagation of cracks within the samples, which clearly affected the suction measurements.
Based on these observations, it was decided to only use the short tensiometer shaft, so as to minimize their disturbing effect on the sample. As a consequence, only one suction measurement was performed and the gradient of the hydraulic head could not be tracked.

Effect of Initial Water Content on the Measurements

Negative suctions were observed at the beginning of drying in samples with high initial water contents (above the liquid limit) indicating water pressures raising above the atmospheric pressure during the initial stages of the test. For the soils with relatively low initial water content (e.g. samples A and B, below the liquid limit), these negative suction values were measured at the beginning of the tests as a transient pressure during the brief adjustment period right after the sample was placed.
In the case of the samples with initial water contents above the liquid limit, the suction remained negative for a longer period, ranging from half a day for sample C to three days for sample E. The problem arises when trying to determine the instant at which the "true suction" begins to be measured, i.e. suction associated to a water deficit. When measuring slurries, this problem is compounded by the fact that the measurements from the tensiometer are a combination of several pressures acting together, but each one with a different magnitude. The pressures acting on the tensiometer can be classified as follows:

- The hydrostatic pressure produced by the water in the slurry. Initially it should increase linearly with depth, as long as the soil is fully saturated. Nevertheless, it is impossible to determine how the hydrostatic pressure will evolve as the soil dries. As described in Chapter 4, the water content will not evolve linearly with depth and it will depend directly on the evaporation rate
- The consolidation pressure which is generated right after the slurry is placed in the equipment and that is represented by an excess pore water pressure. It is not possible to accurately estimate it, since it will depend on the speed at which the soil settles, how long the soil is allowed to settle, if drying is involved during the settling process, etc.
- The water deficit pressure (i.e. suction) that will be produced as the soil dries. As observed in Chapter 4, the generation of suction in the soil changes with depth depending on the evaporation rate. As the drying process inside the HYPROP is time and space dependent, there can be parts of the soil in the device where suction is generated, while at the same time there can be other places where the soil remains fully saturated with no suction;
- The pressure shift that comes from the initial pressure offset of the equipment (it must be noted that the newer software provided by UMS (2016) does allow

A

for the possibility to reset the tensiometer to zero before a measurement campaign starts, which eliminates the need for correcting the initial measured value).

Figure A.1 presents a test performed in the HYPROP using only water. Since in this case there is no influence of consolidation, nor soil suction and the hydrostatic pressure always increases linearly with depth, the test exemplifies in a simple manner the effects of the initial equipment offset and the hydrostatic pressure. Figure A.1 shows the original measurement curve, the curve corrected for the initial equipment offset and the curve corrected for both, the initial offset and the hydrostatic pressure. This last curve provides the true suction measurement.
Until the tensiometer remains submerged under water, the value at the tip gives the pressure at the relevant depth below the water surface (curve corrected for offset). As soon as the tip emerges from the water, it starts measuring suction corresponding to the relative humidity of the air above the water (curve with both corrections), which can be identified as the "true suction". In the uncorrected data the point at which suction should start being measured is identified by the curve deviating from the initial linear slope.

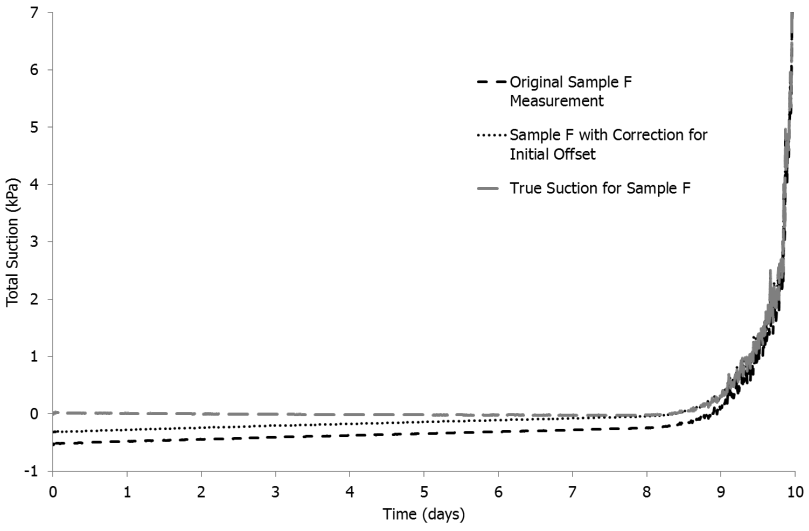

Figure A.1: Example of HYPROP measurements on water and different corrections carried out on the original readings.

The determination of the moment when the true suction is being measured in the HYPROP with slurry is not as easy as in the case of water, because it is affected by consolidation and non-uniform water content distribution. Nonetheless, taking previous considerations into account, it is proposed that a correction is carried out via a graphical method. As an example, Figure A.2 presents a comparison between the data from Sample E, the original data for Sample F (test with water) and the Sample F data corrected for the initial equipment offset. In the case of the slurry,

the correction for the initial offset is not as straightforward as with the water. The proposed method involves fitting a straight line (E'-E") to the initial part of the measured data (Figure A.3). The length and slope of this initial section of the curve will depend on the amount of evaporation. The higher the evaporation rate, the steeper and shorter the initial section is going to be. It is assumed that the point where the measured data deviates from the initial slope (the point is indicated with an arrow in Figure A.3) is the moment in which the equipment starts measuring net true soil suction. This position is considered to be the new zero and the rest of the data is adjusted accordingly giving as a result a corrected curve (Figure A.4).

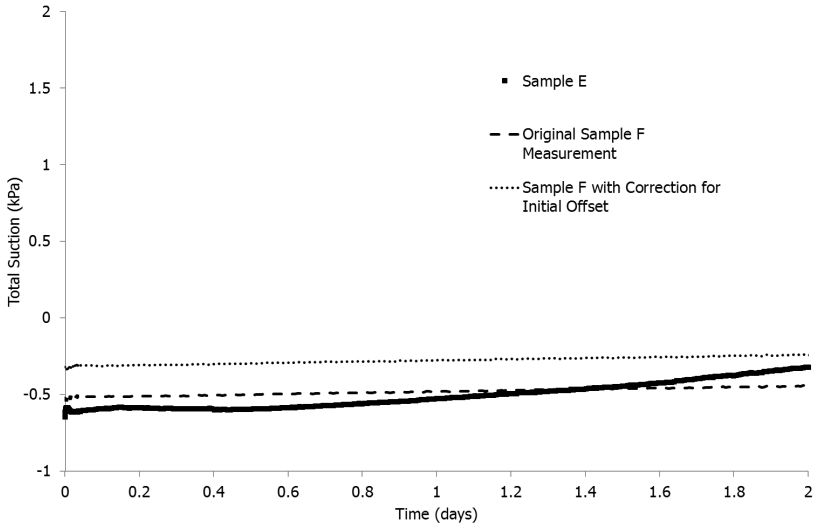

Figure A.2: Comparison between the data from Sample E, the original data for Sample F (test with water) and the Sample F data corrected for the initial equipment offset.

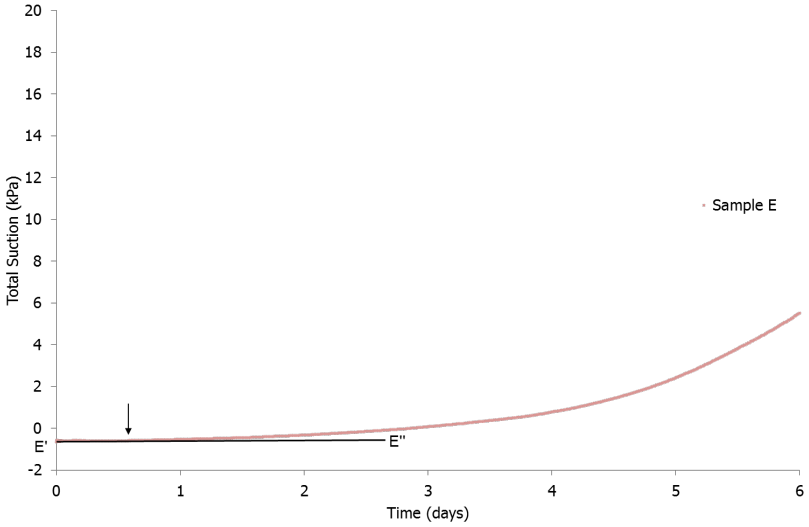

Figure A.3: Example of how to determine the correction, focusing of the first six days of the Sample E curve.

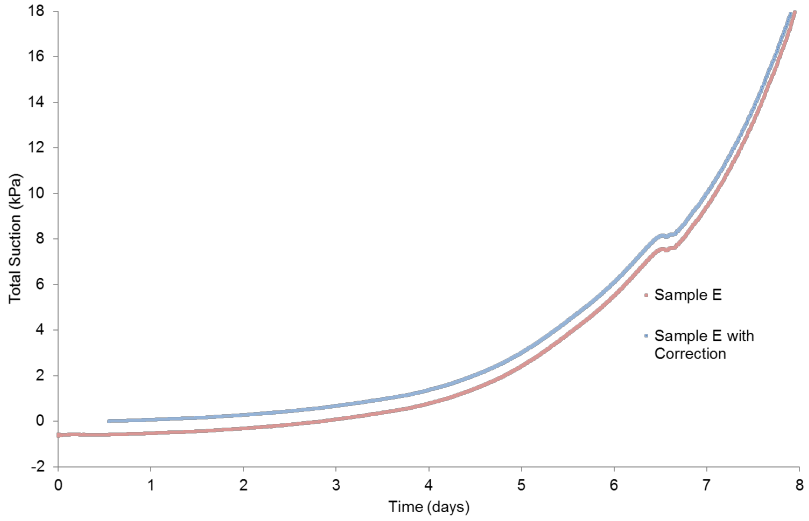

Figure A.4: Comparison of the original curve and the corrected curve.

Figure A.5 displays the results of all the measurements in terms of water ratio and suction. It also provides the results of the corrections for the curves that needed them. As it is clear from the figure, the correction had an effect only in the case of samples with high initial water content and at the suction range below 3 kPa.

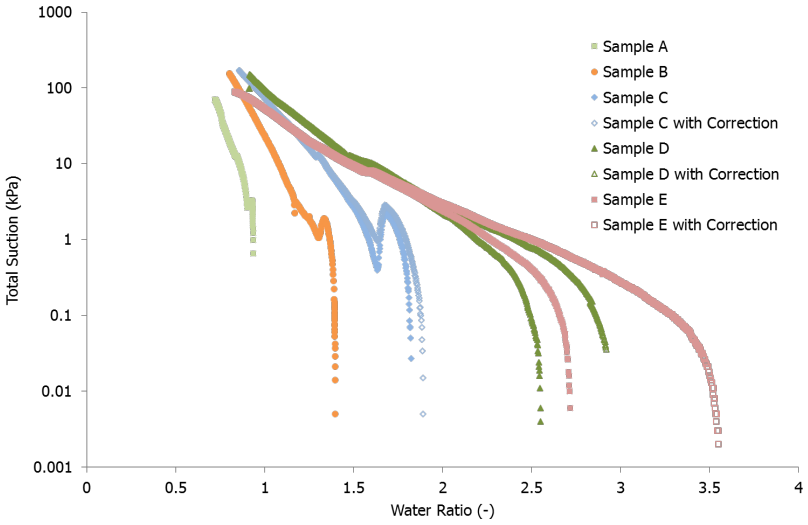

Figure A.5: Water retention curves for samples A to E including the curves with correction for the initial value.

Anomalies during the Measurements

For the tests on samples with different initial water content (A to F) the resulting suction development in time are shown in Figure A.6 and A.7. Most of the tests were stopped before the ceramic air entry point was reached, since the stage up to the boiling point of water was deemed to be the area of interest.

When the low range of suction values during the initial phase of drying were analyzed (Figure A.7), two distinctive features were noted that deviated from the expected results. Initially a temporary drop of tension was observed at relatively low suction values (between 1 and 4 kPa). This was particularly the case for the samples with low initial water content (samples A, B and C). The suction decreased gradually for several hours after which it started to increase again. In some cases the suction drop was related to the soil detachment from the ring. Pressure drops can also be observed in other studies using the HYPROP (Durner et al., 2011; Campbell et al., 2012; Maček et al., 2013; Peters, 2013; Şahin, 2013; Schelle et al., 2013a,b; Dolinar, 2015). Nevertheless, these authors made no mention of the phenomenon, nor did they provide an explanation for it.

Dynamic capillary pressure effects are extensively described in the literature related to multiphase flow in porous media. Rapid pressure drops can occur at pore scale when air suddenly fills a large pore body (Berkowitz & Ewing, 1998; Beliaev &

A

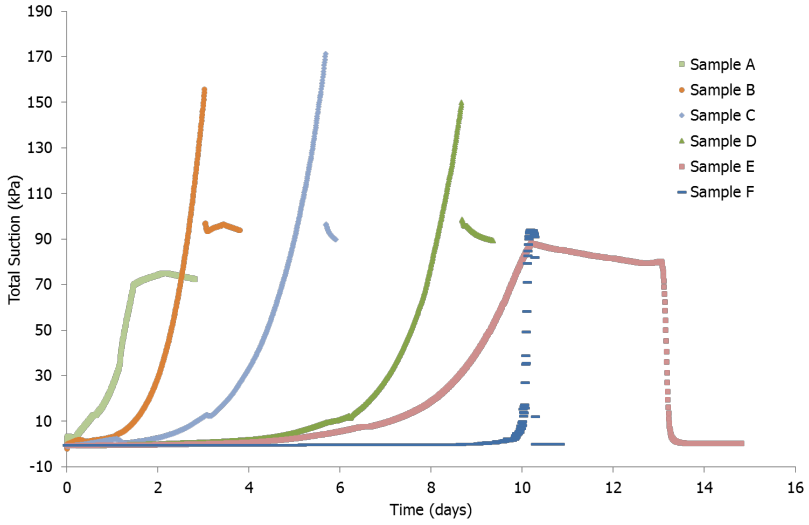

Figure A.6: Results for the entire test length from samples A to F in the HYPROP.

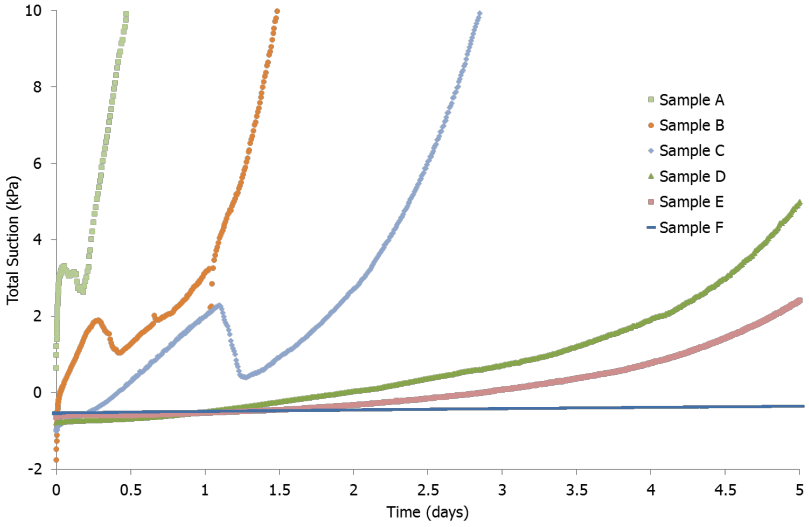

Figure A.7: Detail of the first five days of testing from samples A to F in the HYPROP.

Hassanizadeh, 2001) and they are commonly referred to as Haines jumps (Haines, 1930). In this case, the sudden decrease in suction can hardly be attributed to air entry, unless it occurred through cracks within the sample which were not clearly visible from the outside. Another possible cause for these jumps could be a relaxation of the soil following the detachment from the ring. However, the drop in suction not always happened when the soil separation from the ring was observed at the surface of the sample. It can be presumed that partial or total detachment from other parts of the equipment (e.g. the base of the apparatus) could produce similar pressure drops.

CT-Scan Analysis

The results of the measurements on the sample which was placed in the micro-CT-Scanner are presented in Figure A.8. The CT-scan images display a partial cross section (30 x 45 mm approximately) through the center of the soil sample. The outer portions of the image were discarded because of the disturbances generated by beam hardening and other artifacts during the scanning process.

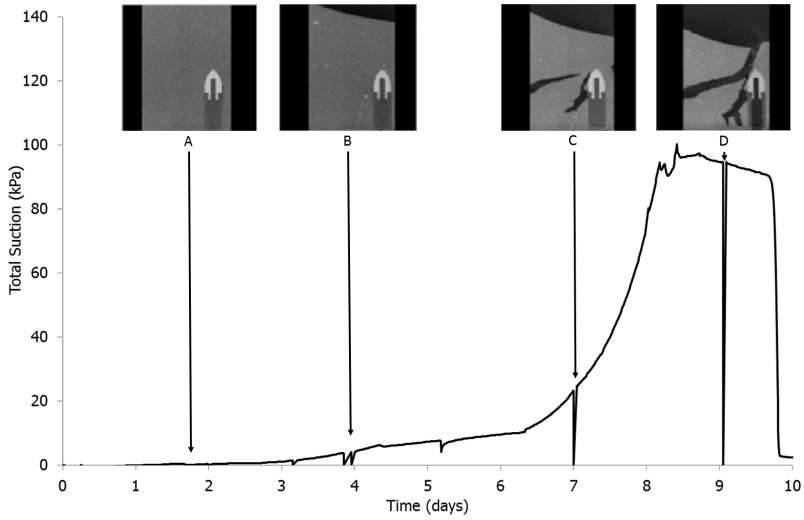

Figure A.8: Results of the HYPROP tests showing the suction development in a drying slurry, and the associated images from CT-scan analysis surrounding the tip of the short tensiometer shaft. The gray tone in the image is related to the material density. It ranges from black (e.g. air = 1 kg/m^3), through intermediate tones of gray (e.g. water = 1000 kg/m^3; soil = 1200-1500 kg/m^3), to white (porous aluminium oxide tip, ≈ 2500 kg/m^3).

Image A shows the condition of the sample after 1.5 days of drying. As time progressed, evaporation and consolidation took place in the soil producing mostly vertical deformation. However, as seen in Image B, the vertical displacement was not uniform. Resistance along the soil-ring interface produced differential settlements within the sample, with the soil in the proximity to the ring exhibiting less vertical displacement than the material towards the center of the sample.

After further evaporation the soil eventually detached from the ring. At this point the first cracks were observed at the surface of the sample. After approximately six days, cracks started to propagate towards the core of the sample, coming in close proximity to the tensiometer shaft (Image C). A second fracture also appeared right beside the shaft, which contributed to the early detachment of the soil from the ceramic tip, and possibly promoted the premature onset of cavitation in the tensiometer. Nonetheless, the measured tension remained below the boiling point of water, and therefore, within the specified allowable measurement range for the HYPROP. Based on the gray tones present in the images at this point, it can be concluded that the cracks were filled with air, whilst the tensiometer and the soil were still close to full saturation. The fact that the cracks did not reach the surface was a contributing factor in keeping the tensiometer at full saturation, since the air inside the crack probably had a relative humidity close to 100%.
After 8.5 days, the suction in the soil reached a stage between the boiling point of the water in the shaft and the air entry point of the ceramic tip. It seems that around this time the cracks around the tensiometer tip reached the surface, connecting the tip to the air outside the soil. The HYPROP manual (UMS, 2012, 2015) indicates that the cavitation point of the water in the tensiometer shaft as being approximately 85 kPa, whereas the air entry point of the tip is 880 kPa. It was found that careful saturation of the tips enabled to significantly delay the boiling point of the water in the tensiometer, increasing the measurement range of the equipment. Image D reveals the tensiometer shaft already full of air after cavitation. The fractures have likewise propagated to the surface of the sample, getting part of the ceramic tip in direct contact with the atmosphere.

A.1.4. Summary and Final Remarks

The HYPROP can be adapted to obtain an approximation of the water retention curve of slurries. Nonetheless, the values acquired link the suction at a fixed point with the average water content of the soil in the device. The use of the two tensiometers, which would give more information on the suction distribution, is not recommended. The soil shrinkage can cause the long tensiometer shafts to bend and get damaged. Moreover, the long tensiometer shaft generally emerges above the surface of soil during the initial consolidation period.
A correction for the hydrostatic water pressure and equipment offset should be implemented. However, this is relevant only for values of suction below 3 kPa.
CT-scans showed that cracks may start in the vicinity of the tensiometer tips while the soil is shrinking. Nevertheless, before the cracks connect the tensiometer tip to the atmosphere, the crack opening does not seem to substantially affect the soil suction measurements.
The fact that the tomographic images clearly display the emergence of cracks within the soil sample in the vicinity of the tensiometer tips, indicates that the assumption of a linear hydraulic gradient with depth is invalid. This and the unsuitability of using the long tensiometer in soils showing significant shrinkage make calculating the hydraulic conductivity from the measured suction data meaningless.

B

Appendix

B

B.1. Crack Patterns of Chapter 2 Experiments

Figure B.1: Crack pattern in 0.3 x 0.3 m board with 20 mm initial thickness and an initial water content of three times liquid limit approx. (170%).

Figure B.2: Crack pattern in 0.3 x 0.3 m board with 50 mm initial thickness and an initial water content of twice the liquid limit approx. (114%).

Figure B.3: Crack pattern in 0.3 x 0.3 m board with 50 mm initial thickness and an initial water content of three times liquid limit approx. (170%).

Figure B.4: Crack pattern in 0.5 x 0.5 m board with 20 mm initial thickness and an initial water content of three times liquid limit approx. (170%).

Figure B.5: Crack pattern in 0.5 x 0.5 m board with 50 mm initial thickness and an initial water content of three times liquid limit approx. (170%).

Figure B.6: Crack pattern in 0.5 x 0.5 m board with 100 mm initial thickness and an initial water content of twice the liquid limit approx. (114%).

Figure B.7: Crack pattern in 1 x 1 m board with 20 mm initial thickness and an initial water content of three times liquid limit approx. (170%).

Figure B.8: Crack pattern in 1 x 1 m board with 50 mm initial thickness and an initial water content of three times liquid limit approx. (170%).

Figure B.9: Crack pattern in 1 x 1 m board with 100 mm initial thickness and an initial water content of twice the liquid limit approx. (114%).

Figure B.10: Crack pattern in 0.4 x 0.4 m board with 40 mm initial thickness and an initial water content of twice the liquid limit approx. (114%).

Figure B.11: Crack pattern in 0.4 x 0.4 m board with 40 mm initial thickness and an initial water content of three times liquid limit approx. (170%).

Figure B.12: Crack pattern in 0.35 x 0.5 m board with 50 mm initial thickness and an initial water content of twice the liquid limit approx. (114%).

Figure B.13: Crack pattern in 0.35 x 0.5 m board with 50 mm initial thickness and an initial water content of three times liquid limit approx. (170%).

C

Appendix

C

C.1. Output of Chapter 3 Tests

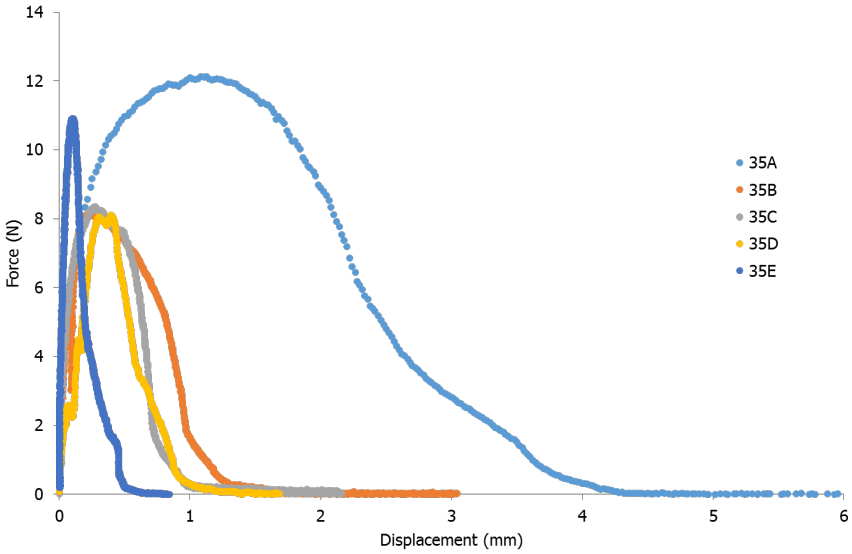

Figure C.1: Results for Test Set 35.

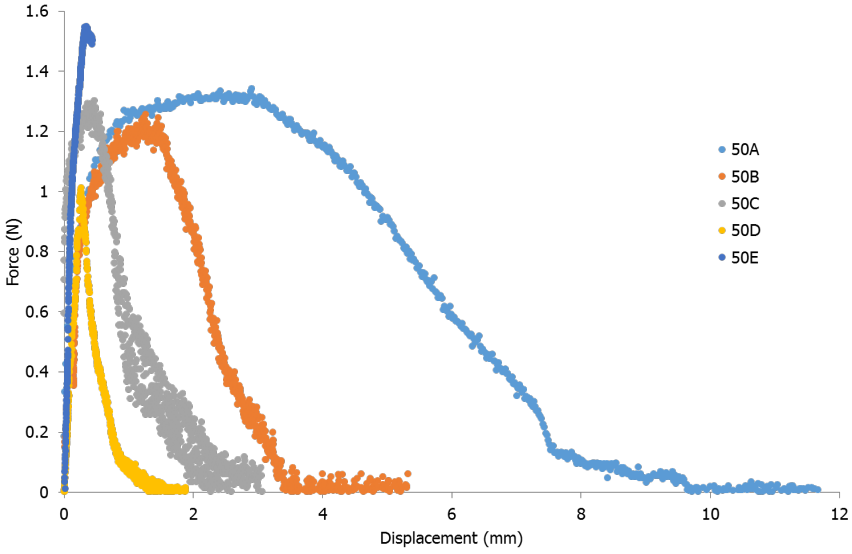

Figure C.2: Results for Test Set 50.

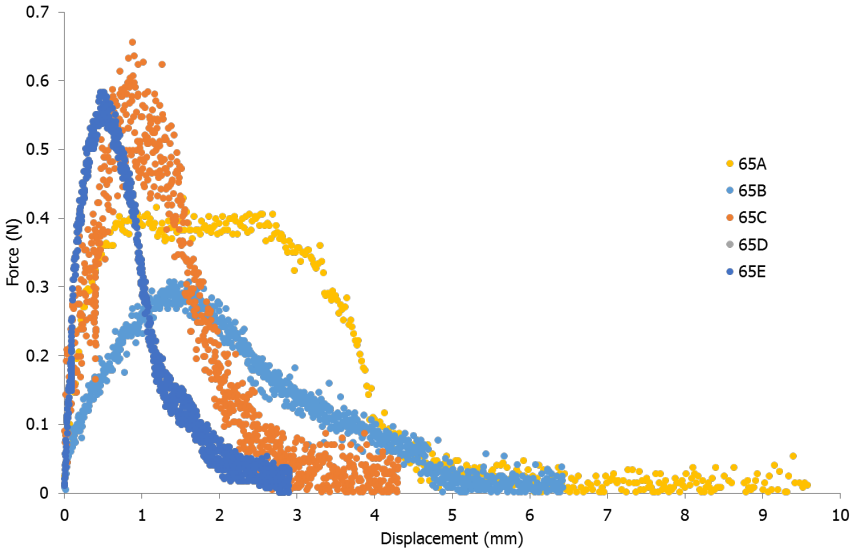

Figure C.3: Results for Test Set 65.

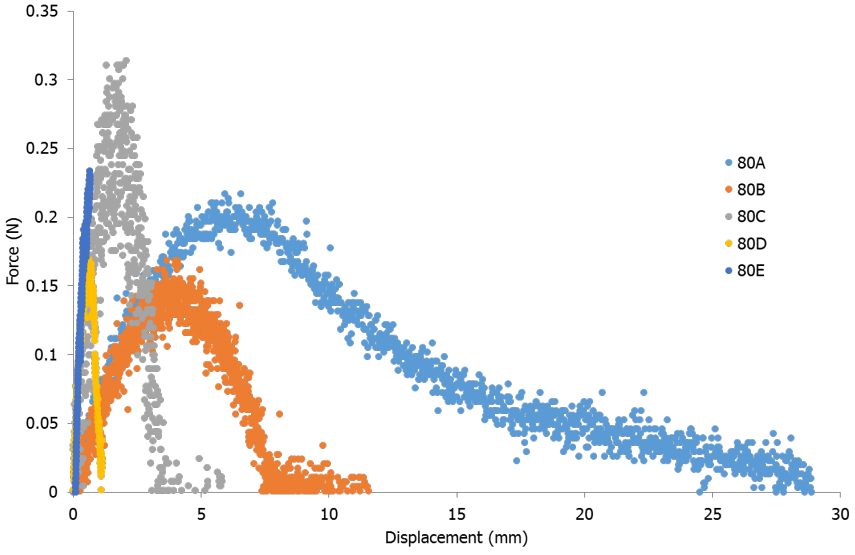

Figure C.4: Results for Test Set 80.

References

Abu-Hejleh, A., & Znidarčić, D. (1995). Desiccation theory for soft cohesive soils. *Journal of Geotechnical Engineering*, *121*, 493–502.

Ajaz, A., & Parry, R. H. G. (1974). Unconfined direct tension test for compacted clays. *Journal Testing and Evaluation*, *2*, 163–172.

Al Qadad, A., Shahrour, I., & Rouainia, M. (2012). Influence of the soil-atmosphere exchange on the hydric profile induced in soil-structure system. *Nat. Hazards Earth Syst. Sci.*, *12*, 2039–2049. NHESS.

Beckett, C. T. S., Smith, J. C., Ciancio, D., & Augarde, C. E. (2015). Tensile strengths of flocculated compacted unsaturated soils. *Géotechnique Letters*, *5*, 254–260.

Beliaev, A. Y., & Hassanizadeh, S. M. (2001). A theoretical model of hysteresis and dynamic effects in the capillary relation for two-phase flow in porous media. *Transport in Porous Media*, *43*, 487–510.

Berkowitz, B., & Ewing, R. P. (1998). Percolation theory and network modeling applications in soil physics. *Surveys in Geophysics*, *19*, 23–72.

Bittelli, M., Ventura, F., Campbell, G. S., Snyder, R. L., Gallegati, F., & Pisa, P. R. (2008). Coupling of heat, water vapor, and liquid water fluxes to compute evaporation in bare soils. *Journal of Hydrology*, *362*, 191–205.

Blazejczak, D., Horn, R., & Pytka, J. (1995). Soil tensile strength as affected by time, water content and bulk density. *Int. Agrophysics*, *9*, 179–188.

Blight, G. E. (2002). Measuring evaporation from soil surfaces for environmental and geotechnical purposes. *Water SA*, *28*, 381–394.

Blight, G. E. (2009). Solar heating of the soil and evaporation from a soil surface. *Géotechnique*, *59*, 355–363.

Briones, A. A., & Uehara, G. (1977). Soil elastic constants: II. Application to analysis of soil cracking. *Soil Sci. Soc. Am. J.*, *41*, 26–29.

Bronswijk, J. J. B. (1988). Modeling of water balance, cracking and subsidence of clay soils. *Journal of Hydrology*, *97*, 199–212. Doi: 10.1016/0022-1694(88)90115-1.

Campbell, C. S., Cobos, D. R., Rivera, L. D., Dunne, K. M., & Campbell, G. S. (2012). Constructing fast, accurate soil water characteristic curves by combining the wind/schindler and vapor pressure techniques. In *Unsaturated soils: Research and applications* (pp. 55–62). Springer.

Chandler, H. W. (1984). The use of non-linear fracture mechanics to study the fracture properties of soils. *Journal of Agricultural Engineering Research*, *29*, 321–327.

Corte, A., & Higashi, A. (1960). *Experimental Research on Desiccation Cracks in Soil, Research Report 66*. Technical Report , Wilmette, Illinois: US Army Snow Ice and Permafrost Research Establishment.

Corti, T., Wüest, M., Bresch, D., & Seneviratne, S. I. (2011). Drought-induced building damages from simulations at regional scale. *Nat. Hazards Earth Syst. Sci.*, *11*, 3335–3342.

Costa, S., Kodikara, J. K., & Shannon, B. (2013). Salient factors controlling desiccation cracking of clay in laboratory experiments. *Géotechnique*, *63*, 18–29.

Şahin, Y. (2013). *Laboratory Tests to Study Stability Mechanism of Rainfall Infiltrated Unsaturated Fine-grained Soil Slopes Developing Into Shallow Landslides and Their Hydraulic Properties*. Master's thesis İzmir Institute of Technology.

Cui, Y. J., & Zornberg, J. G. (2008). Water balance and evapotranspiration monitoring in geotechnical and geoenvironmental engineering. *Geotechnical and Geological Engineering*, *26*, 783–798.

Davidson, J. M., Nielsen, D. R., & Biggar, J. W. (1966). The dependence of soil water uptake and release upon the applied pressure increment. *Soil Science Society of America Journal*, *30*, 298–304.

De Souza Villar, L. F., De Campos, T. M. P., Azevedo, R. F., & Zornberg, J. G. (2009). Tensile strength changes under drying and its correlations with total and matric suctions. In *Proceedings of the 17th International Conference on Soil Mechanics and Geotechnical Engineering* (pp. 793–796). volume 1.

Dolinar, B. (2015). Prediction of the soil-water characteristic curve based on the specific surface area of fine-grained soils. *Bulletin of Engineering Geology and the Environment*, *74*, 697–703.

Durner, W., Iden, S. C., Schelle, H., & Peters, A. (2011). Determination of hydraulic properties of porous media across the whole moisture range. In *Schuhmann, R.(Hrsg): Workshop Innovative Feuchtemessung in Forschung und Praxis-Materialeigenschaften und Prozesse , 12.10.-14.10. 2011 am KIT, Karlsruhe*.

Eibisch, N., Durner, W., Bechtold, M., Fuß, R., Mikutta, R., Woche, S. K., & Helfrich, M. (2015). Does water repellency of pyrochars and hydrochars counter their positive effects on soil hydraulic properties? *Geoderma*, *245*, 31–39.

Elzeftawy, A., & Mansell, R. S. (1975). Hydraulic conductivity calculations for unsaturated steady-state and transient-state flow in sand. *Soil Science Society of America Journal*, *39*, 599–603.

Fang, H. Y., & Chen, W. F. (1972). Further study of double-punch test for tensile strength of soils. In *Proceedings of the 3rd Southeast Asian Conference on Soil Engineering* (pp. 236–242). volume 1.

Fang, H. Y., & Fernandez, J. (1981). Determination of tensile strength of soils by unconfined-penetration test. *ASTM STP*, *740*, 130–144.

Farrell, D. A., Greacen, E. L., & Larson, W. E. (1967). The effect of water content on axial strain in a loam soil under tension and compression. *Soil Sci. Soc. Am. J.*, *31*, 445–450.

Favaretti, M. (1995). Tensile strength of compacted clays. In E. E. Alonso, & P. Delage (Eds.), *Proceedings of the First International Conference on Unsaturated Soils, UNSAT'95, Paris, France. 6-8 September 1995* (pp. 51–56). Balkema, Rotterdam, Netherlands volume 1.

FEI (2013). *Avizo (Version 8.0)*. FEI Company, Hillsboro, Oregon, USA.

Garnier, P., Rieu, M., Boivin, P., Vauclin, M., & Baveye, P. (1997). Determining the hydraulic properties of a swelling soil from a transient evaporation experiment. *Soil Science Society of America Journal*, *61*, 1555–1563.

van Genuchten, M. T. (1980). A closed-form equation for predicting the hydraulic conductivity of unsaturated soils. *Soil Science Society of America Journal*, *44*, 892–898.

Groisman, A., & Kaplan, E. (1994). An experimental study of cracking induced by desiccation. *EPL (Europhysics Letters)*, *25*, 415–420.

Haberfield, C. M., & Johnston, I. W. (1989). Relationship between fracture toughness and tensile strength for geomaterials. In *International Conference on Soil Mechanics and Foundation Engineering, 12th, 1989, Rio de Janiero, Brazil* (pp. 47–52). volume 1.

Haines, W. B. (1923). The volume changes associated with variations of water content in soil. *J. Agric. Sci*, *13*, 296–310.

Haines, W. B. (1930). Studies in the physical properties of soil. v. the hysteresis effect in capillary properties, and the modes of moisture distribution associated therewith. *The Journal of Agricultural Science*, *20*, 97–116.

Haliburton, T. A. (1978). *Guidelines for dewatering/densifying confined dredged material, (No. WES-TR-DS-78-11)*. Technical Report , DTIC Document, Army Engineer Waterways Experiment Station, Vicksburg, Mississippi.

Hallett, P. D., Dexter, A. R., & Seville, J. P. K. (1995). The application of fracture mechanics to crack propagation in dry soil. *European Journal of Soil Science*, *46*, 591–599.

Hallett, P. D., & Newson, T. A. (2001). A simple fracture mechanics approach for assessing ductile crack growth in soil. *Soil Sci. Soc. Am. J.*, *65*, 1083–1088.

Hallett, P. D., & Newson, T. A. (2005). Describing soil crack formation using elastic–plastic fracture mechanics. *European Journal of Soil Science*, *56*, 31–38.

Harison, J., Hardin, B., & Mahboub, K. (1994). Fracture toughness of compacted cohesive soils using ring test. *Journal of Geotechnical Engineering*, *120*, 872–891.

Hasegawa, H., & Ikeuti, M. (1966). On the tensile strength test of disturbed soils. In *Rheology and Soil Mechanics/Rhéologie et Mécanique des Sols* (pp. 405–412). Springer.

Hassanizadeh, S. M., Celia, M. A., & Dahle, H. K. (2002). Dynamic effect in the capillary pressure–saturation relationship and its impacts on unsaturated flow. *Vadose Zone Journal*, *1*, 38–57.

Heibrock, G., Zeh, R. M., & Witt, K. J. (2005). Tensile strength of compacted clays. In T. Schanz (Ed.), *Unsaturated Soils: Experimental Studies* chapter 30. (pp. 395–412). Springer Berlin Heidelberg volume 93 of *Springer Proceedings in Physics*.

Hellwig, D. H. R. (1973). Evaporation of water from sand, 4: The influence of the depth of the water-table and the particle size distribution of the sand. *Journal of Hydrology*, *18*, 317–327.

Hillel, D. (1980). *Applications of soil physics*. New York: Academic Press.

Holmes, R. M. (1961). Estimation of soil moisture content using evaporation data. In *Proceedings of Hydrology Symposium* (pp. 184–196). Queen's Printer, Ottawa volume 2.

Ibarra, S. Y., McKyes, E., & Broughton, R. S. (2005). Measurement of tensile strength of unsaturated sandy loam soil. *Soil and Tillage Research*, *81*, 15–23.

Jommi, C., Valimberti, N., Tollenaar, R. N., Della Vecchia, G., & van Paassen, L. A. (2016). Modelling desiccation cracking in a homogenous soil clay layer: comparison between different hypotheses on constitutive behaviour. In *E3S Web of Conferences* (p. 08006). EDP Sciences volume 9.

Kayyal, M. K. (1995). Effect of the moisture evaporative stages on the development of shrinkage cracks in soil. In *Proceedings of First International Conference on Unsaturated Soils* (pp. 373–379).

Kies, J. A., Sullivan, A. M., & Irwin, G. R. (1950). Interpretation of fracture markings. *Journal of Applied Physics*, *21*, 716–720.

Kim, T. H., Kim, C. K., Jung, S. J., & Lee, J. H. (2007). Tensile strength characteristics of contaminated and compacted sand-bentonite mixtures. *Environmental Geology*, *52*, 653–661.

Kim, T. H., Kim, T. H., Kang, G., & Ge, L. (2012). Factors influencing crack-induced tensile strength of compacted soil. *Journal of Materials in Civil Engineering*, *24*, 315–320.

Kindle, E. M. (1917). Some factors affecting the development of mud-cracks. *The Journal of Geology*, *25*, 135–144.

Kitsunezaki, S. (2009). Crack propagation speed in the drying process of paste. *Journal of the Physical Society of Japan*, *78*, 064801.

Knight, J. (2005). Processes of soft-sediment clast formation in the intertidal zone. *Sedimentary Geology*, *181*, 207–214.

Kodikara, J. K., Barbour, S. L., & Fredlund, D. G. (1999). Changes in clay structure and behaviour due to wetting and drying. In N. D. Vitharana, & R. Colman (Eds.), *Proceedings 8th Australia New Zealand Conference on Geomechanics: Consolidating Knowledge* (pp. 179–185). Barton, ACT: Australian Geomechanics Society.

Kodikara, J. K., Barbour, S. L., & Fredlund, D. G. (2000). Desiccation cracking of soil layers. In *Proceedings of the Asian Conference on Unsaturated Soils, UNSAT-Asia 2000, Singapore* (pp. 693–698). Balkema.

Kodikara, J. K., Nahlawi, H., & Bouazza, A. (2004). Modelling of curling in desiccating clay. *Canadian Geotechnical Journal*, *41*, 560–566.

Konrad, J. M., & Ayad, R. (1997). A idealized framework for the analysis of cohesive soils undergoing desiccation. *Canadian Geotechnical Journal*, *34*, 477–488.

Lakshmikantha, M. R., Prat, P. C., & Ledesma, A. (2006). An experimental study of cracking mechanisms in drying soils. In *Proceedings of the 5th international conference on environmental geotechnics. Thomas Telford, London* (pp. 533–540).

Lakshmikantha, M. R., Prat, P. C., & Ledesma, A. (2012). Experimental evidence of size effect in soil cracking. *Canadian Geotechnical Journal*, *49*, 264–284.

Lakshmikantha, M. R., Reig, R., Prat, P. C., & Ledesma, A. (2013). Origin and mechanism of cracks seen at the bottom of a desiccating soil specimen. In *Geo-Congress 2013 Stability and Performance of Slopes and Embankments III* (pp. 790–799). ASCE.

Lau, J. T. K. (1987). *Desiccation cracking of clay soils*. Master's thesis Department of Civil Engineering, University of Saskatchewan, Saskatoon, Canada.

Leavell, D. A., & Peters, J. F. (1987). *Uniaxial Tensile Test for Soil, (No. WES/TR/GL-87-10)*. Technical Report , Army Engineer Waterways Experiment Station, Geotechnical Lab, Vicksburg, Mississippi.

Lee, F. H., Lo, K. W., & Lee, S. L. (1988). Tension crack development in soils. *Journal of Geotechnical Engineering*, *114*, 915–929.

Maček, M., Smolar, J., & Petkovšek, A. (2013). Extension of measurement range of dew-point potentiometer and evaporation method. In *Proceedings of the 18th International Conference on Soil Mechanics and Geotechnical Engineering, Paris* (pp. 1137–1142).

MedCalc (2016). *Digimizer, version 4.6.1*. MedCalc Software bvba, Acacialaan 22, 8400 Ostend, Belgium.

Mikulitsch, W. A., & Gudehus, G. (1995). Uniaxial tension, biaxial loading and wetting tests on loess. In *Proceedings of the First International Conference on Unsaturated Soils, UNSAT'95, Paris, France. 6-8 September 1995* (pp. 145–150). volume 1.

Müller, G., & Dahm, T. (2000). Fracture morphology of tensile cracks and rupture velocity. *Journal of Geophysical Research: Solid Earth*, *105*, 723–738.

Morris, P. H., Graham, J., & Williams, D. J. (1992). Cracking in drying soils. *Canadian Geotechnical Journal*, *29*, 263–277.

Morris, P. H., Graham, J., & Williams, D. J. (1994). Crack depths in drying clays using fracture mechanics. In *Fracture mechanics applied to geotechnical engineering* (pp. 40–53). ASCE.

Murray, I., Tarantino, A., & Francescon, F. (2014). Crack formation in clayey geomaterials subjected to tensile (total) stress. In *Unsaturated Soils: Research and Applications* (pp. 823–828). CRC Press. Doi:10.1201/b17034-117.

Nahlawi, H., Chakrabarti, S., & Kodikara, J. K. (2004). A direct tensile strength testing method for unsaturated geomaterials. *ASTM Geotechnical Testing Journal*, *27*, 356–361.

Nahlawi, H., & Kodikara, J. K. (2002). Experimental observations on curling of desiccating clay. In J. F. T. Juca, T. M. P. De Campos, & F. A. M. Marinho (Eds.), *Proc. 3rd International Conference on Unsaturated Soils, UNSAT 2002, Recife, Brazil* (pp. 553–556). A. A. Balkema, Rotterdam, The Netherlands.

Nahlawi, H., & Kodikara, J. K. (2006). Laboratory experiments on desiccation cracking of thin soil layers. *Geotechnical and Geological Engineering*, *24*, 1641–1664.

Nearing, M. A., Parker, S. C., Bradford, J. M., & Elliot, W. J. (1991). Tensile strength of thirty-three saturated repacked soils. *Soil Sci. Soc. Am. J*, *55*, 1546–1551.

Nearing, M. A., West, L. T., & Bradford, J. M. (1988). Consolidation of an unsaturated illitic clay soil. *Soil Sci. Soc. Am. J.*, *52*, 929–933.

Penman, H. L. (1941). Laboratory experiments on evaporation from fallow soil. *The Journal of Agricultural Science*, *31*, 454–465.

Penman, H. L. (1948). Natural evaporation from open water, bare soil and grass. In *Proceedings of the Royal Society of London A: Mathematical, Physical and Engineering Sciences* (pp. 120–145). The Royal Society volume 193.

Peron, H., Hu, L. B., Laloui, L., & Hueckel, T. (2007). Mechanisms of desiccation cracking of soil: Validation. In *Numerical Models in Geomechanics: Numog X* (pp. 277–282). Taylor and Francis Inc, 1900 Frost Road, Suite 101, Bristol, Pa 19007 USA.

Peron, H., Hueckel, T., Laloui, L., & Hu, L. B. (2009). Fundamentals of desiccation cracking of fine-grained soils: experimental characterisation and mechanisms identification. *Canadian Geotechnical Journal*, *46*, 1177–1201.

Peters, A. (2013). Simple consistent models for water retention and hydraulic conductivity in the complete moisture range. *Water Resources Research*, *49*, 6765–6780.

Peters, A., & Durner, W. (2008). Simplified evaporation method for determining soil hydraulic properties. *Journal of Hydrology*, *356*, 147–162.

Philip, J. R. (1957). Evaporation, and moisture and heat fields in the soil. *Journal of Meteorology*, *14*, 354–366.

Prat, P. C., Ledesma, A., Lakshmikantha, M. R., Levatti, H., & Tapia, J. (2008). Fracture mechanics for crack propagation in drying soils. In *Proceedings of the 12th International Conference of the International Association for Computer Methods and Advances in Geomechanics, IACMAG* (pp. 1060–1067). volume 12.

Rodríguez, R. (2006). Hydrogeotechnical characterization of a metallurgical waste. *Canadian Geotechnical Journal*, *43*, 1042–1060.

Rodríguez, R., Sánchez, M., Ledesma, A., & Lloret, A. (2007). Experimental and numerical analysis of desiccation of a mining waste. *Canadian Geotechnical Journal*, *44*, 644–658.

Rodríguez, R. (2002). *Estudio experimental de flujo y transporte de cromo, níquel y manganeso en residuos de la zona minera de Moa (Cuba): influencia del comportamiento hidromecánico*. Ph.D. thesis Universidad Politécnica de Cataluña. Escuela Técnica Superior de ingenieros de caminos, canales y puertos de Barcelona. Departamento de ingeniería y terreno y cartografía. Barcelona.

Sattler, P., & Fredlund, D. G. (1989). Use of thermal conductivity sensors to measure matric suction in the laboratory. *Canadian Geotechnical Journal*, *26*, 491–498.

Schelle, H., Heise, L., Jänicke, K., & Durner, W. (2013a). Wasserretentionseigenschaften von böden über den gesamten feuchtebereich-ein methodenvergleich. In *Beiträge zur 15. Lysimetertagung, 16.-17.4.2013, HBFLA Raumberg-Gumpenstein*.

Schelle, H., Heise, L., Jänicke, K., & Durner, W. (2013b). Water retention characteristics of soils over the whole moisture range: A comparison of laboratory methods. *European Journal of Soil Science*, *64*, 814–821.

Scherer, G. W. (1990). Theory of drying. *Journal of the American Ceramic Society*, *73*, 3–14.

Scherer, G. W., & Smith, D. M. (1995). Cavitation during drying of a gel. *Journal of Non-Crystalline Solids*, *189*, 197–211.

Schindler, U. (1980). Ein schnellverfahren zur messung der wasserleitfahigkeit im teilgesattigten boden and stechzylinderproben. *Archiv fur Acker-und Pflanzenbau und Bodenkunde, Berlin*, *24*, 1–7.

Schindler, U., Doerner, J., & Mueller, L. (2015). Simplified method for quantifying the hydraulic properties of shrinking soils. *Journal of Plant Nutrition and Soil Science*, *178*, 136–145.

Schindler, U., Durner, W., von Unold, G., Mueller, L., & Wieland, R. (2010). The evaporation method: Extending the measurement range of soil hydraulic properties using the air-entry pressure of the ceramic cup. *J. Plant Nutr. Soil Sci*, *173*, 563–572.

Schindler, U., & Müller, L. (2006). Simplifying the evaporation method for quantifying soil hydraulic properties. *Journal of plant nutrition and soil science*, *169*, 623–629.

Schindler, U., & Mueller, L. (2013). Novel method for the simultaneous quantification of soil hydraulic functions in the laboratory under consideration of shrinkage. In *EGU General Assembly Conference Abstracts* (pp. 14–15). volume 15.

Schindler, U., Mueller, L., da Veiga, M., Zhang, Y., Schlindwein, S., & Hu, C. (2012). Comparison of water□retention functions obtained from the extended evaporation method and the standard methods sand/kaolin boxes and pressure plate extractor. *Journal of Plant Nutrition and Soil Science*, *175*, 527–534.

Schroeder, W. (2017). *Perspective Image Correction, version 2.0.0.3*. Wolfgang.Schroeder2@gmx.de.

Schultze, B., Ippisch, O., Huwe, B., & Durner, W. (1997). Dynamic nonequilibrium during unsaturated water flow. In M. T. van Genuchten, F. J. Leij, & L. Wu (Eds.), *Proceedings of the international workshop on characterization and measurement of the hydraulic properties of unsaturated porous media, October 22-24, 1997, University of California, Riverside, California, USA* (pp. 877–892). Citeseer.

Shin, H., & Santamarina, J. C. (2011). Desiccation cracks in saturated fine-grained soils: particle-level phenomena and effective-stress analysis. *Géotechnique*, *61*, 961–972.

Silvestri, V., Soulié, M., Lafleur, J., Sarkis, G., & Bekkouche, N. (1990). Foundation problems in champlain clays during droughts. i: Rainfall deficits in montréal (1930–1988). *Canadian Geotechnical Journal*, *27*, 285–293.

Smiles, D. E., Vachaud, G., & Vauclin, M. (1971). A test of the uniqueness of the soil moisture characteristic during transient, nonhysteretic flow of water in a rigid soil. *Soil Science Society of America Journal*, *35*, 534–539.

Snyder, V. A., & Miller, R. D. (1985). A pneumatic fracture method for measuring the tensile strength of unsaturated soils1. *Soil Sci. Soc. Am. J.*, *49*, 1369–1374.

Song, W. K. (2014). *Experimental investigation of water evaporation from sand and clay using an environmental chamber*. Ph.D. thesis Université Paris Est.

Song, W. K., Cui, Y. J., Tang, A. M., Ding, W. Q., & Wang, Q. (2016). Experimental study on water evaporation from compacted clay using environmental chamber. *Canadian Geotechnical Journal*, *53*, 1293–1304.

Stanier, S. A., Blaber, J., Take, W. A., & White, D. J. (2015). Improved image-based deformation measurement for geotechnical applications. *Canadian Geotechnical Journal*, *53*, 727–739.

Stirling, R. A., Hughes, P., Davie, C. T., & Glendinning, S. (2015). Tensile behaviour of unsaturated compacted clay soils - A direct assessment method. *Applied Clay Science*, *112*, 123–133.

Tamrakar, S. B., Mitachi, T., & Toyosawa, Y. (2007). Factors affecting tensile strength measurement and modified tensile strength measuring apparatus for soil. In *Experimental Unsaturated Soil Mechanics* (pp. 207–218). Springer.

Tamrakar, S. B., Toyosawa, Y., Mitachi, T., & Itoh, K. (2005). Tensile strength of compacted and saturated soils using newly developed tensile strength measuring apparatus. *Soils and Foundations*, *45*, 103–110.

Tang, C. S., Cui, Y. J., Tang, A. M., & Shi, B. (2010a). Experiment evidence on the temperature dependence of desiccation cracking behavior of clayey soils. *Engineering Geology*, *114*, 261–266.

Tang, C. S., Shi, B., Liu, C., Gao, L., & Inyang, H. I. (2010b). Experimental investigation of the desiccation cracking behavior of soil layers during drying. *Journal of Materials in Civil Engineering*, *23*, 873–878.

Tang, C. S., Shi, B., Liu, C., Suo, W. B., & Gao, L. (2011). Experimental characterization of shrinkage and desiccation cracking in thin clay layer. *Applied Clay Science*, *52*, 69–77.

Tang, C. S., Shi, B., Liu, C., Zhao, L., & Wang, B. (2008). Influencing factors of geometrical structure of surface shrinkage cracks in clayey soils. *Engineering Geology*, *101*, 204–217.

Tollenaar, R. N., Paassen, L. A. v., & Jommi, C. (2017a). Experimental evaluation of the effects of pull rate on the tensile behaviour of a clay. Applied Clay Science (accepted for publication, CLAY 4269).

Tollenaar, R. N., Paassen, L. A. v., & Jommi, C. (2017b). Observations on the desiccation and cracking of clay layers. Engineering Geology (revised, after acceptance subject moderate revision, ENGEO 2017 95).

Tollenaar, R. N., Paassen, L. A. v., & Jommi, C. (2017c). Small scale evaporation tests on a clay: Influence of drying rate on a clayey soil layer. Canadian Geotechnical Journal (revised, after acceptance subject to major revision, cgj-2017-0061).

Topp, G. C., Klute, A., & Peters, D. B. (1967). Comparison of water content-pressure head data obtained by equilibrium, steady-state, and unsteady-state methods. *Soil Science Society of America Journal*, *31*, 312–314.

Towner, G. D. (1987). The tensile stress generated in clay through drying. *Journal of Agricultural Engineering Research*, *37*, 279–289.

Trabelsi, H., Jamei, M., Zenzri, H., & Olivella, S. (2012). Crack patterns in clayey soils: Experiments and modeling. *International Journal for Numerical and Analytical Methods in Geomechanics*, *36*, 1410–1433.

Tripathy, S., Bag, R., & Thomas, H. R. (2010). Desorption and consolidation behaviour of initially saturated clays. In E. E. Alonso, & A. Gens (Eds.), *Proceedings of the 5th International Conference on Unsaturated Soils, Barcelona* (pp. 381–386). Taylor and Francis, London volume 1.

Tripathy, S., Tadza, M. Y. M., & Thomas, H. R. (2014). Soil-water characteristic curves of clays. *Canadian Geotechnical Journal*, *51*, 869–883.

Tschebotarioff, G. P., Ward, E. R., & DePhilippe, A. A. (1953). The tensile strength of disturbed and recompacted soils. In *Proc. of the 3rd Int. Conf. Soil. Mech. Fond. Eng.* (pp. 207–210). volume 1.

Turner, C. E., & Kolednik, O. (1994). Application of energy dissipation rate arguments to stable crack growth. *Fatigue and Fracture of Engineering Materials and Structures*, *17*, 1109–1127.

Turner, C. E., & Kolednik, O. (1997). A simple test method for energy dissipation rate, CTOA and the study of size and transferability effects for large amounts of ductile crack growth. *Fatigue and Fracture of Engineering Materials and Structures*, *20*, 1507–1528.

UMS (2012). *User Manual HYPROP, version 02.13*. UMS GmbH, Munich, Germany.

UMS (2013). *tensioVIEW, version 1.9.104*. UMS GmbH, Munich, Germany.

UMS (2015). *Operation Manual HYPROP, version 2015.01*. UMS GmbH, Munich, Germany.

UMS (2016). *HYPROP-VIEW, version 1.2.2*. UMS GmbH, Munich, Germany.

Vogel, H. J., Hoffmann, H., & Roth, K. (2005). Studies of crack dynamics in clay soil: I. Experimental methods, results, and morphological quantification. *Geoderma*, *125*, 203–211.

VolumeGraphics (2013). *VGStudio Max (Version 2.2)*. Volume Graphics GmbH.

Vomocil, J. A., Waldron, L. J., & Chancellor, W. J. (1961). Soil tensile strength by centrifugation1. *Soil Sci. Soc. Am. J.*, *25*, 176–180.

Wana-Etyem, C. (1984). *Static and dynamic water content-pressure head relations of porous media*. Ph.D. thesis Colorado State University.

Wang, J., Zhu, J., Chiu, C. F., & Chai, H. (2007). Experimental study on fracture behavior of a silty clay. *Geotechnical Testing Journal*, *30*, 303.

Watson, K. K., & Whisler, F. D. (1968). System dependence of the water content-pressure head relationship. *Soil Science Society of America Journal*, *32*, 121–123.

Weinberger, R. (1999). Initiation and growth of cracks during desiccation of stratified muddy sediments. *Journal of Structural Geology*, *21*, 379–386.

Weinberger, R. (2001). Evolution of polygonal patterns in stratified mud during desiccation: The role of flaw distribution and layer boundaries. *Bulletin of the Geological Society of America*, *113*, 20–31.

White, D. J., Take, W. A., & Bolton, M. D. (2003). Soil deformation measurement using particle image velocimetry (PIV) and photogrammetry. *Géotechnique*, *53*, 619–632.

White, W. N. (1932). *A method of estimating ground-water supplies based on discharge by plants and evaporation from soil: results of investigations in Escalante Valley, Utah* volume 659. US Government Printing Office.

Wildenschild, D., Hopmans, J. W., & Simunek, J. (2001). Flow rate dependence of soil hydraulic characteristics. *Soil Science Society of America Journal*, *65*, 35–48.

Wilson, G. W., Fredlund, D. G., & Barbour, S. L. (1994). Coupled soil-atmosphere modelling for soil evaporation. *Canadian Geotechnical Journal*, *31*, 151–161.

Wilson, G. W., Fredlund, D. G., & Barbour, S. L. (1997). The effect of soil suction on evaporative fluxes from soil surfaces. *Canadian Geotechnical Journal*, *34*, 145–155.

Wind, G. P. (1966). Capillary conductivity data estimated by a simple method. In P. Rijtema, & H. Wassink (Eds.), *International Association of Scientific Hydrology, Proceedings of the Wageningen Symposium, Water in the Unsaturated Zone, 19-23 June 1966*. Int. Assoc. Sci. Hydrol. Publ. (IASH), Gentbrugge, The Netherlands and UNESCO, Paris.

Woodworth, J. B. (1895). Some features of joints. *Science*, *2*, 903–904.

Woodworth, J. B. (1896). On the fracture system of joints: With remarks on certain fractures. *Boston Society of Natural History Proceedings*, *27*, 163–184.

Yanful, E. K., & Choo, L.-P. (1997). Measurement of evaporative fluxes from candidate cover soils. *Canadian Geotechnical Journal*, *34*, 447–459.

Yanful, E. K., Mousavi, S. M., & Yang, M. (2003). Modeling and measurement of evaporation in moisture-retaining soil covers. *Advances in Environmental Research*, *7*, 783–801.

Yang, M., & Yanful, E. K. (2002). Water balance during evaporation and drainage in cover soils under different water table conditions. *Advances in Environmental Research*, *6*, 505–521.

Yoshida, S., & Hallett, P. D. (2008). Impact of hydraulic suction history on crack growth mechanics in soil. *Water Resources Research*, *44*, W00C01.

Zabat, M., Vayer-Besançon, M., Harba, R., Bonnamy, S., & Van Damme, H. (1997). Surface topography and mechanical properties of smectite films. In *Trends in Colloid and Interface Science XI* (pp. 96–102). Springer.

Zielinski, M., Sánchez, M., Romero, E., & Atique, A. (2014). Precise observation of soil surface curling. *Geoderma*, *226-227*, 85–93.

Summary

Waterways and lakes in low-lying delta areas require regular dredging for maintenance. Reuse of dredged sediments has been proposed for various applications. However, directly after dredging the physical characteristics of these sediments make them generally unsuited for immediate reuse. They are often placed on land, where they are allowed to ripen through a combination of drainage, consolidation and evaporation. At a certain stage during the desiccation process cracks will develop, affecting the physical properties of the material. These include its strength, stiffness and hydraulic conductivity, as well as drainage, water infiltration and evaporation. The soil composition can be likewise altered by biochemical processes, which are stimulated by the ingress of oxygen through the cracked surface. Consequently, identifying how cracks develop in the soil is essential for understanding the behavior of the material.

Much investigation has been performed studying desiccation cracks, but the underlying mechanisms are still not fully understood. It is known that the drying speed affects the final amount of cracks in a soil, which points out to the potential impact of rate effects in soil cracking. The effects of the drying rate might be related to variations in the tensile strength influenced by different shrinkage rates, as well as its impact on the suction development in the soil.

In this thesis different sets of experiments were carried out to study the phenomenon of desiccation fracturing in soil. The first series of tests were carried out in a controlled laboratory environment to study the crack development in drying clay slurries under different initial and boundary conditions. The outcomes of those tests indicated that cracks can propagate in a different way than commonly assumed (namely under the surface) and that fracture characteristics strongly depend on the initial and boundary conditions.

A second series of tests examined the combined effects of pull rates and high water contents on the tensile strength. Particle Image Velocimetry analysis was also carried out on pictures taken during the tests to examine the strains generated. It was found that the effect of pull rate on the tensile strength of the clay was negligible compared to the effect of the water content. Pull rate did affect the stiffness response of the soil. The findings revealed that the influence of the evaporation rate on soil fracturing might be related more to the rate dependency of the stiffness rather than to significant changes in tensile strength.

The last series of experiments investigated the drying behaviour of a clay with different initial water contents and under different evaporative conditions. The small scale evaporation experiments carried out using commercially available suction measuring equipment with an adjusted test procedure. The results showed that the initial conditions have great influence on the drying performance of a soil, which can be partly attributed to the influence of the surface texture and the pore

structure. It was observed that under certain circumstances, the evaporation of a soil surface can be higher than that of open water. The different evaporation rates had a marked effect on the water distributions with depth within the soil. The evaporation rate also produced a dynamic response of the soil water retention curve.
At the end, a simple one-dimensional model was set up to try to capture the behavior observed during all the laboratory tests. It also served to analyze the consequences of different hypotheses about the material behaviour on the crack onset in a homogenous soil layer undergoing surface drying.

Samenvatting

Het onderhoud van waterwegen en meren in laaggelegen delta's vereist regelmatig baggeren. Hergebruik van vrijgekomen baggerslib is voor diverse toepassingen voorgesteld. Echter, de fysieke eigenschapen van deze sedimenten direct na het baggeren maken ze ongeschikt voor onmiddellijk hergebruik. Ze worden vaak op land gebracht om te rijpen door een combinatie van drainage, consolidatie en verdamping. Tijdens dit proces ontwikkelen zich op een bepaald moment verdrogingsscheuren. Deze scheuren hebben invloed op de materiaaleigenschappen zoals de sterkte, stijfheid, doorlatendheid, drainage, waterinfiltratie en verdamping. De bodemsamenstelling kan ook worden veranderd door biochemische processen die gestimuleerd worden door het indringen van zuurstof door het gebarsten oppervlak. Daarom, is het identificeren hoe scheuren in de bodem zich ontwikkelen essentieel voor het begrijpen van het materiaalgedrag.

Veel onderzoek in het bestuderen van verdrogingsscheuren is al verricht, maar de onderliggende mechanismen zijn nog niet volledig begrepen. Het is bekend dat de snelheid van drogen van invloed is op het uiteindelijke scheurgedrag in de bodem. Dit duidt op de mogelijke invloed van de belastingssnelheidseffecten in de scheurvorming. De effecten van de droogsnelheid kunnen worden gerelateerd aan de variaties in de treksterkte onder invloed van verschillende krimpsnelheiden, alsook aan het effect van de ontwikkeling van zuigspanning in de bodem.

In dit proefschrift werden verschillende sets experimenten uitgevoerd om het verschijnsel van scheurvorming in klei te bestuderen. De eerste reeks proeven werden in een gecontroleerde laboratoriumomgeving uitgevoerd om de scheurontwikkeling als het gevolg van het drogen van kleislib onder verschillende begin- en randvoorwaarden te analyseren. De resultaten van deze tests lieten zien dat scheuren zich anders dan algemeen aangenomen verspreiden (namelijk onder het oppervlak) en dat de scheureigenschappen sterk afhankelijk zijn van de begin- en randvoorwaarden.

Een tweede reeks proeven onderzocht de gecombineerde effecten van trekkracht en een hoge watergehalte op de treksterkte. Particle Image Velocimetry analyse werd ook uitgevoerd op de foto's die tijdens de tests waren genomen om de ontwikkelde rekvelden te onderzoeken. Het bleek dat het effect van de treksnelheid op de treksterkte van de klei verwaarloosbaar is in verhouding tot het effect van het watergehalte. De treksnelheid heeft wel invloed op de stijfheidsrespons van de bodem. De bevindingen lieten zien dat de invloed van de verdampingssnelheid op de scheurvorming meer afhankelijk is van de belastingssnelheid afhankelijke stijfheid dan aan significante veranderingen in treksterkte.

De laatste reeks experimenten onderzocht het drooggedrag van de klei met verschillende initiële watergehaltes en onder verschillende verdampingsomstandigheden. De kleinschalige verdamping experimenten werden uitgevoerd met behulp van

commercieël verkrijgbare zuigkracht meetapparatuur met een aangepaste testprocedure. De resultaten toonden aan dat het watergehalte aan het begin van de experimenten een grote invloed heeft op de droogcapaciteit van de grond, die gedeeltelijk toegeschreven kunnen worden aan de invloed van de oppervlaktestructuur en het poriënnetwerk. Onder bepaalde omstandigheden werd waargenomen dat de verdamping aan het maaiveld hoger was dan dat van open water. De verschillende verdampingssnelheden hadden een duidelijk effect op het watergehalteprofiel in de grond. De verdampingssnelheid produceerde ook een dynamische respons in de waterretentiecapaciteit van de grond.
Aan het eind werd een eenvoudige eendimensionaal model opgezet om het in de laboratoriumproeven geobserveerde gedrag vast te leggen. Het diende ook om de gevolgen van verschillende hypotheses over het materiaalgedrag gedurende scheurvorming in een drogende homogene grondlaag te analyseren.

Acknowledgements

First I would like to thank my supervisors prof. Cristina Jommi and Leon van Paassen for their support and the freedom they gave me in my research. I want to additionally acknowledge prof. Frits van Tol, who was my promotor during the first year.
The research presented in this thesis had the financial support the Dutch Technology Foundation STW, which is part of the Netherlands Organization for Scientific Research (NWO). It was also partly funded by the Ministry of Economic Affairs, via the perspective program BioGeoCivil (grant 11344), and through the CEAMaS (Civil Engineering Applications for Marine Sediments) project, which was supported by the European Regional Development Funding Through INTERREG IV B.
Most of my experiments were performed smoothly thanks to the help of Arno Mulder, who aided me with the construction and refinement of my experimental set ups. I would also like to thank the help of Ellen Meijvogel-de Koning and Wim Verwaal.
Niccolò Valimberti provided me with great assistance during the image processing with GeoPIV-RG and the Matlab programming.
During my Ph.D. I was grateful to have shared an office with prof. Frans Molenkamp, Stefano Muraro and Tom de Gast. Thanks for your friendship, help, the interesting conversations and the good laughs.
I want to thank all my Ph.D. colleagues and staff members of the Geo-Engineering section, and also friends and colleagues from other sections and places, in particular: Alex, Anna, André, Bruna, Hongfen, Jelke, Joana, Jon, Ngan, Nor, Patrick, Phil, Rafael, Richard, Shirish and Vinh. Likewise, I want to thank my friends from the MV, especially the members of the Ph.D. Committee and "De Elephanten".
Finally I would like to thank my parents and family for all their support and encouragement during all these years.

Curriculum Vitæ

Roderick Nicolaas TOLLENAAR

06-07-1979 Born in Chillán, Chile.

Education

2012–2017 Ph.D. Candidate in Geotechnical Engineering
Technische Universiteit Delft, the Netherlands
Thesis: Experimental Investigation on the Desiccation and Fracturing of Clay
Promotor: Prof. dr. C. Jommi

2005–2008 Master of Applied Science in Mining Engineering (Geomechanics)
The University of British Columbia, Vancouver, Canada

2001–2005 Bachelor of Applied Science in Geological Engineering
The University of British Columbia, Vancouver, Canada

Work

2007–2011 Geotechnical Engineer
AMEC Earth and Environmental, Vancouver, Canada

2005–2007 Geotechnical Engineer
Rio Tinto T.S., Vancouver, Canada